

**JAERI-M**  
**88-166**

**EFFECT OF CORE INLET WATER FLOW RATE ON REFLOODING  
PHENOMENA IN THE FORCED FEED SCTF CORE-I TESTS**

September 1988

Akira OHNUKI, Takamichi IWAMURA and  
Hiromichi ADACHI

日本原子力研究所  
Japan Atomic Energy Research Institute

JAERI-M レポートは、日本原子力研究所が不定期に公刊している研究報告書です。  
入手の問合せは、日本原子力研究所技術情報部情報資料課（〒319-11 茨城県那珂郡東海村）あて、お申しこしください。なお、このほかに財団法人原子力弘済会資料センター（〒319-11 茨城県那珂郡東海村日本原子力研究所内）で複写による実費頒布をおこなっております。

JAERI-M reports are issued irregularly.

Inquiries about availability of the reports should be addressed to Information Division  
Department of Technical Information, Japan Atomic Energy Research Institute, Tokaimura,  
Naka-gun, Ibaraki-ken 319-11, Japan.

©Japan Atomic Energy Research Institute, 1988

編集兼発行 日本原子力研究所  
印 刷 いばらき印刷株

Effect of Core Inlet Water Flow Rate on Reflooding  
Phenomena in the Forced Feed SCTF Core-I Tests

Akira OHNUKI, Takamichi IWAMURA and Hiromichi ADACHI

Department of Reactor Safety Research  
Tokai Research Establishment  
Japan Atomic Energy Research Institute  
Tokai-mura, Naka-gun, Ibaraki-ken

(Received August 5, 1988)

The present report investigates the effects of core inlet water flow rate ( $M_i$ ) on the reflooding phenomena in the core observed in the Slab Core Test Facility (SCTF) Core-I tests. The effects on the two-dimensional core thermal-hydraulic phenomena are emphasized. The following forced feed test results are examined : Tests S1-01 [ $M_i$  in Acc injection period = 16 kg/s (flooding velocity = 6.6 cm/s),  $M_i$  in LPCI injection period = 10 kg/s (4.1 cm/s)], S1-SH1 [29 (12.0), 10 (4.1)], S1-05 [16 (6.6), 6 (2.1)] and S1-09 [29 (12.0), 19 (7.8)].

Major conclusions derived from this study are as follows :

- (1) Larger core inlet flow rate gave larger water accumulation rate in the core and resultantly better core cooling. Larger core inlet flow rate gave larger water accumulation rate in the upper planum and larger water flow rate through the hot leg.
- (2) The two-dimensional thermal-hydraulic behaviors in the core (radial differences on void fraction and on heat transfer coefficient) were not significantly affected by the magnitude on the core inlet flow rate.
- (3) The dependency of heat transfer coefficients on the core inlet flow rate was qualitatively consistent with modified Murao-Sugimoto correlation which includes the correction factor of liquid flow rate. The correlation slightly underestimated the heat transfer coefficients quantitatively. The cause of the underestimation was discussed by

---

This work was performed under a contract with the Atomic Energy Bureau of the Science and Technology Agency of Japan.

evaluating the flow circulation in the core.

Keywords : Reflood, PWR-LOCA, SCTF, ECCS, Two-Phase Flow, Void Fraction, Heat Transfer, Quench, Cross Flow, Two-Dimensional Thermal-Hydraulic Behavior

S C T F 第一次炉心強制注入試験における  
炉心入口水流量の再冠水現象に及ぼす効果

日本原子力研究所東海研究所原子炉安全工学部

大貫 晃・岩村 公道・安達 公道

(1988年8月5日受理)

本報告書では、平板炉心試験装置（SCTF）第一次炉心においてみられた炉心入口水流量( $M_i$ )の炉心内再冠水現象に及ぼす効果を調べる。特に炉心内の二次元熱水力学的挙動に及ぼす効果に重点をおく。強制注入試験 S1-01 [蓄圧系 (Acc) 注入期間の  $M_i = 16 \text{ kg/s}$  (冠水速度 = 6.6 cm/s), 低圧系 (LPCI) 注入期間の  $M_i = 10 \text{ kg/s}$  (4.1 cm/s)], S1-SH1 [29 (12.0), 10 (4.1)], S1-05 [16 (6.6), 6 (2.1)] 及び S1-09 [29 (12.0), 19 (7.8)] の結果を比較検討する。

本研究から得られた主な結論は以下の通りである。

- (1) 炉心入口流量が大きいほど炉心内の蓄水速度が大きく、その結果炉心冷却は促進された。  
また、炉心入口流量が大きいほど上部プレナム内の蓄水速度は大きく、ホットレグを流れる水流量は増加した。
- (2) 炉心内の二次元熱水力学的挙動、すなわちボイド率や熱伝達率の半径方向の差といったものは炉心入口流量の大きさによらずほぼ同程度であった。
- (3) 熱伝達率の炉心入口流量に対する依存性は、水流量補正係数を含む修正村尾・杉本の式により定性的に表すことができた。定量的には同相関式は熱伝達率をわずかに過小評価した。  
炉心内の循環流の評価により過小評価の原因を考察した。

---

本報告書は、電源開発促進対策特別会計法に基づき科学技術庁からの受託によって行った研究の成果である。

## Contents

1. Introduction .....	1
2. Test Description .....	3
2.1 Test Facility .....	3
2.2 Test Conditions and Procedure .....	3
3. Test Results and Discussions .....	6
3.1 Overall Fluid Behavior in Pressure Vessel and Primary Loops .....	6
3.2 Overall Core Thermal Behavior .....	7
3.3 Two-Dimensional Hydraulic Behavior .....	8
3.4 Two-Dimensional Heat Transfer Behavior .....	11
4. Summary and Conclusions .....	15
Acknowledgement .....	17
References .....	18
Appendix A Schematic of Slab Core Test Facility (SCTF) Core-I ...	70
Appendix B Selected Heater Rod Cladding Temperatures of SCTF Test S1-SH1 .....	87
Appendix C Selected Heater Rod Cladding Temperatures of SCTF Test S1-05 .....	91
Appendix D Selected Heater Rod Cladding Temperature of SCTF Test S1-09 .....	95

## 目 次

1. 序 .....	1
2. 試験 .....	3
2.1 試験装置 .....	3
2.2 試験条件と手順 .....	3
3. 試験結果及び考察 .....	6
3.1 圧力容器及び1次系における流体挙動 .....	6
3.2 炉心の熱的挙動 .....	7
3.3 2次元流体挙動 .....	8
3.4 2次元熱伝達挙動 .....	11
4. まとめ及び結論 .....	15
謝辞 .....	17
参考文献 .....	18
付録A 平板炉心(SCTF)第一次炉心の試験装置 .....	70
付録B SCTF試験S1-SH1のデータ抄 .....	87
付録C SCTF試験S1-05のデータ抄 .....	91
付録D SCTF試験S1-09のデータ抄 .....	95

## Nomenclature

BOCREC	bottom of core recovery = time of reflood initiation
$C_D$	drag coefficient / one rod
$dP_h$	horizontal differential pressure (Pa)
$E$	emissivity
$f$	correction factor defined in section 3.4
$G_h$	horizontal mass velocity (kg/m <sup>2</sup> s)
$g$	acceleration due to gravity (m/s <sup>2</sup> )
HTC	heat transfer coefficients (W/m <sup>2</sup> K)
$H_{re}$	latent heat of evaporation (J/kg)
$h_f$	film boiling term in Murao-Sugimoto correlation
$h_m$	measured heat transfer coefficients
$h_r$	radiation term in Murao-Sugimoto correlation
$L_q$	distance from quench front (m)
$M_i$	core inlet mass flow rate (kg/s)
$N_T$	number of rods
$T_b$	maximum cladding temperature at reflood initiation(K)
$T_w$	cladding temperature (K)
$T_s$	saturation temperature (K)
$\Delta T_s$	= $T_w - T_s$ (K)
$T_q$	quench temperature (K)
$t_q$	quench time (s)
$\Delta T_r$	temperature rise after reflood initiation (K)

## Greek symbols

$\alpha$	void fraction
$\rho$	density (kg/m <sup>3</sup> )
$\rho_m$	density of mixture = $\rho_g \alpha + \rho_l (1-\alpha)$
$\lambda$	thermal conductivity (W/mK)
$\mu$	dynamic viscosity (Pa·s)
$\varepsilon$	Stefan Boltzmann constant (W/m <sup>2</sup> K <sup>4</sup> )

## Subscripts

$g$	gas phase
$l$	liquid phase

## List of Tables

- Table 2-1 List of Major Measured Test Conditions  
 Table 2-2 Accuracy of Instruments

## List of Figures

- Fig. 2-1 Schematic Diagram of Slab Core Test Facility  
 Fig. 2-2 Vertical Cross Section of Pressure Vessel  
 Fig. 2-3 Comparison of Core Inlet Water Flow Rate and Flooding Velocity  
 Fig. 2-4 Comparison of Pressure, Core Inlet Subcooling and Supplied Power  
 Fig. 3-1 Comparison of Core Full Height Differential Pressure in Bundle 4  
 Fig. 3-2 Comparison of Sectional Void Fraction at Three Axial Regions in Bundle 4  
 Fig. 3-3 Comparison of Steam Mass Flow Rate Generated in Core  
 Fig. 3-4 Comparison of Core Mass Effluent Rate  
 Fig. 3-5 Comparison of Water Mass in Upper Plenum  
 Fig. 3-6 Comparison of Water Mass in Steam/Water Separator  
 Fig. 3-7 Terminology : Cladding Temperature History  
 Fig. 3-8(1) Effect of Core Inlet Water Flow Rate on  $t_q$   
     (Comparison of high Acc and LPCI test with base case test)  
 Fig. 3-8(2) Effect of Core Inlet Water Flow Rate on  $t_q$   
     (Comparison of high Acc and low  $T_b$  test with base case test)  
 Fig. 3-8(3) Effect of Core Inlet Water Flow Rate on  $t_q$   
     (Comparison of low LPCI test with base case test)  
 Fig. 3-9(1) Effect of Core Inlet Water Flow Rate on  $T_q$   
     (Comparison of high Acc and LPCI test with base case test)  
 Fig. 3-9(2) Effect of Core Inlet Water Flow Rate on  $T_q$   
     (Comparison of high Acc and low  $T_b$  test with base case test)  
 Fig. 3-9(3) Effect of Core Inlet Water Flow Rate on  $T_q$   
     (Comparison of low LPCI test with base case test)  
 Fig. 3-10(1) Effect of Core Inlet Water Flow Rate on  $\Delta T_r$   
     (Comparison of high Acc and LPCI test with base case test)  
 Fig. 3-10(2) Effect of Core Inlet Water Flow Rate on  $\Delta T_r$   
     (Comparison of high Acc and low  $T_b$  test with base case test)  
 Fig. 3-10(3) Effect of Core Inlet Water Flow Rate on  $\Delta T_r$   
     (Comparison of low LPCI test with base case test)  
 Fig. 3-11 Comparison of HTC at Three Axial Elevations in Bundle 4

- Fig. 3-12 Comparison of Core Full Height Differential Pressure in Bundles 2, 4 and 8
- Fig. 3-13 Comparison of Horizontal Differential Pressure between Bundles 5 and 8 at 1.905m and 3.235m elevations
- Fig. 3-14(1) Comparison of Sectional Void Fraction between 0.085m and 0.575m elevations in Bundles 2, 4 and 8
- Fig. 3-14(2) Comparison of Sectional Void Fraction between 0.7m and 1.24m elevations in Bundles 2, 4 and 8
- Fig. 3-14(3) Comparison of Sectional Void Fraction between 1.365m and 1.905m elevations in Bundles 2, 4 and 8
- Fig. 3-14(4) Comparison of Sectional Void Fraction between 2.03m and 2.57m elevations in Bundles 2, 4 and 8
- Fig. 3-14(5) Comparison of Sectional Void Fraction between 2.695m and 3.235m elevations in Bundles 2, 4 and 8
- Fig. 3-14(6) Comparison of Sectional Void Fraction between 3.36m and 3.685m elevations in Bundles 2, 4 and 8
- Fig. 3-15 Comparison of Differential Pressure across End Box Tie Plate above Bundles 2, 4, 6 and 8
- Fig. 3-16 Comparison of Liquid Level in End Box above Bundles 2, 4, 6 and 8
- Fig. 3-17 Comparison of Liquid level in Upper Plenum above Bundles 1, 4 and 8
- Fig. 3-18 Comparison of Difference of Liquid Level between above Bundles 1 and 8
- Fig. 3-19(1) Comparison of HTC at 0.95m elevation in Bundles 2, 4 and 8
- Fig. 3-19(2) Comparison of HTC at 1.905m elevation in Bundles 2, 4 and 8
- Fig. 3-19(3) Comparison of HTC at 2.33m elevation in Bundles 2, 4 and 8
- Fig. 3-20(1) Relationship between HTC and Distance from Quench Front at 0.95m elevation in Bundles 2,4,6 and 8
- Fig. 3-20(2) Relationship between HTC and Distance from Quench Front at 1.905m elevation in Bundles 2,4,6 and 8
- Fig. 3-20(3) Relationship between HTC and Distance from Quench Front at 2.33m elevation in Bundles 2,4,6 and 8
- Fig. 3-21 Difference of HTC between Maximum or Minimum HTC and Average HTC at Three Axial Elevations
- Fig. 3-22(1) Comparison of HTC at 1.905m and 2.33m elevations in Bundles 2,4 and 8 with Murao-Sugimoto Correlation in Base Case Test

Fig. 3-22(2) Comparison of HTC at 1.905m and 2.33m elevations in Bundles 2,4 and 8 with Murao-Sugimoto Correlation in High Acc and Low Tb Test

Fig. 3-22(3) Comparison of HTC at 1.905m and 2.33m elevations in Bundles 2,4 and 8 with Murao-Sugimoto Correlation in Low LPCI Test

Fig. 3-22(4) Comparison of HTC at 1.905m and 2.33m elevations in Bundles 2,4 and 8 with Murao-Sugimoto Correlation in High Acc and LPCI Test

Fig. 3-23(1) Correction Factor for Film Boiling Term of Murao-Sugimoto Correlation in Base Case Test

Fig. 3-23(2) Correction Factor for Film Boiling Term of Murao-Sugimoto Correlation in High Acc and Low Tb Test

Fig. 3-23(3) Correction Factor for Film Boiling Term of Murao-Sugimoto Correlation in Low LPCI Test

Fig. 3-23(4) Correction Factor for Film Boiling Term of Murao-Sugimoto Correlation in High Acc and LPCI Test

Fig. 3-24 Comparison of Correction Factor in SCTF Tests with Correlation from Small Scale Reflood Test

Fig. 3-25(1) Horizontal Mass Velocities in Base Case Test

Fig. 3-25(2) Horizontal Mass Velocities in High Acc and LPCI Test

## 1. Introduction

The Slab Core Test Facility (SCTF) Test Program<sup>(1)-(4)</sup> is being performed as a part of the Large Scale Reflood Test Program in which the Cylindrical Core Test Facility (CCTF) Test Program is also conducted. The principal purposes of both test programs are to clarify thermal-hydraulic behavior in the primary coolant system of a pressurized water reactor (PWR) during a reflood phase of a large break loss-of-coolant accident (LOCA) and to demonstrate and quantify the safety margin of the emergency core coolant system (ECCS) against the accident.

In the CCTF test program, primary objective is to study the system behavior. On the other hand, the SCTF test is a separate effect test. The SCTF has electrically heated rod bundles with a full height, full radial width and single bundle along the azimuthal direction. The major objectives of the SCTF test program are to clarify the following items:

- (1) Two-dimensional thermal-hydraulic behavior in the core (e.g., chimney effect),
- (2) Two-dimensional flow interaction between the core and the upper plenum (e.g., fall back of water, counter-current flow at tie plates) and
- (3) Hot leg carry-over characteristics.

Many small scale reflood experiments<sup>(5)</sup> have been performed in the past. However, the above items have not been clarified, especially for the first item, because the flow area of the core was much smaller than that in an actual reactor. Therefore, the effects of various test parameters<sup>(1)-(4)</sup> on two-dimensional reflooding phenomena have been studied in the SCTF test series. Recent analysis showed that a steep radial power profile gave higher heat transfer coefficients in higher power bundles under the same total core power<sup>(6)</sup>. And it was reported in reference (7) that a larger cross flow between rod bundles was induced under steeper radial power profile. So the cross flow between bundles is important to investigate the heat transfer enhancement in the higher power bundles.

The present report describes the effects of core inlet water mass flow rate mainly on the two-dimensional thermal-hydraulic behavior in the core and clarifies the effect on the heat transfer enhancement due to the cross flow.

A brief description of the facility is given in Appendix A. More detailed information is available in reference (8). Tests investigated in

this report are Tests S1-SH1,S1-01,S1-05 and S1-09 in the SCTF Core-I tests. The selected heater rod cladding temperatures obtained in those tests are presented in Appendices B through D for respective tests,except those for S1-01 which have been presented in reference (1).

## 2. Test Description

### 2.1 Test Facility

The schematic diagram of SCTF is shown in Fig.2-1.

The primary coolant loops consist of a hot leg equivalent of the four actual hot leg, a steam/water separator corresponding to the four actual steam generator inlet plenums, an intact cold leg equivalent to the three actual intact cold legs, a broken cold leg on the pressure vessel side and a broken cold leg on the steam/water separator side. The two-broken cold legs are connected to two containment tanks, respectively.

The flow area scaling ratio is 1/21 to a 1,100 MWe PWR, whereas the height of each component simulates the actual PWR.

The emergency core cooling system (ECCS) consists of an accumulator (Acc) system and a low pressure coolant injection (LPCI) system. The injection ports for the Acc and LPCI systems are the lower plenum and the intact cold leg, respectively.

Figure 2-2 shows the vertical cross section of the pressure vessel. The pressure vessel includes a simulated core, an upper plenum with internals, a lower plenum, a core baffle and a downcomer.

The simulated core consists of 8 bundles arranged in a row with full radial width. Each bundle consists of 234 heater rods and 22 non-heated rods arranged 16x16 array. The outer diameter and the heated length of the heater rod are 10.7mm and 3,660 mm, respectively. The dimensions of rod bundle are based on those for a 15x15 fuel rod bundle of a Westinghouse type PWR.

The core and the upper plenum are enveloped by honeycomb thermal insulators to minimize the wall thermal effects.

More detailed information on the SCTF is available in reference (8) and brief description is presented in Appendix A.

### 2.2 Test Conditions and Procedure

Emergency core cooling (ECC) water was injected directly into the lower plenum in the tests examined in this study. The downcomer had been isolated from the lower plenum by inserting a blocking plate. Therefore, reliable test data were obtained because core inlet coolant (water) flow rate could be measured accurately at the ECC water injection piping. This method is called the forced-feed reflooding.

Four forced feed tests were adopted in this report to meet objectives mentioned in Introduction, those are Tests S1-01, S1-SH1, S1-05 and S1-09. These four tests were performed under almost the same conditions except for the core inlet flow rate. Additionally, the maximum cladding temperature at the reflood initiation in Test S1-SH1 was different from that in other tests. The time when the ECC water reaches the bottom of the core heated length is called BOCREC (bottom-of-core recovery) in this report and the cladding temperature at the BOCREC is represented as Tb. Major measured test conditions are listed in Table 2-1. And the accuracy of instruments used in this report is listed in Table 2-2.

The estimated core inlet flow rate ( $M_i$ ) for each test is shown in Fig. 2-3. These flow rates were calculated by subtracting the water accumulation rate in the baffle region and in the lower plenum from the ECC water injection rate. The core inlet water velocity (flooding velocity) is also shown in Fig. 2-3. These velocities were calculated by using the nominal core flow area  $0.259\text{m}^2$  shown in Table A-1 in Appendix-A. In the Acc injection period, the core inlet flow rates for Tests S1-SH1 and S1-09 were larger than those for Tests S1-01 and S1-05. In the LPCI injection period, the core inlet flow rate for Test S1-09 was larger than those for Tests S1-01 and S1-SH1 and that for Test S1-05 was lower than those for Tests S1-01 and S1-SH1. Therefore, in this report Test S1-SH1 is called "High Acc and Low Tb", Test S1-05 is "Low LPCI" and Test S1-09 is "High Acc and LPCI" as compared to Test S1-01 (Base Case).

The other test conditions which are intended to be common to these four tests are shown in Figs. 2-4(a), (b) and (c). Pressure in the core center and in the containment tank and core inlet subcooling were almost the same with each other. Total core power and its profile over eight bundles were identical for the four tests. The radial power profile was based on the radial profile of a 1,100 MWe Westinghouse initial core. The normalized radial power factors in Bundles 1 and 2, 3 and 4, 5 and 6 and 7 and 8 are 1.001, 1.065, 1.015 and 0.919, respectively, for all the tests.

The test procedure for these four tests is as follows. After setting the initial conditions (pressure and saturation condition etc.), core heating was initiated. When four cladding temperatures 842K and 926K for Test S1-SH1 and for other three tests, respectively, the Acc injection into the lower plenum was initiated. The initial saturation water level in the lower plenum was about 0.4 m below the bottom of heated part. After keeping the core power constant for 2 s in Test S1-SH1 and for 5 s in other Tests from the

Acc injection start, the core power decay simulation started from the value at 30 s after shutdown of an actual reactor. The decay curve was based on the "ANS standard + actinides + delayed neutron effect for voided core". The maximum cladding temperature at the BOCREC ( $T_b$ ) was intended to be 873K in Test S1-SH1 and 973K in other Tests. The injection was switched from the Acc injection to the LPCI at about 10 through 15 s after the BOCREC. At 900 s after the initiation of LPCI, the test was terminated.

### 3. Test Results and Discussions

#### 3.1 Overall Fluid Behavior in Pressure Vessel and Primary Loops

Figure 3-1 shows the comparison of differential pressures across the core full height in bundle 4 (highest power bundle) for four tests examined in this report. Figures 3-2 (a),(b) and (c) show the comparison of void fractions at three axial sections in bundle 4 for all the tests. These void fractions were calculated from the measured vertical differential pressures by neglecting the effects of frictional and accelerational pressure drops. From the comparisons among Tests S1-01, S1-05 and S1-09, it is found that the larger core inlet flow rate ( $M_i$ ) gives larger amount of water accumulation (smaller void fraction) in the core. From the comparison between Tests S1-01 and S1-SH1, it is found that the larger core water accumulation rate (gradient of accumulation curve) in the Acc injection period is realized by the larger  $M_i$  in that period under the different condition for  $T_b$ . The difference of about 100K for  $T_b$  has been reported in ref.(9) to give no significant difference of accumulation rate of water. From the comparison between Tests S1-01 and S1-05, the smaller accumulation rate is found to be realized by the smaller  $M_i$  in the LPCI injection period. Therefore, the amount of core inlet flow rate both in the Acc and the LPCI injection periods affects the accumulation rate of water in the core.

Steam mass flow rates generated in the core are shown in Fig.3-3. These flow rates were measured at the primary loop by the ventury and the orifice flow meters. The result of Test S1-SH1 is not presented in this figure because of malfunction of the flow meters. The larger  $M_i$  gave the larger steam generation rate in the early period (until about 100 seconds) and after that period the larger decreasing rate of steam generation was observed under the condition of larger  $M_i$ . The different characteristics of steam generation in the early period are caused by the faster quench velocity under the larger  $M_i$  as will be discussed in the core thermal behavior.

Carry-over characteristics out of the core are shown in Figs.3-4, 3-5 and 3-6. Figure 3-4 shows the comparison of core mass effluent rate (that is water plus steam mass flow rates) obtained by subtracting the core water accumulation rate from  $M_i$ . The larger  $M_i$  gave the larger core mass effluent rate. The results of high Acc and low  $T_b$  test were almost the same value as those of base case test in the LPCI injection period. This result suggests that the difference of  $T_b$  and  $M_i$  in the Acc injection period have no sig-

nificant effects on the core mass effluent rate in the LPCI injection period. Figures 3-5 and 3-6 show the comparison of amount of water accumulation in the upper plenum and in the steam/water(S-W)separator,respectively. The larger  $M_i$  gave the larger water mass in the upper plenum and gave the larger water accumulation rate in the S-W separator. And the larger  $M_i$  gave the earlier initiation time of water accumulation in the S-W separator.

### 3.2 Overall Core Thermal Behavior

The terminology is defined in Fig.3-7 for a typical cladding temperature history in the SCTF tests. In this section, the effects of core inlet flow rate ( $M_i$ ) are presented on the quench time ( $t_q$ ), the quench temperature ( $T_q$ ) and the temperature rise ( $\Delta T_r$ ). The effects of  $M_i$  on the heat transfer coefficients (HTC) are also discussed.

During the SCTF tests, the quench front progressed upward from the bottom to the top (bottom quench) or downward from the top to the bottom (top quench). Bottom quench always occurred below the 2.33m elevation (T/C elevation No's. 1 through 7 shown in Fig. A-10 in Appendix-A). Top quench always occurred at No.10 elevation and sometimes occurred at some part of a bundle (1D,1B and 2B regions,etc.,shown in Fig. A-10) at No's.8 and 9 elevations though bottom quench was still dominant even at these elevations. Top quench tended to occur randomly. However, bottom quench propagation was almost uniform throughout the core and the quench time and temperature were clearly defined. Therefore, in order to distinguish the thermal characteristics in the bottom quench region from those in the top quench region, the subsequent comparison plots are separately presented for the two regions: one for the T/C elevation No's. 1 through 7 and the other for No's. 8 through 10.

Figures 3-8(1),(2) and (3) show the comparison of  $t_q$  for Tests S1-09,S1-SH1 and S1-05 with that for Test S1-01. Shorter quench times for almost all elevations resulted from the larger  $M_i$  only in the Acc injection period (Fig.3-8(2)) and both in the Acc and LPCI injection period (Fig.3-8(1)). On the other hand, the smaller  $M_i$  only in the LPCI injection period gave longer quench times except at T/C elevation No's. 1,2,3 and 10 at which the quench times were less than 100 seconds (Fig.3-8(3)).

Figures 3-9(1),(2) and (3) show the comparison of  $T_q$ . No significant effect of the amount of  $M_i$  both in the Acc and LPCI injection period was observed on  $T_q$  from these figures.

Figures 3-10(1),(2) and (3) show the comparison of  $\Delta T_r$ . Since the  $T_b$  in

Test S1-SH1 is relatively lower than the other tests due to the lower preset temperature as mentioned in section 2.2,  $\Delta Tr$  is a more suitable value than the turnaround temperature to evaluate the effects of Mi independently of the difference of Tb. As shown in these figures, the larger Mi gave a smaller  $\Delta Tr$ . In particular, the smaller Tr was observed in Test S1-09 (Fig.3-10(1)) at all elevations. The larger Mi in the Acc injection period with an equal one in the LPCI injection period also resulted in a smaller  $\Delta Tr$  at almost all elevations (Fig.3-10(2)). The smaller Mi in the LPCI injection period with an equal one in the Acc injection period resulted in the larger  $\Delta Tr$  except at T/C elevation No's. 1 through 5 and 10 (Fig.3-10(3)).

Figure 3-11 (a),(b) and (c) show the comparison of HTC at three elevations in bundle 4 (highest power bundle). These HTC were calculated by the cladding temperature transients<sup>(10)</sup> and smoothed by the moving averaged method. As shown in these figures, the larger Mi both in the Acc and the LPCI injection periods gave the higher HTC during the whole transients at all elevations. This result is consistent with the better core cooling on tq and on  $\Delta Tr$  as shown in Figs 3-8(1) and 3-10(1).

In the case of larger Mi only in the Acc injection period, the tendency of higher HTC still existed even in the LPCI injection period. This difference of HTC in the LPCI injection period is quite large against the difference of HTC due to the lower Tb which has been reported in ref.(9). This result giving the higher HTC even in the LPCI injection period is consistent with the lower void fraction which is resulted from the larger Mi in the Acc injection period as shown in Figs.3-2(a),(b) and (c). And this result is also consistent with the better core cooling on tq and on  $\Delta Tr$  as shown in Figs 3-8(2) and 3-10(2).

In the case of lower Mi only in the LPCI injection period, HTC at 0.95m (lower elevation of the core) was almost the same as that in the base case test during the whole transients and almost the same HTC in the Acc injection period was realized at 1.905m and 3.19m elevations. These characteristics are consistent with the result that the smaller Mi only in the LPCI injection period gives the longer quench times above 1.38m elevation and the larger  $\Delta Tr$  also above 1.905m elevation.

### 3.3 Two-Dimensional Hydraulic Behavior

The effects of core inlet flow rate (Mi) on two-dimensional hydraulic behavior in the pressure vessel are presented and discussed in this section.

Two-dimensional hydraulic behaviors in the wide core of SCTF are expected due to the non-uniform power profile over the eight bundles<sup>(6)</sup>. Two-dimensional hydraulic behaviors are examined from the comparisons of : (I) core full height differential pressures and sectional void fractions, (II) horizontal differential pressures in the core, (III) fluid behavior around the end box tie plates and (IV) water level distribution above the upper core support plate (UCSP).

Figures 3-12 (a) through (d) show the comparisons of core full height differential pressures in bundles 2,4 and 8 for each test. It is observed from these figures that the differential pressures in these bundles were almost the same at any time regardless of the differences of bundle power and Mi. This result indicates the existence of cross flow between the bundles because under the no cross flow condition the differential pressure at each bundle should be different to each other due to the different bundle power. This uniform distribution of the core full height differential pressure has been also observed in the other SCTF test under a steeper radial power profile<sup>(7)</sup>.

Figures 3-13 (a) and (b) show the comparisons of horizontal differential pressure transients between bundles 5 and 8 at 3.235m (top region of the core) and at 1.905m (almost middle elevation of the core) elevations, respectively. The signs and the magnitudes of these differential pressures can be considered to indicate the direction and the intensity of cross flows between bundles.

At the top region of the core, the cross flow for each test were almost zero until about 240 seconds for low LPCI test and about 150 seconds for the others. After that, the cross flow from bundle 8 to bundle 5 was getting large with time and reached to some constant value. The intensity of the cross flow for each test was almost the same except for the low LPCI test in which the intensity was slightly smaller than those in the other tests.

On the other hand, at the middle elevation of the core, the cross flow from bundle 5 to bundle 8 was realized until about the quench time of this elevation or of the whole core. In the high Acc and LPCI test, the slightly larger intensity of the cross flow was realized until about 260 seconds (this time is correspond to the whole core quench time of this test) and no significant cross flow was realized after that. In the low LPCI test, the cross flow was realized until about 310 seconds (this time is also correspond to the whole core quench time of this test). On the contrary, for the other tests the cross flow from bundle 8 to bundle 5 was realized after

the quench time of this elevation. Though the different signs and intensity of the cross flow at this elevation were recognized at a specified time for each test, the maximum plus or minus value was almost the same among tests except for the high Acc and LPCI test.

Figures 3-14 (1) through (6) show the comparison of void fraction at six axial sections in bundle 2,4 and 8 for each test. The calculating method of these void fractions was the same as that presented in Fig.3-2. The following results are observed in these figures,

- (1) In the lower part of the core (0.085m through 1.24m), the distribution of void fractions is almost uniform until about the whole core quench time irrespective of the amount of  $M_i$ . After the whole core quench time, the void fraction in bundle 8 becomes higher for all the tests.
- (2) In the middle part of the core (1.365m through 2.57m), the distribution of void fractions is also almost uniform except for high Acc and LPCI test. In that test, the void fraction at the section of 1.365m-1.905m in bundle 8 becomes lower after about 90 s.
- (3) In the top part of the core (2.695m through 3.685m), the distribution of void fractions is also almost uniform though the void fraction in bundle 8 tends to be a little higher in some time before the whole core quench time.

The higher void fraction in bundle 8 after about the whole core quench time mentioned in the above first item is supposed to be realized by the reduction of vertical flow rate of water due to the water cross flow from bundle 8 to bundle 5 sides since the cross flow of that direction is dominant in that period as shown in Fig.3-13(b). The result of lower void fraction in bundle 8 in high Acc and LPCI test mentioned in the above second item is supposed to be caused by the following two effects; one is that the increase of vertical flow rate of water due to the larger intensity of cross flow from bundle 5 to bundle 8 is realized until about 300 seconds as shown in Fig.3-13(b) and another is the smaller steam generation rate in bundle 8 due to the lowest power under no significant cross flow condition after about 300 seconds as also shown in Fig.3-13(b).

Figures 3-15 through 3-18 show the comparisons of the fluid behaviors at around the end boxes and in the upper plenum. Figure 3-15 shows the comparisons of differential pressures across the end box tie plates above bundles 2,4,6 and 8. The larger  $M_i$  gave the larger positive differential pressure above each bundle, which meant the larger mass flow rate of two-phase up-flow. Besides, the differential pressure above bundle 8 became much lower than those above the other bundles after about the whole core quench

time. The negative differential pressure above bundle 8 indicates the possibility of water fall back into the core through the end box tie plate holes. This fall back water might increase the water cross flow at the top region of the core due to the cross flow mentioned in Fig.3-13 (a).

Figure 3-16 shows the comparisons of liquid levels in the end boxes above bundles 2,4,6 and 8. The liquid levels above bundle 8 in all the tests became much higher than those above the other bundles after about the whole core quench time of each test.

Figure 3-17 shows the comparisons of collapsed liquid levels in the upper plenum above bundles 1,4 and 8 in each test. The liquid levels above these bundles increased gradually and at about the whole core quench time the levels increased rapidly and remained at almost constant value.

The liquid levels above bundle 8 in all the tests were higher than those above the other bundles and the difference of liquid levels between bundle 8 and the other bundles increased gradually with time. Figure 3-18 shows the difference of the liquid levels between above bundle 8 and above bundle 1. No significant effect of  $M_i$  is observed on the magnitudes of this difference except only for the low LPCI test in which the difference is much smaller than that in other tests until about the whole core quench time.

The development of non-uniform pressure distribution at the interface between the core and the upper plenum mentioned above is supposed to develop the cross flow from bundle 8 to bundle 5 sides shown in Fig.3-13 (a). This effect has been reported as non-uniform water head effect<sup>(7)</sup>. The smaller intensity of cross flow in the low LPCI test shown in Fig.3-13(a) is consistent with the smaller difference of liquid levels in the upper plenum.

### 3.4 Two-Dimensional Heat Transfer Behavior

The effects of core inlet flow rate ( $M_i$ ) are presented and discussed on the two-dimensional thermal behavior in this section. Figures 3-19(1) through (3) show the comparison of transients of heat transfer coefficients (HTC) in bundles 2,4 and 8 at three axial elevations (0.95m, 1.905m and 2.33m) for each test. At 0.95m elevation, no difference was observed among these bundles for all the tests. However, at 1.905m and 2.33m elevations, the HTC in bundles 2 and 4 were higher than that in bundle 8 during almost whole transients. The two-dimensionality of HTC is also observed in Figs. 3-20(1) through (3). The HTC in bundles 2,4,6 and 8 are plotted against the distance from the quench front of each bundle in these figures.

In order to clarify the effects of  $M_i$  on the two-dimensionality of HTC, the following two differences, which are shown in Fig.3-21, are examined for each test; (1) (maximum HTC-average HTC) on HTC in bundles 2,4,6 and 8 at a certain distance from the quench front and (2) (minimum HTC-average HTC) at the same location. It is found from this figure that the magnitude of heat transfer enhancement and reduction is not significantly affected by  $M_i$  though the magnitudes scattered at 1.905m elevation.

The two-dimensionality of HTC is examined in Figs.3-22(1)through(4) by comparing data with Murao-Sugimoto film boiling heat transfer correlation<sup>(11)</sup>. The structure of the correlation is as follows,

$$h = h_r + h_f = 0.94[\lambda_g^3 \rho_g \rho_f H_{fg} g / L_g \mu_g \Delta T_s]^{1/4} (1-\alpha)^{1/4} + E \epsilon (1-\alpha)^{1/2} (T_w^4 - T_s^4) / \Delta T_s.$$

The emissivity  $E$  is assumed to be 0.65.

This correlation has successfully predicted the slug flow film boiling heat transfer coefficient during reflood phase in a relatively small bundle with full height of an actual reactor<sup>(11)</sup>. This correlation includes the effects of the different clad surface temperature, different distance from the quench front and different void fraction on the heat transfer coefficient. Therefore, by using this correlation, those effects can be examined on the two-dimensionality of HTC. As shown in Figs.3-22(1) through (4), the calculated results by the correlation show almost uniform distribution of HTC among bundles. This result indicates that the two-dimensionality of the data is induced by the other effect. These different characteristics between data and calculations were also observed in CCTF data<sup>(12)</sup>. In reference (12), the differences were considered to be induced by the effect of radial power profile. The differences in CCTF data in this report are also considered to be caused by the same reason. However, the real physical reason induced by the radial power profile has not been made clear against producing the two-dimensionality of HTC yet.

As shown in Figs.3-22(1) through (4), the Murao-Sugimoto correlation underestimates HTC and the degree of underestimation became larger with  $M_i$ . The following factor  $f$  representing the disagreement between the correlation and data was obtained for each test and shown in Figs.3-23(1) through (4),

$$f = (h_M - h_r) / h_f$$

where  $h_M$ : measured HTC ,

$h_r$ : radiation term in Murao-Sugimoto correlation and

$h_f$ : film boiling term in Murao-Sugimoto correlation.

It is found from these figures that the factor  $f$  becomes larger than unity

with increasing  $M_i$  and is larger in bundles 2 and 4 than that in bundle 8. The dependency of  $f$  on  $M_i$  has been investigated in small scale reflood tests<sup>(13)</sup>. The comparison is shown in Fig.3-24. The axis of abscissas in this figure is the superficial liquid velocity obtained by the heat balance method<sup>(7)</sup>. The data of SCTF are at the elevations of 1.905m and 2.33m. The amount of  $f$  of SCTF is found to depend on the amount of  $M_i$ , that is similar to the correlation obtained by the data of small scale reflood tests. However, the  $f$  of SCTF is relatively larger than the correlation and some SCTF data are located above the scattering band ( 25 ) of small scale reflood test data. The reason of this difference is not clear and however the increase of superficial liquid velocity along the axial direction is supposed to be occurred in SCTF by the following examination.

The horizontal mass velocity through the gap between rods was estimated with using the data of horizontal differential pressures based on the homogeneous two-phase flow model. The basic equation is as follows,

$$G_h = \rho_m V_h = (2 \rho_m dP_h / C_D N_T)^{1/2}$$

where  $G_h$  : horizontal mass velocity,

$\rho_m$  : density of mixture =  $\rho_g \alpha + \rho_l (1 - \alpha)$

$dP_h$  : horizontal differential pressure,

$C_D$  : drag coefficient and

$N_T$  : number of rods.

The drag coefficient,  $C_D$ , is assumed to be 0.5 in accordance with COBRA-IV code model<sup>(14)</sup>.

The results for base case and high Acc and LPCI tests are shown in Figs. 3-25(1) and (2). The locations A and B in these figures are between bundles 1 and 5 and C,D and E are between bundles 5 and 8. The plus sign indicates the cross flow from bundles 1 to 5 and from 5 to 8, respectively. At 3.235m elevation (top region of the core), the direction of the cross flow is from bundle 8 to bundle 1 sides. On the other hand, the direction of the cross flow tends to be from the center bundle to the peripheral bundle above the quench front, while the direction is reversed below the quench front with significant oscillation except for the location D for high Acc and LPCI test. Since the core inlet mass velocity in the LPCI injection period was about 40 kg/m<sup>2</sup>s and 74 kg/m<sup>2</sup>s for base case and high Acc and LPCI tests, respectively, almost the same amount of mass velocity was able to flow horizontally at the middle elevations. These results indicate the existence of the flow circulation in the core and the possibility of the increase of liquid flow rate along the axial direction. Thus, the quantitative dif-

ference of the factor  $f$  between SCTF data and the correlation from the small scale reflood test data mentioned before is supposed to be related to the underestimation of the amount of the axial liquid flow rate.

#### 4. Summary and Conclusions

The present evaluation study on SCTF tests revealed the following facts concerning the effects of the core inlet water mass flow rate ( $M_i$ ) on the reflooding phenomena. The ranges of core inlet flooding velocity examined in this report were as follows, 6.6 to 12.0cm/s in the Acc injection period and 2.1 to 7.8cm/s in the LPCI one.

##### [1] Hydraulic behavior including two-dimensional behavior

- (1) Larger  $M_i$  gave larger water accumulation rate in the core and in the upper plenum.
- (2) Larger  $M_i$  gave larger core mass effluent rate, larger carry-over water mass flow rate into the steam/water separator and earlier initiation time of carry-over into the steam/water separator
- (3) The distribution of core full height differential pressures was almost uniform throughout the entire width of the core irrespective of  $M_i$ . This indicates the existence of cross flow between bundles which compensates the effect of difference of steam generation rate due to the different bundle power on the void fraction. This characteristic has been also observed in the other SCTF test under a steeper radial power profile.
- (4) The distribution of sectional void fraction was almost uniform at the top region of the core irrespective of  $M_i$ , and the intensity of cross flow was determined by the degree of difference of water head in the upper plenum. The degree of that difference was not affected by  $M_i$  for core inlet flooding velocities greater than 6.6cm/s(Acc) and 4.1cm/s(LPCI).
- (5) At the middle region of the core, the cross flow was occurred from the higher power bundle to the lower one mainly above the quench front and the direction was reversed after passing the quench front or after the time of whole core quench. The maximum intensity of the cross flow was not affected by  $M_i$  and the distribution of sectional void fraction at this region was almost uniform except for high Acc(12.0cm/s) and LPCI(7.8cm/s) test. In that test the slightly larger intensity of cross flow from the highest to the lowest power bundles was realized until about the whole core quench time than the other tests and after the quench the intensity of cross flow was slightly smaller than the other tests.

(6) After about the time of whole core quench, the water fall back through the end box tie plate was realized into the bundles near hot leg for all the tests in this report and this fall back water might increase the water cross flow at the top region of the core due to the cross flow mentioned in the above item [1]~(4).

[2] Thermal behavior including two-dimensional behavior

- (1) Larger  $M_i$  gave shorter quench time, almost the same quench temperature and smaller temperature rise. Larger  $M_i$  only in the Acc injection period gave the same tendency of better core cooling even in the LPCI injection period. This was realized by the larger amount of water accumulation in the core even in the LPCI injection period.
- (2) No significant influence of  $M_i$  was observed on the two-dimensional heat transfer characteristics among the bundles. Namely, the heat transfer coefficients were always larger at the higher power bundles and the differences of heat transfer coefficients between at the higher power and at the lower power bundles were almost the same irrespective of  $M_i$ .
- (3) The dependency of the heat transfer coefficients on  $M_i$  was qualitatively consistent with modified Murao-Sugimoto correlation which includes the correction factor of liquid flow rate. The correlation slightly underestimated the heat transfer coefficients quantitatively. The cause of the underestimation was discussed by evaluating the flow circulation in the core.

Acknowledgement

The authors are much indebted to Drs. K. Sato, T. Shimooke and Y. Murao for their guidance and encouragement for this program.

They would like to express their appreciation to Drs. Y. Sudo, M. Sobajima, M. Osakabe and Mr. Y. Abe and to Messrs. T. Iguchi, J. Sugimoto, T. Okubo and Dr. H. Akimoto of CCTF analysis group for their useful discussions.

## References

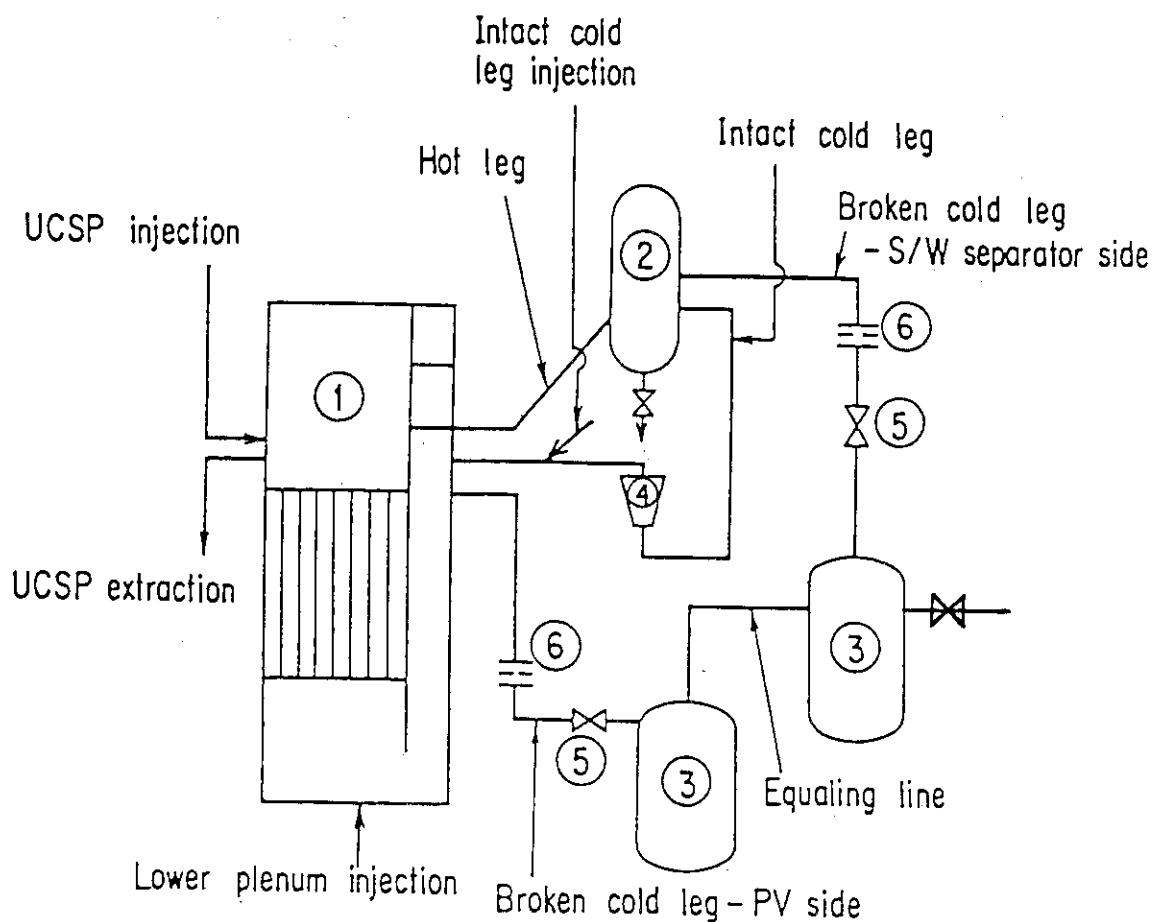
- (1) H. Adachi, et al., System Pressure Effects on Reflooding Phenomena observed in the SCTF Core-I Forced Flooding Tests, JAERI-M 83-079, (1983).
- (2) Y. Sudo, et al., Effect of Upper Plenum Water Accumulation on Reflooding Phenomena under Forced Flooding in SCTF Core-I Test, JAERI-M 83-114, (1983).
- (3) T. Iwamura, et al., Effects of Core Inlet Water Subcooling on Reflooding Phenomena -- SCTF Core-I Forced Feed Flooding Test --, JAERI-M 83-122, (1983).
- (4) M. Sobajima, et al., Examination of Repeatability in Reflood Phenomena under Forced Flooding in SCTF Core-I Tests, JAERI-M 83-237, (1984).
- (5) For instance, N. Lee, et al., NURGE/CR-2256, (1981).
- (6) T. Iwamura, et al., Effects of Radial Core Power Profile on Core Thermo-Hydraulic Behavior during Reflood Phase in PWR-LOCA, J. Nucl. Sci. Tech., Vol.20, No.9, pp.743~751, 1983.
- (7) T. Iwamura, et al., Two-Dimensional Thermal-Hydraulic Behavior In Core In SCTF Core-II Cold Leg Injection Tests (Radial Power Profile Test Results), JAERI-M 85-106, (1985).
- (8) H. Adachi, et al., Design of Slab Core Test Facility (SCTF) in Large Scale Reflood Test Program, Part I : Core-I, JAERI-M 83-080, (1983).
- (9) J. Sugimoto, et al., Experimental Study of Effect of Initial Clad Temperature on Reflood Phenomena during PWR-LOCA, J. Nucl. Sci. Tech., Vol.20, No.8, pp.656~667, 1983.
- (10) M. Osakabe, et al., Heat Transfer Calculation of Simulated Heater Rods throughout Reflood Phase in Postulated PWR-LOCA Experiments, J. Nucl. Sci. Tech., Vol.20, No.7, pp.559~570, 1983.
- (11) Y. Murao, et al., Correlation of Heat Transfer Coefficient for Saturated Film Boiling during Reflood Phase Prior to Quenching, J. Nucl. Sci. Tech., Vol.18, No.4, pp.275~284, 1981.
- (12) H. Akimoto, et al., Core Radial Power Profile Effect on System and Core Cooling Behavior during Reflood Phase of PWR-LOCA with CCTF Data, J. Nucl. Sci. Tech., Vol.22, No.7, pp.538~550, 1985.
- (13) A. Ohnuki, et al., to be published.
- (14) C.W. Stewart, et al., COBRA-IV, The model and the method, BNWL-2214, (1977).

Table 2-1 List of Major Measured Test Conditions

Test No.	Objective	Initial pressure (MPa)	Max. rod surface temp. at BOCREC (K) - T <sub>b</sub> -	ECC water injection rate (kg/s)		Max. core inlet water subcooling (K)	Decay curve	Radial power ratio			
				Acc max.	LPCI			Bundles 1 & 2	Bundles 3 & 4	Bundles 5 & 6	Bundles 7 & 8
S1-01	Base case	0.195	970	22	11.4						
S1-SH1	High Acc injection rate and Low T <sub>b</sub>	0.200	873	40	11.1	19.0	ANS+Actinides +D.N. from 30S from scram	1.001	1.065	1.015	0.919
S1-05	Low LPCI injection rate	0.200	952	25	6	18.0	ANS+Actinides +D.N. from 30S from scram	1.001	1.065	1.015	0.919
S1-09	High Acc and LPCI inj. rate	0.201	961	45	19	22.0	ANS+Actinides +D.N. from 30S from scram	1.001	1.065	1.015	0.919

Table 2-2 Accuracy of Instruments

Item	Range	Accuracy	Error band
Heater rod temperature	273~1273 (K)	±1%	10 K
Fluid temperature	273~873 (K)	±1%	6K
Liquid level above UCSP	0~2.5 MAQ	±1%	0.025 MAQ
Liquid level above end box tie plate	0~0.25 MAQ	±1%	0.0025 MAQ
Differential pressure across core full height	-2~5 MAQ	±1%	0.07 MAQ
Differential pressure across end box tie plate	-0.5~0.5 MAQ	±1%	0.05 MAQ
Horizontal differential pressure between bundles 5 and 8	-0.2~0.2 MAQ	±1%	0.002 MAQ



- |                             |                                |
|-----------------------------|--------------------------------|
| (1) Pressure vessel         | (5) Break valves               |
| (2) Steam / water separator | (6) Flow resistance simulators |
| (3) Containment tanks       |                                |
| (4) Pump simulator          |                                |

Fig. 2-1 Schematic Diagram of Slab Core Test Facility

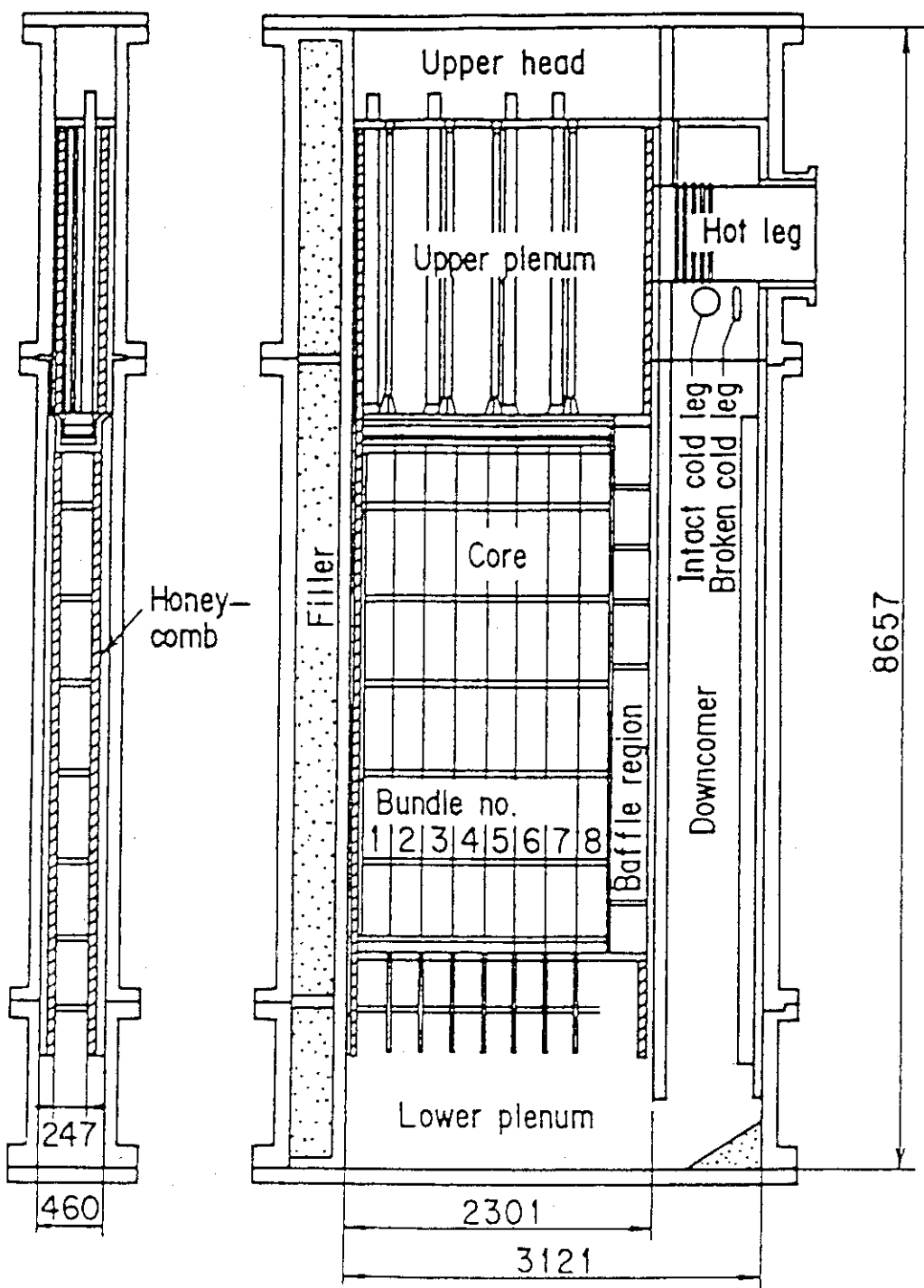


Fig. 2-2 Vertical Cross Section of Pressure Vessel

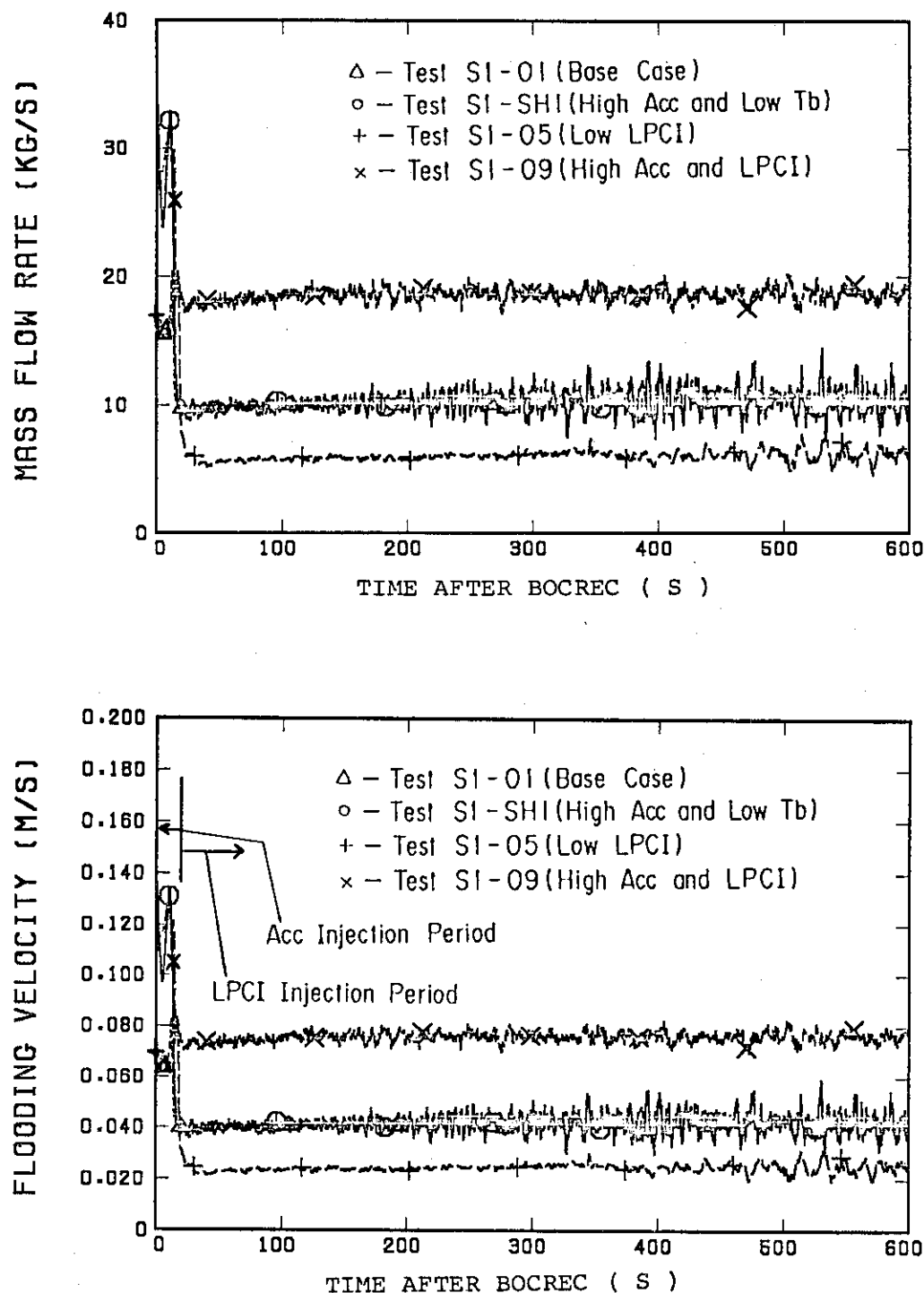


Fig. 2-3 Comparison of Core Inlet Water Flow Rate and Flooding Velocity

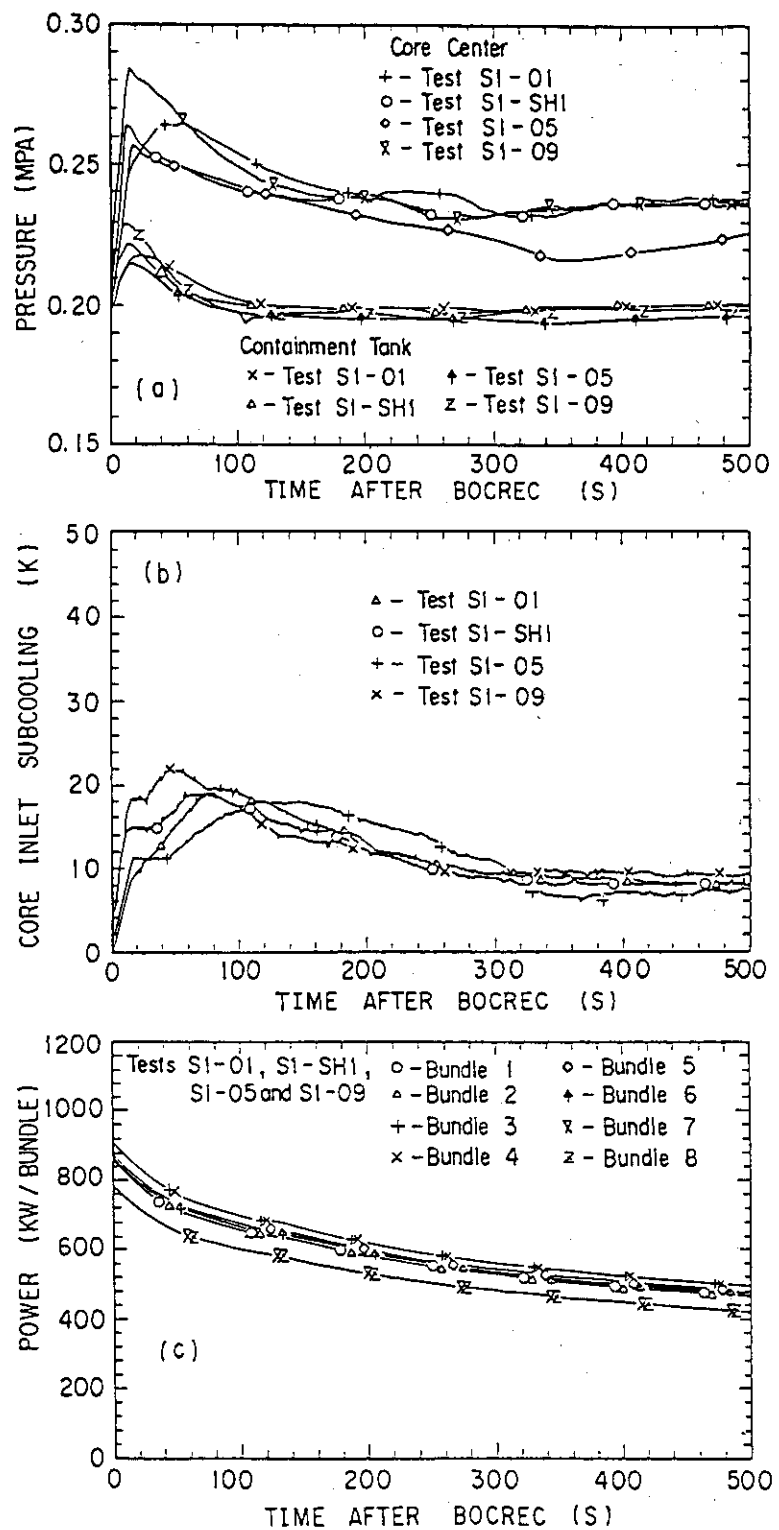


Fig. 2-4 Comparison of Pressure, Core Inlet Subcooling and Supplied Power

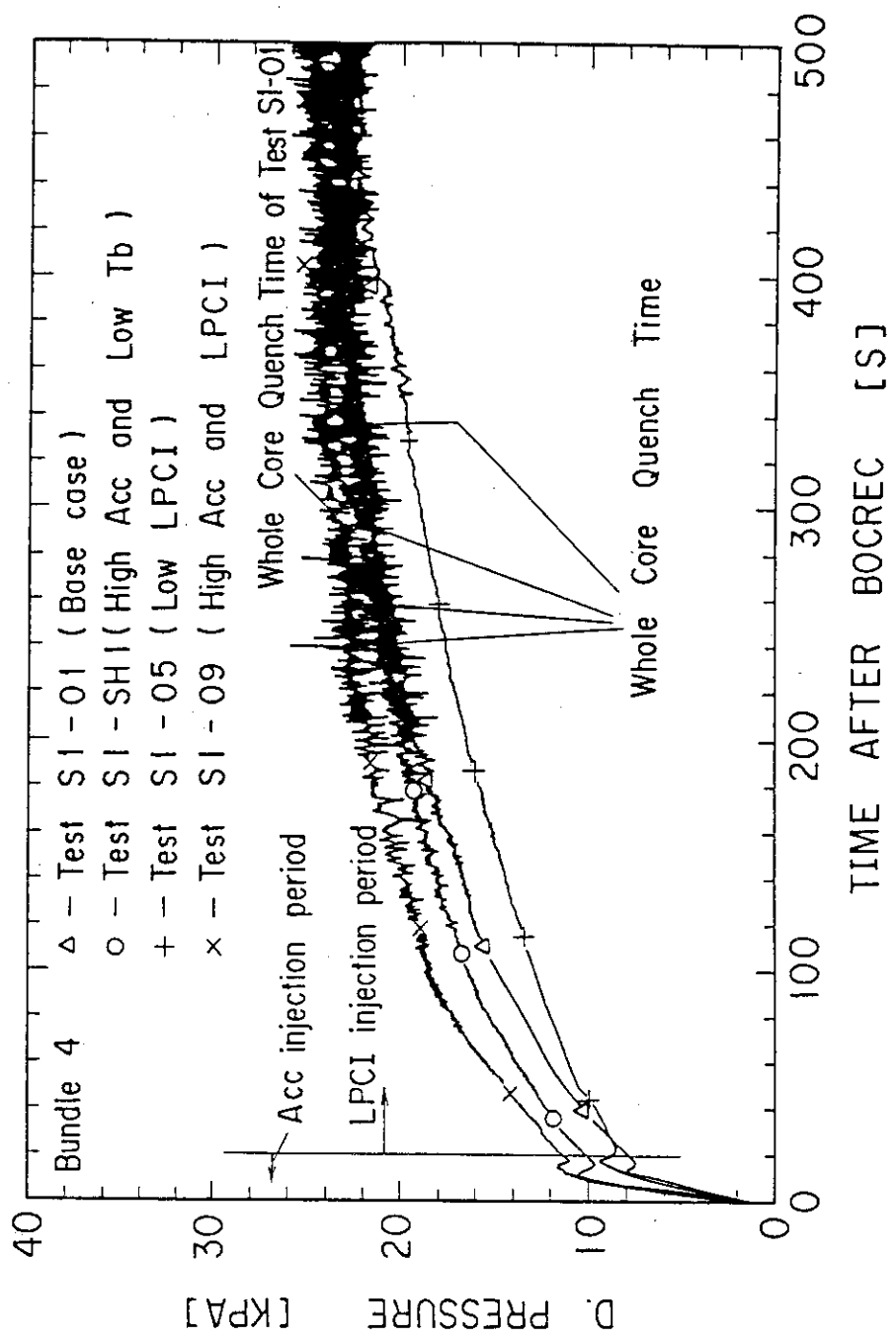


Fig. 3-1 Comparison of Core Full Height Differential Pressure in Bundle 4

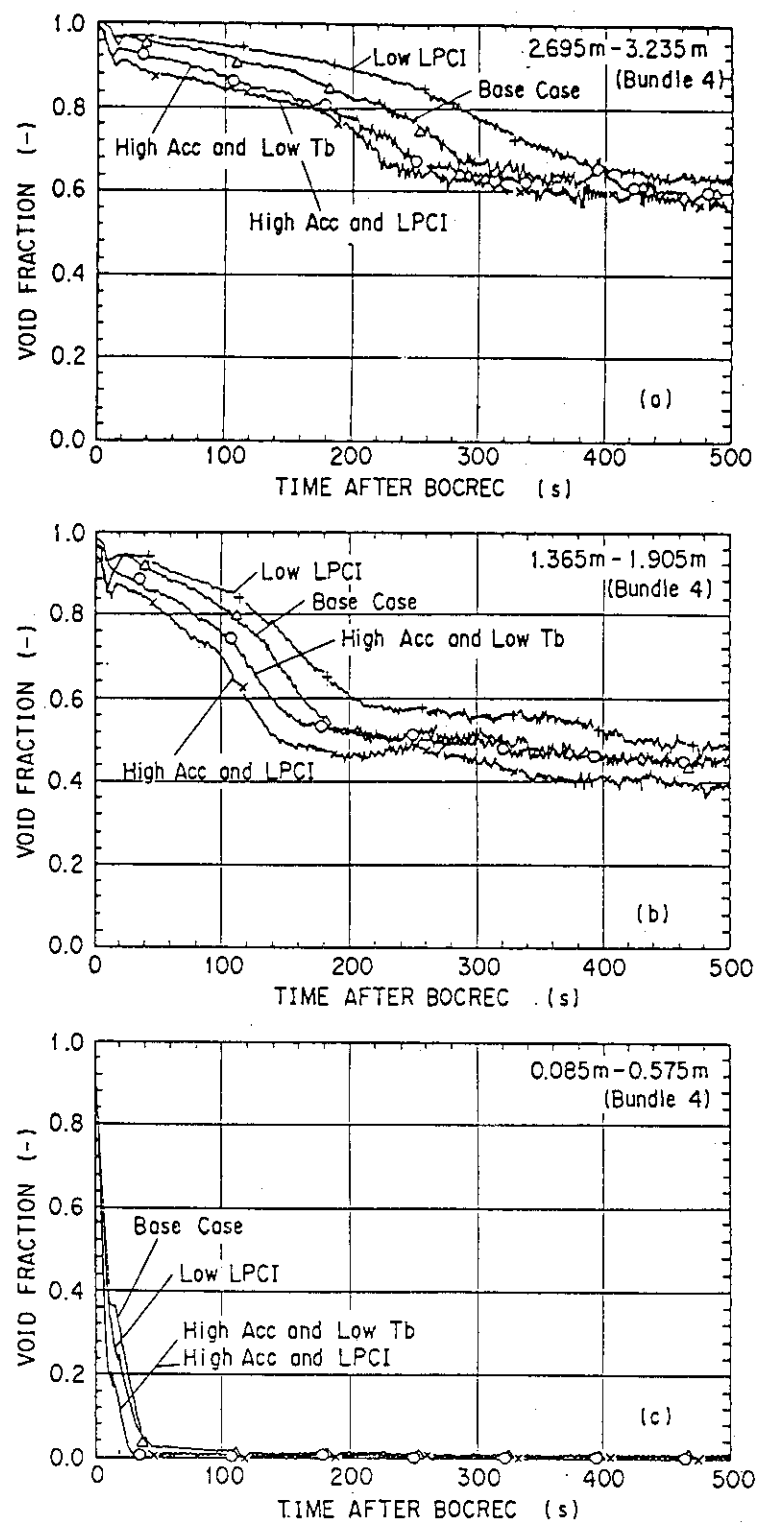


Fig. 3-2 Comparison of Sectional Void Fraction at Three Axial Regions in Bundle 4

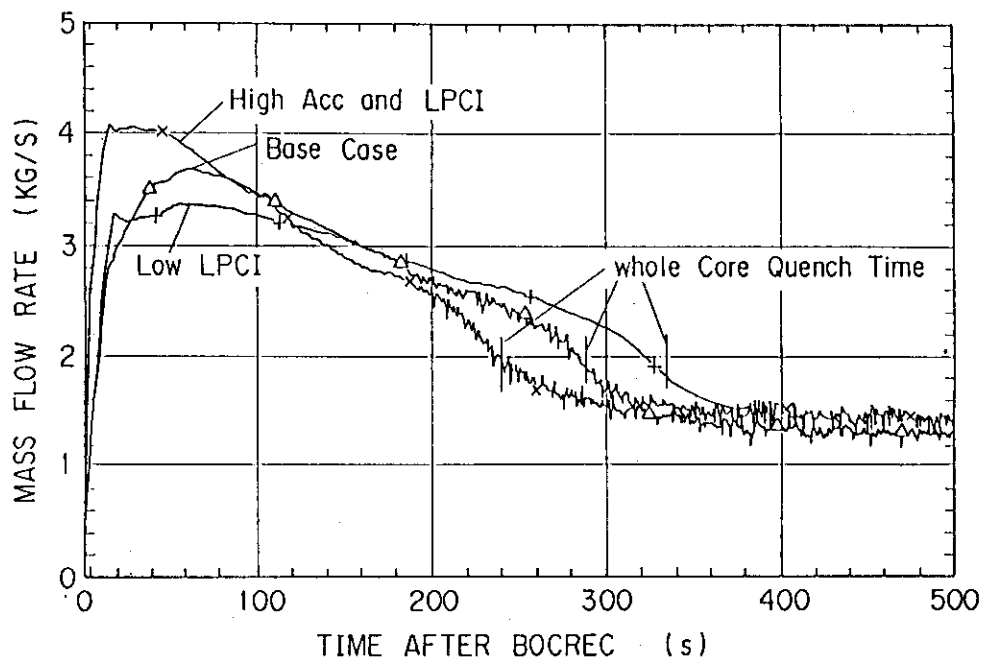


Fig. 3-3 Comparison of Steam Mass Flow Rate Generated in Core

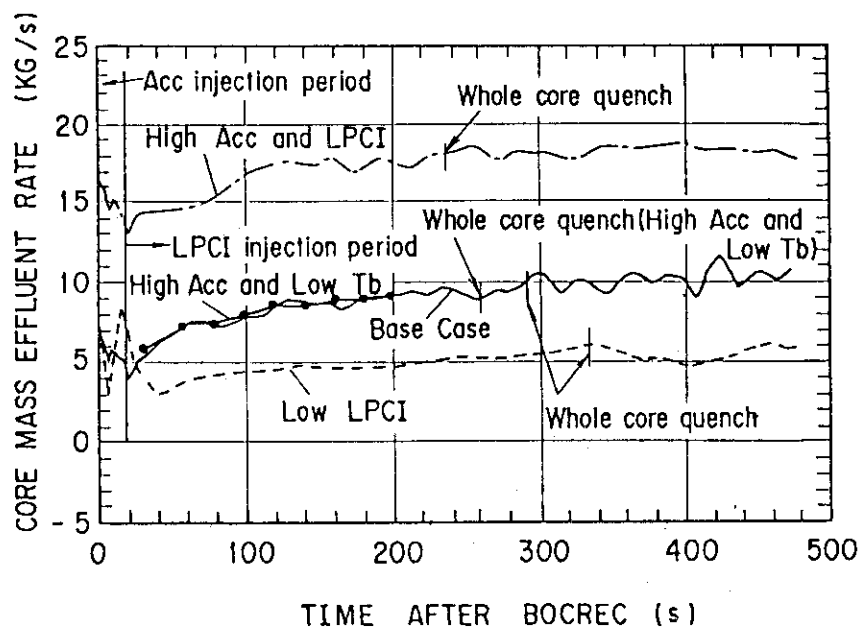


Fig. 3-4 Comparison of Core Mass Effluent Rate

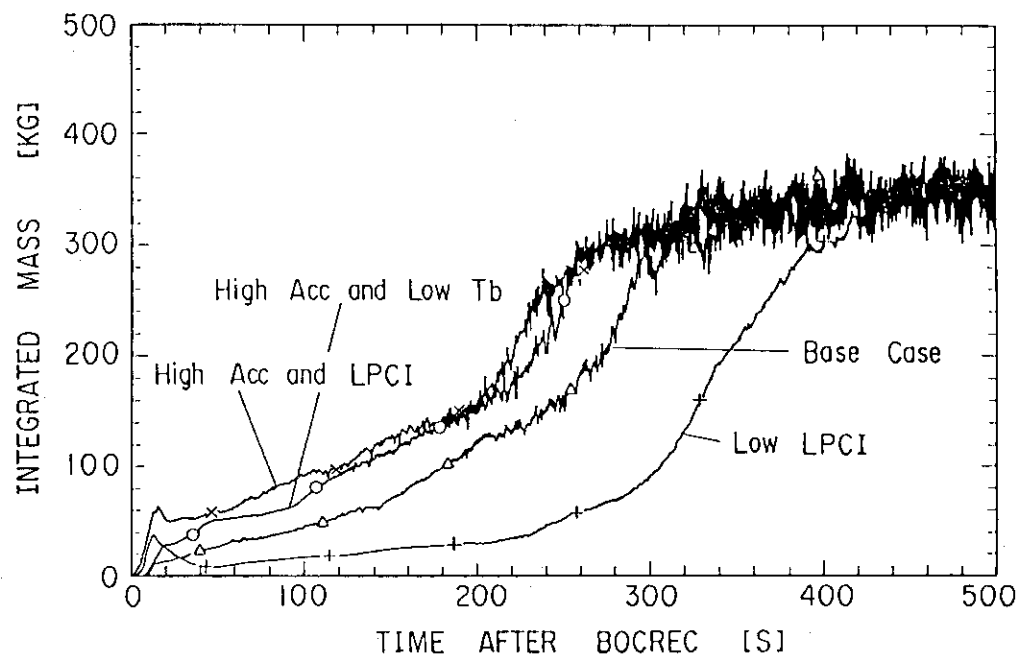


Fig. 3-5 Comparison of Water Mass in Upper Plenum

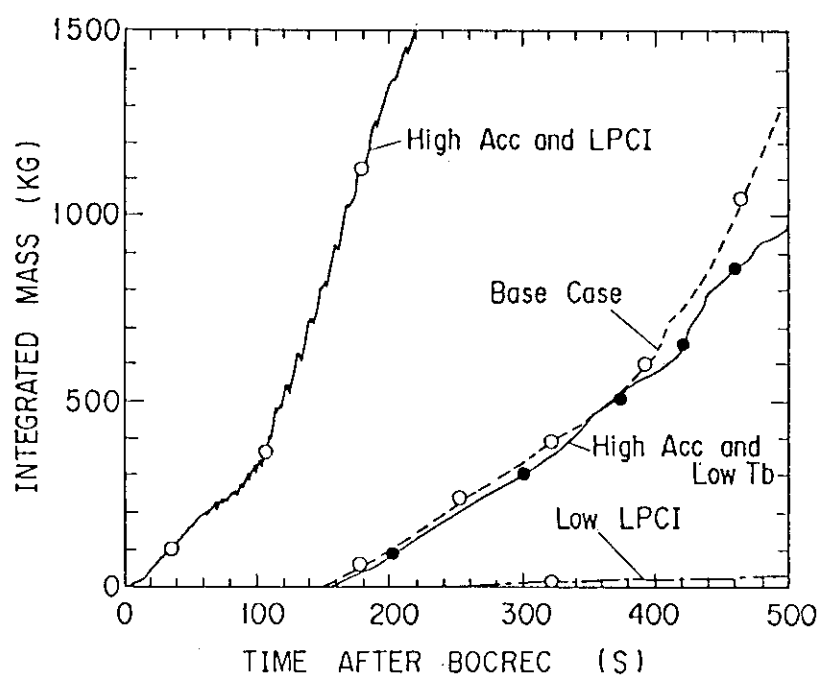


Fig. 3-6 Comparison of Water Mass in Steam/Water Separator

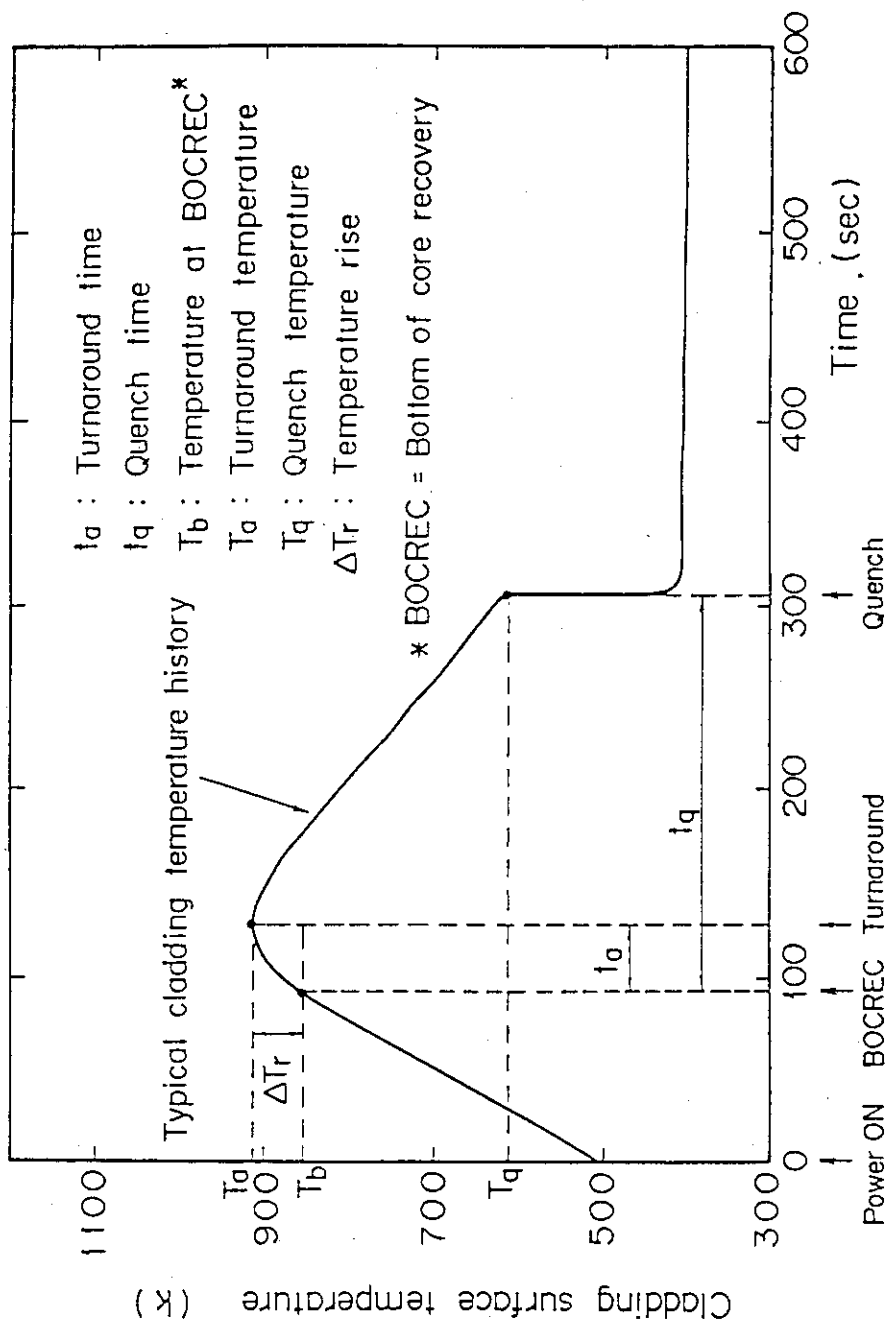


Fig. 3-7 Terminology : Cladding Temperature History

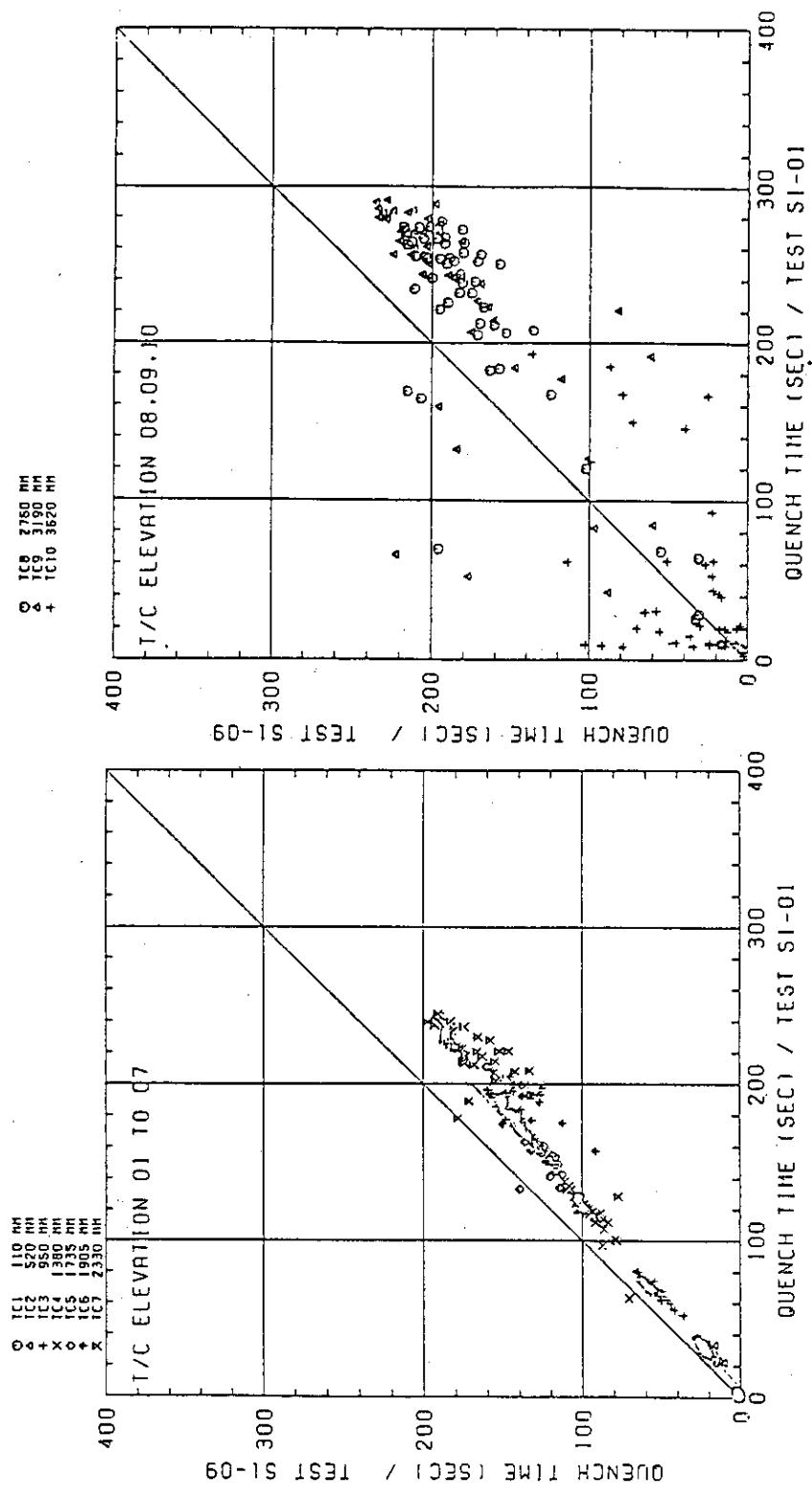


Fig. 3-8(1) Effect of Core Inlet Water Flow Rate on  $t_{q}$   
(Comparison of high Acc and LPCI test with base case test)

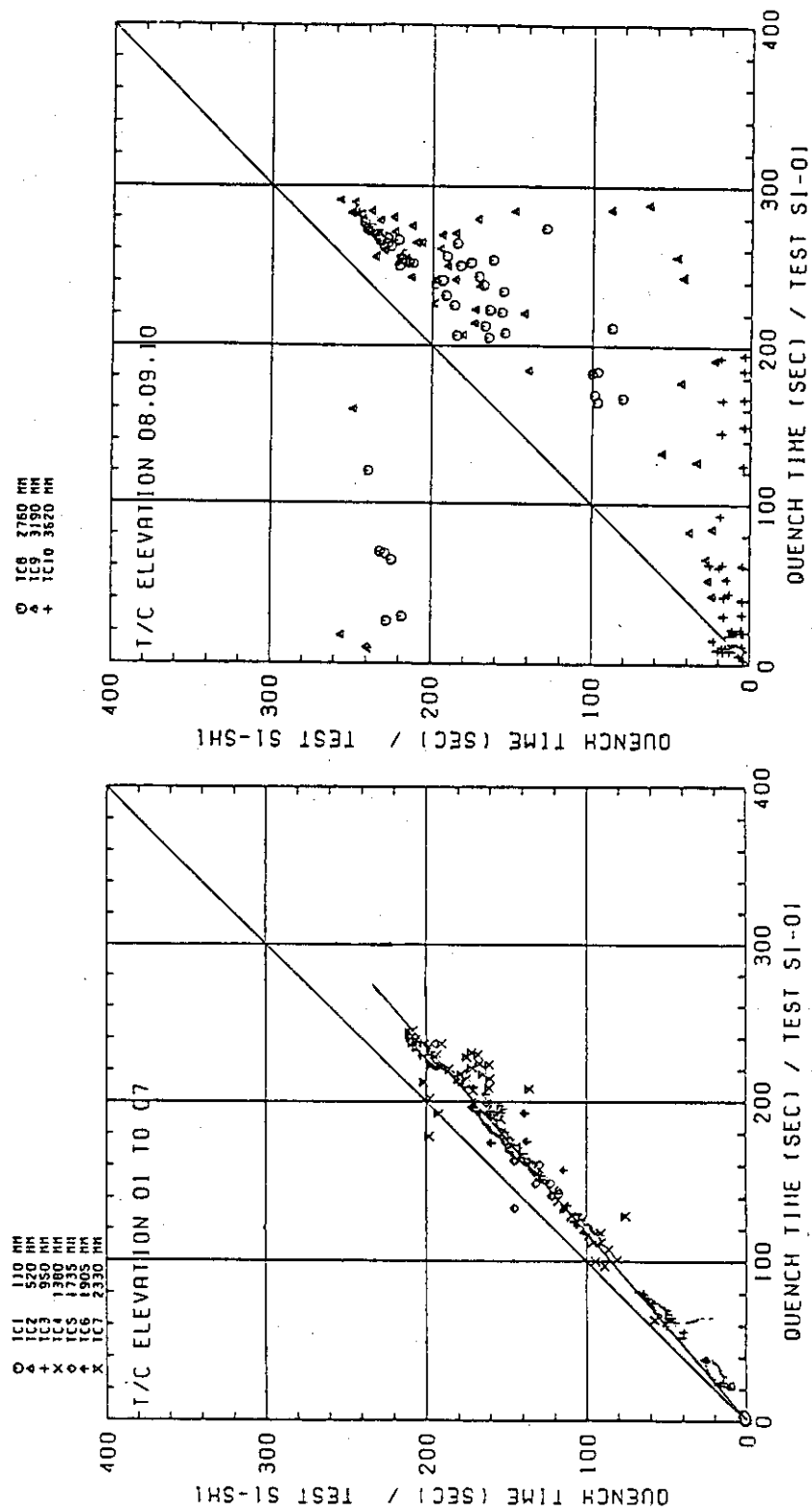


Fig. 3-8(2) Effect of Core Inlet Water Flow Rate on  $t_q$   
(Comparison of high Acc and low  $T_b$  test with base case test)

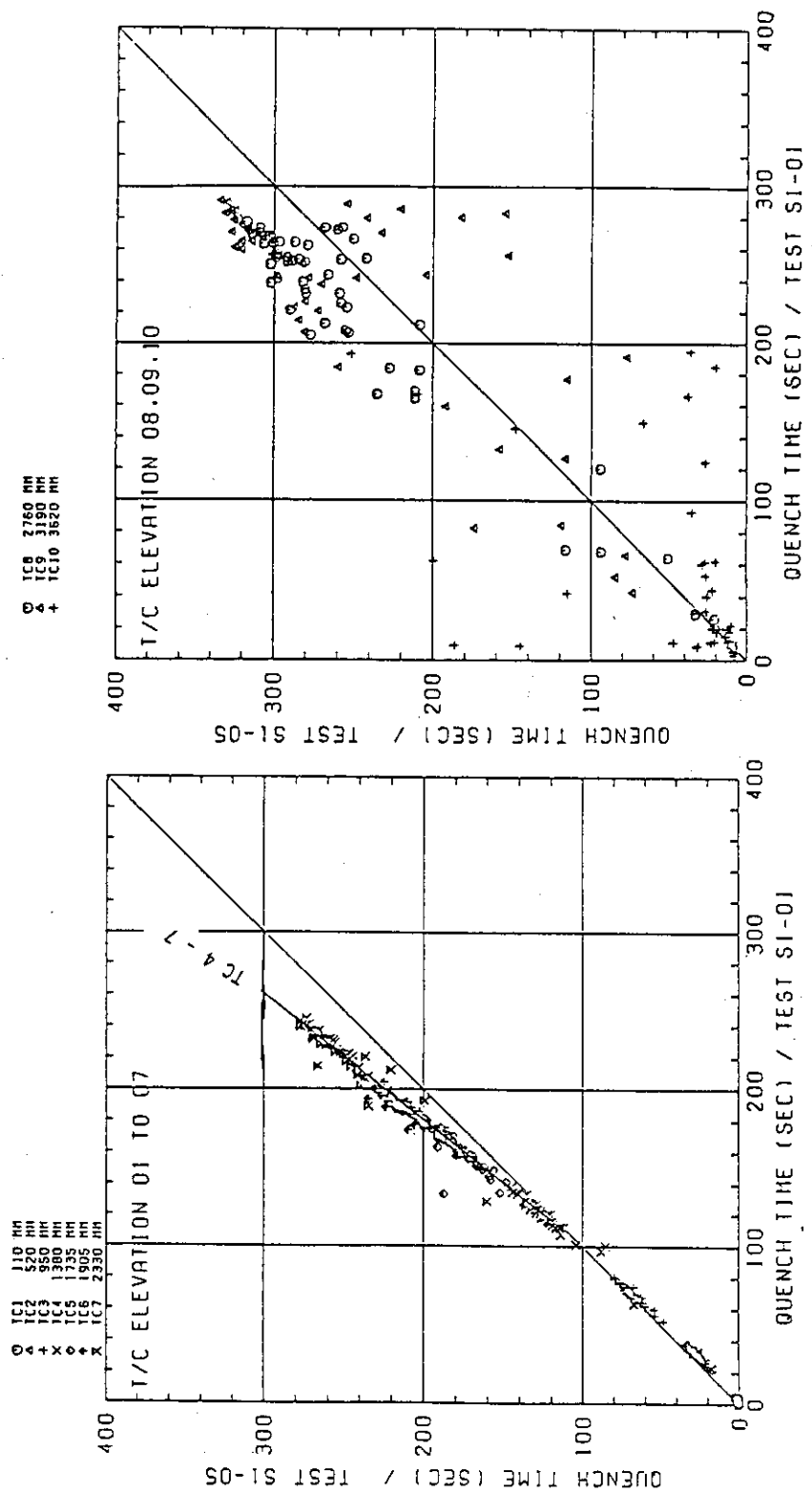


Fig. 3-8(3) Effect of Core Inlet Water Flow Rate on tq  
(Comparison of low LPCT test with base case test)

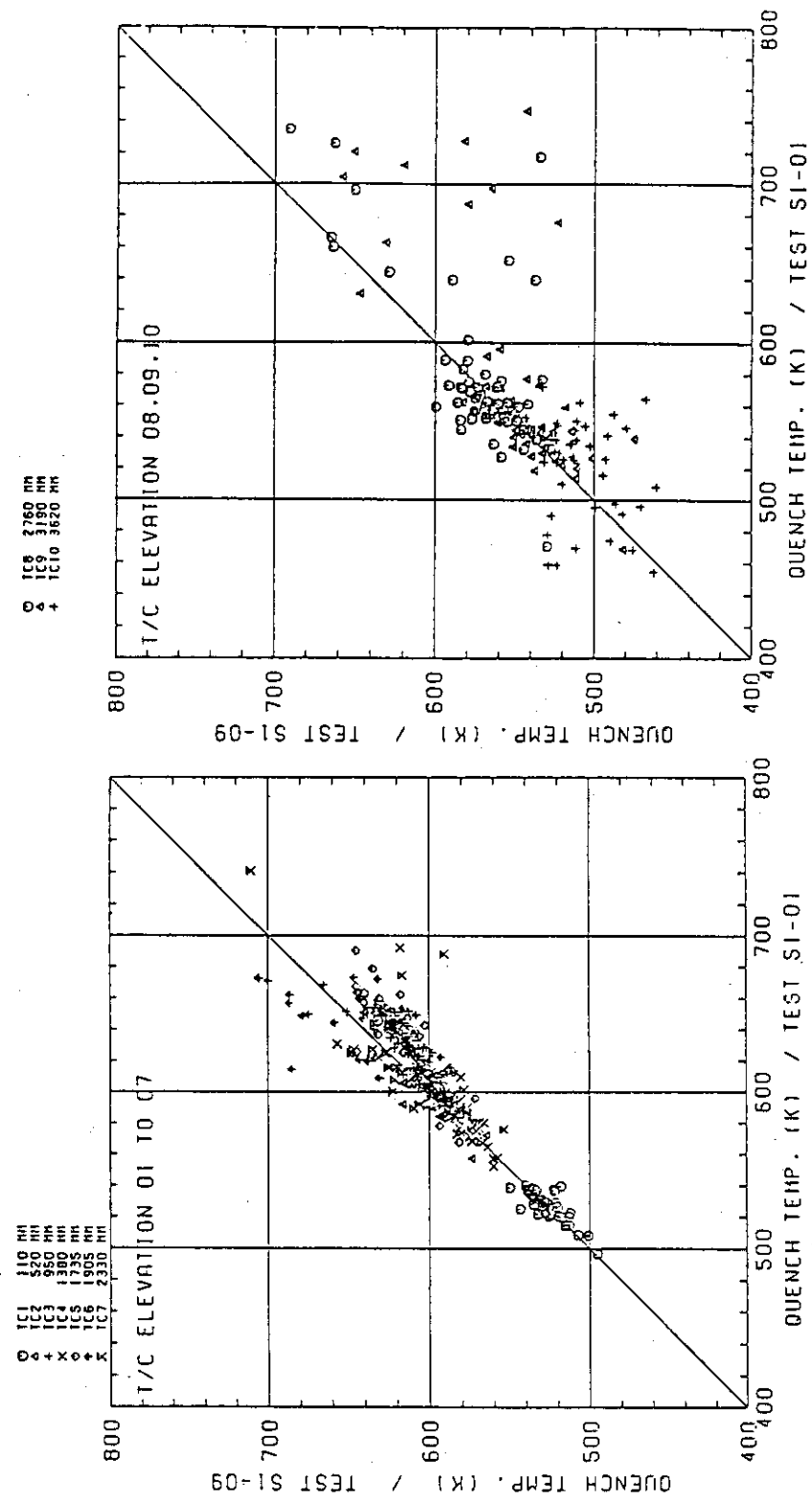


Fig. 3-9(1) Effect of Core Inlet Water Flow Rate on  $T_q$   
(Comparison of high Acc and LPCI test with base case test)

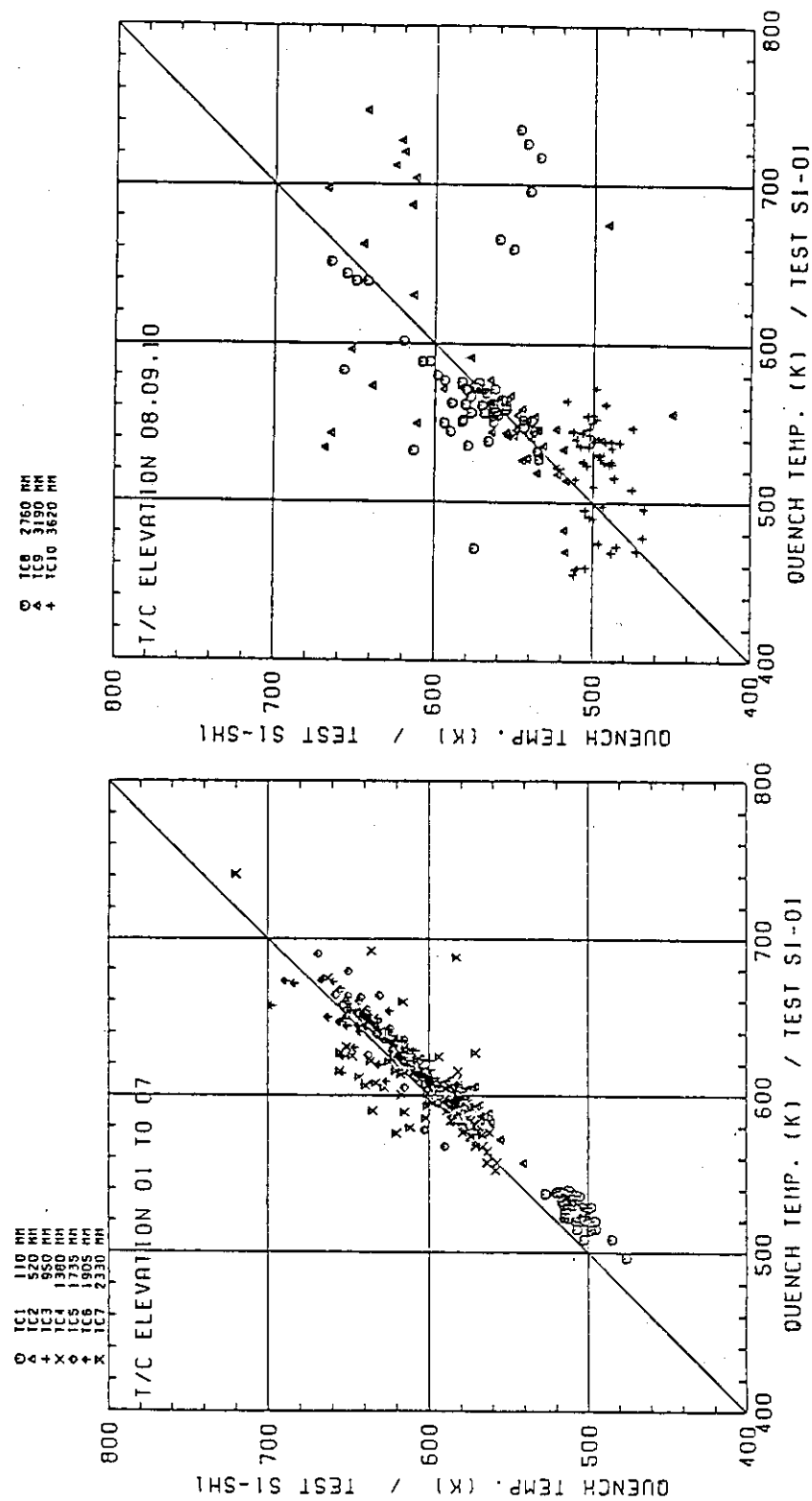


Fig. 3-9(2) Effect of Core Inlet Water Flow Rate on  $T_b$   
(Comparison of high Acc and low Tb test with base case test)

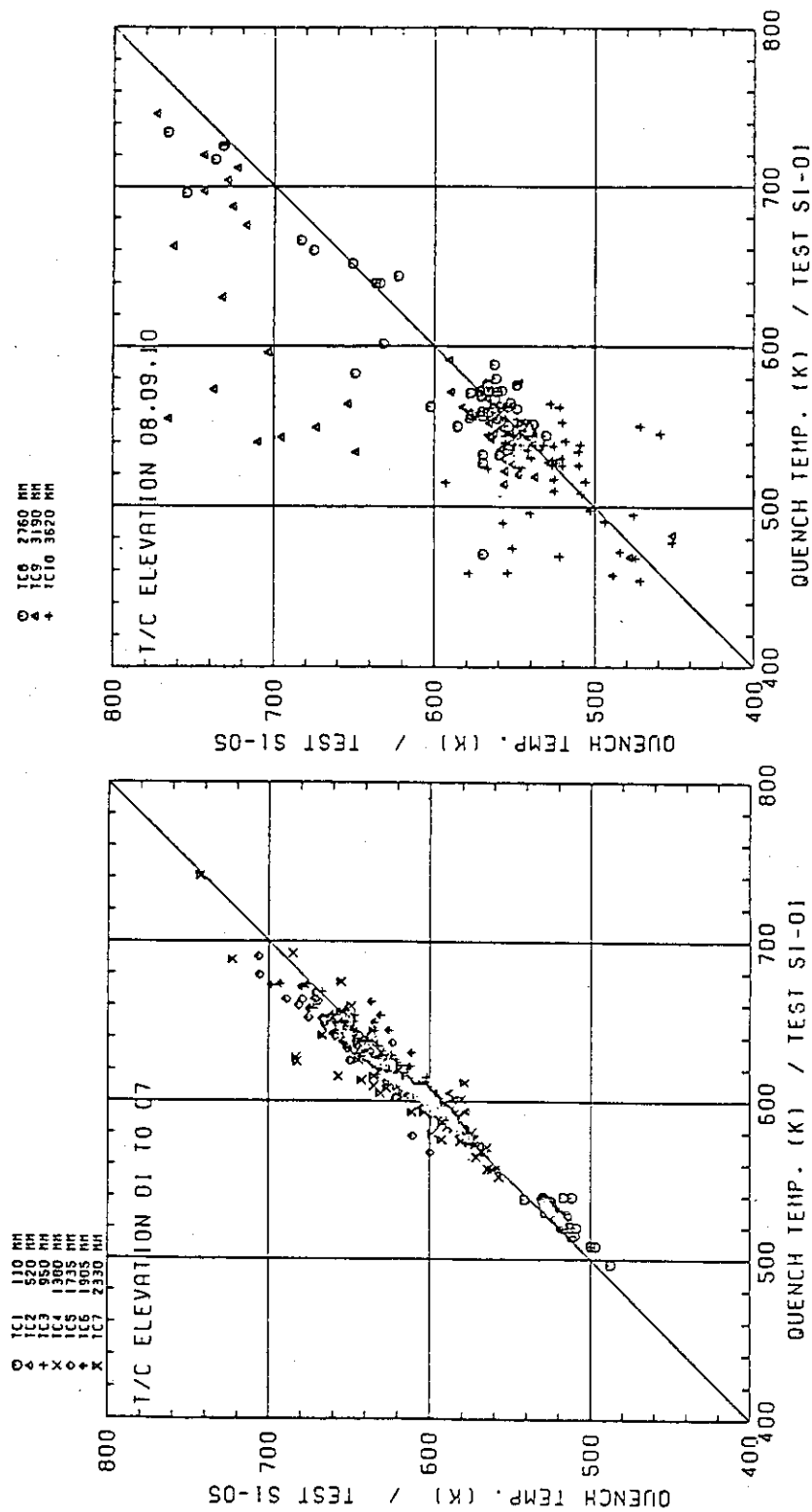


Fig. 3-9(3) Effect of Core Inlet Water Flow Rate on  $T_q$

(Comparison of low LPCI test with base case test)

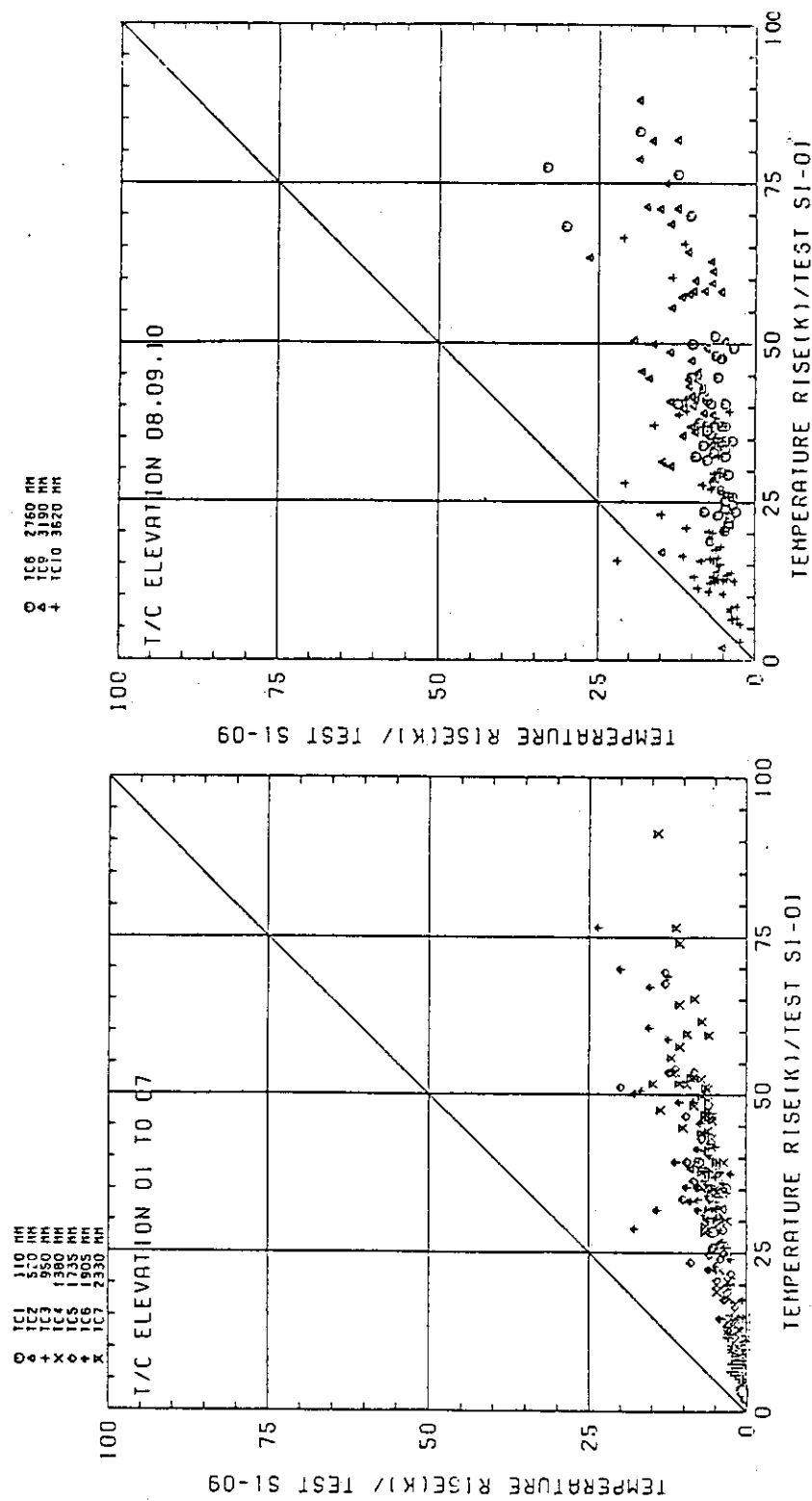


Fig. 3-10(1) Effect of Core Inlet Water Flow Rate on  $\Delta T_r$   
(Comparison of high Acc and LPCI test with base case test)

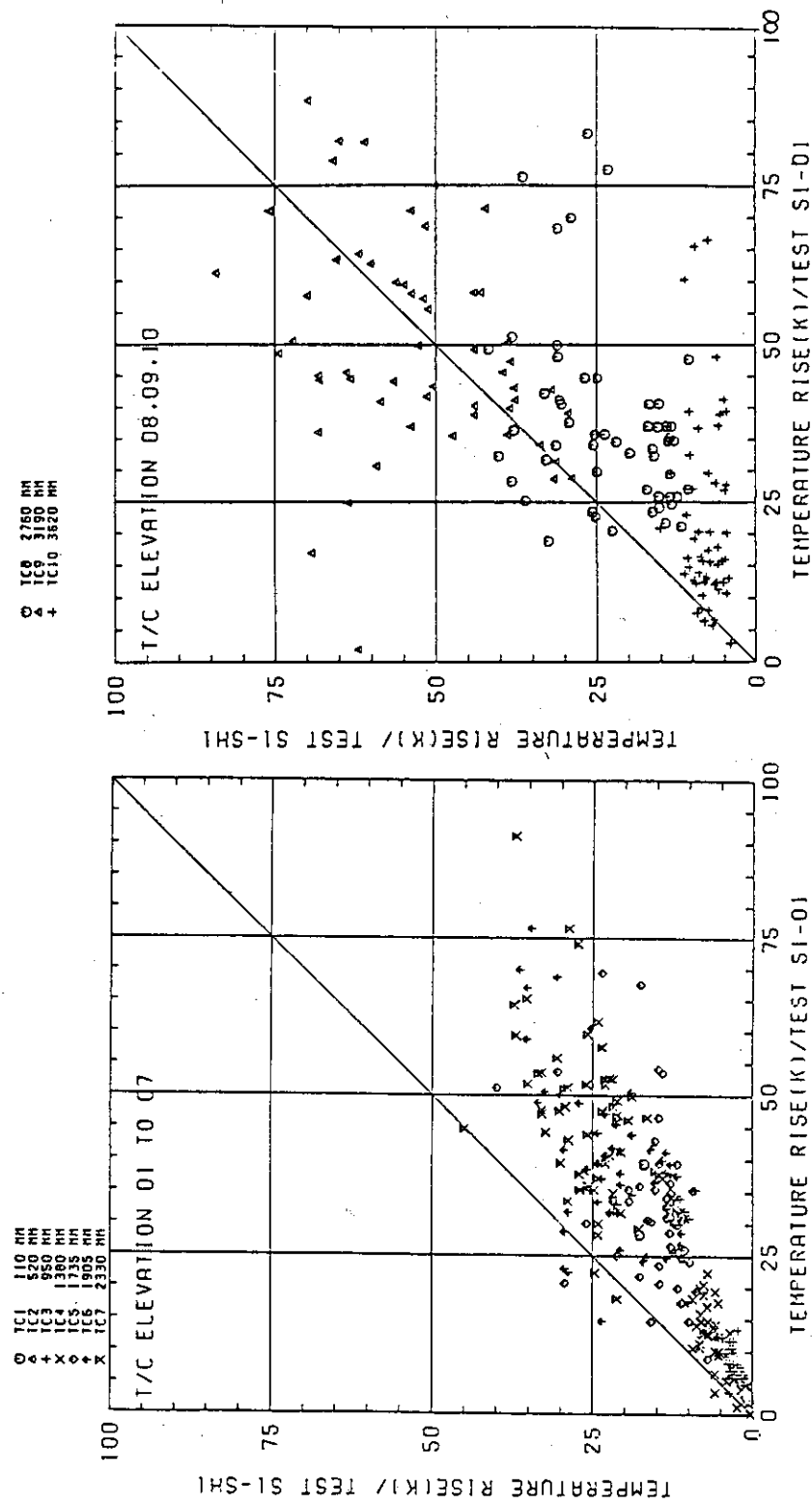


Fig. 3-10(2) Effect of Core Inlet Water Flow Rate on  $\Delta T_r$   
(Comparison of high Acc and low Tb test with base case test)

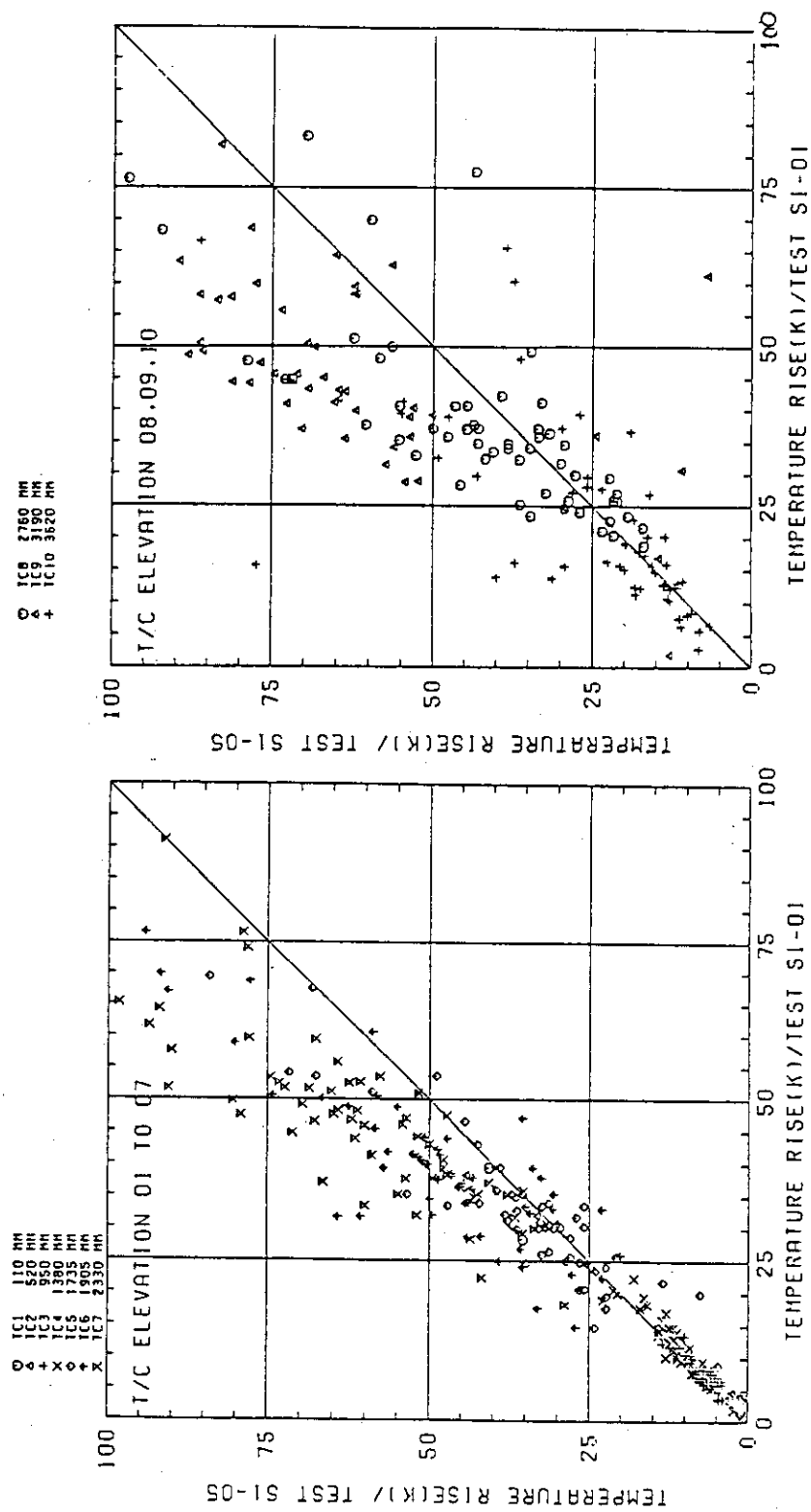


Fig. 3-10(3) Effect of Core Inlet Water Flow Rate on  $\Delta T_r$   
(Comparison of low LPCL test with base case test)

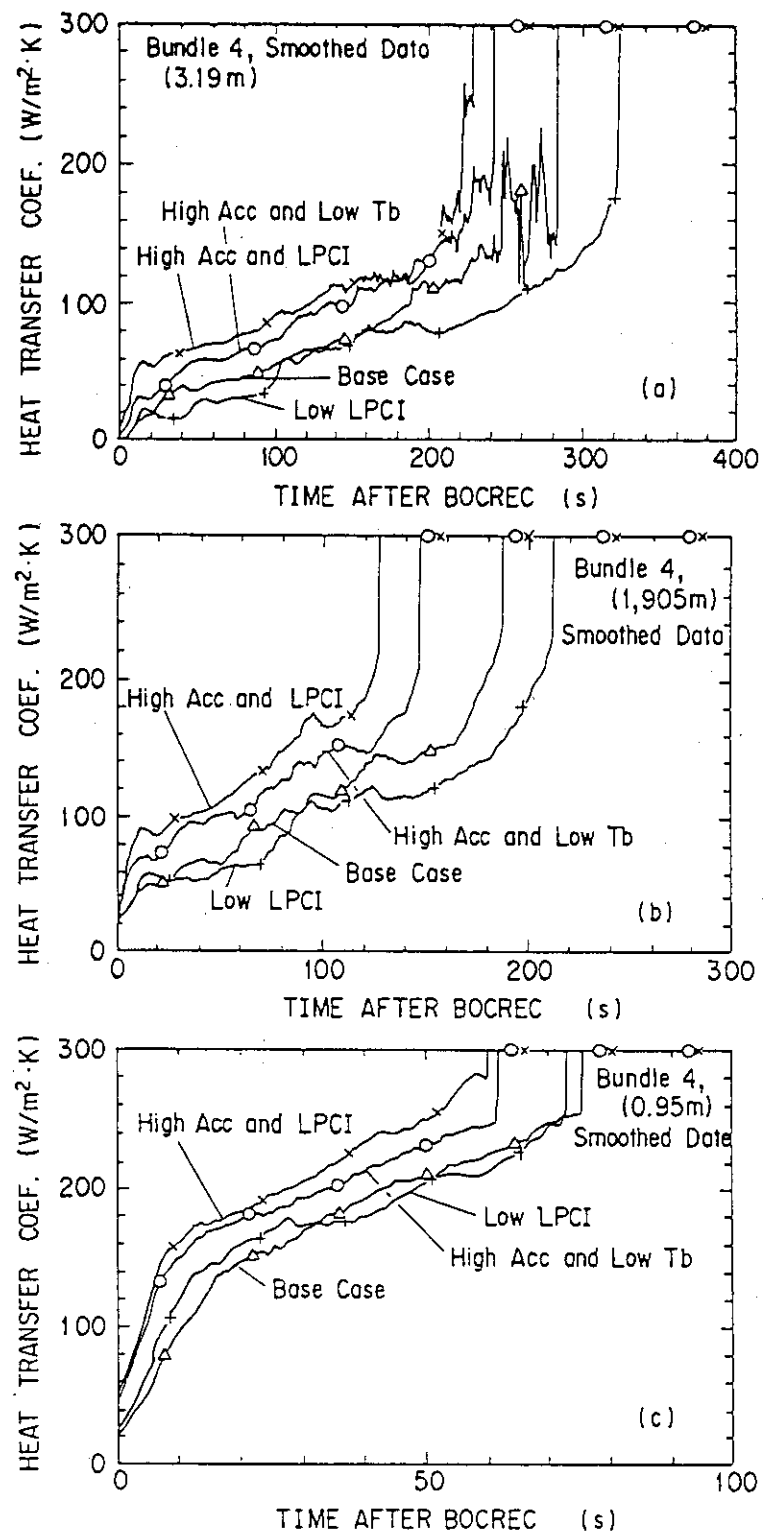


Fig. 3-11 Comparison of HTC at Three Axial Elevations in Bundle 4

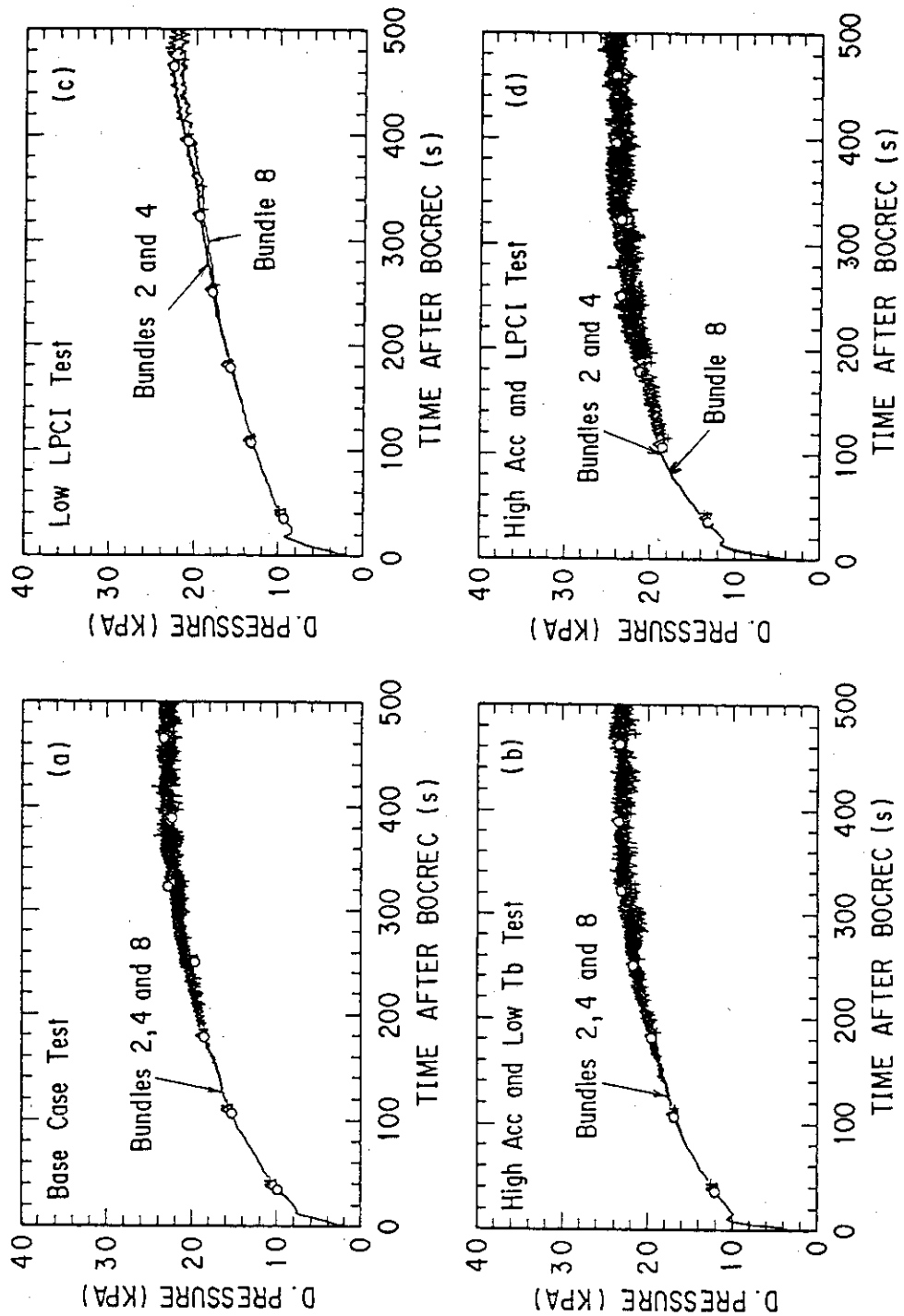


Fig. 3-12 Comparison of Core Full Height Differential Pressure in Bundles  
2, 4 and 8

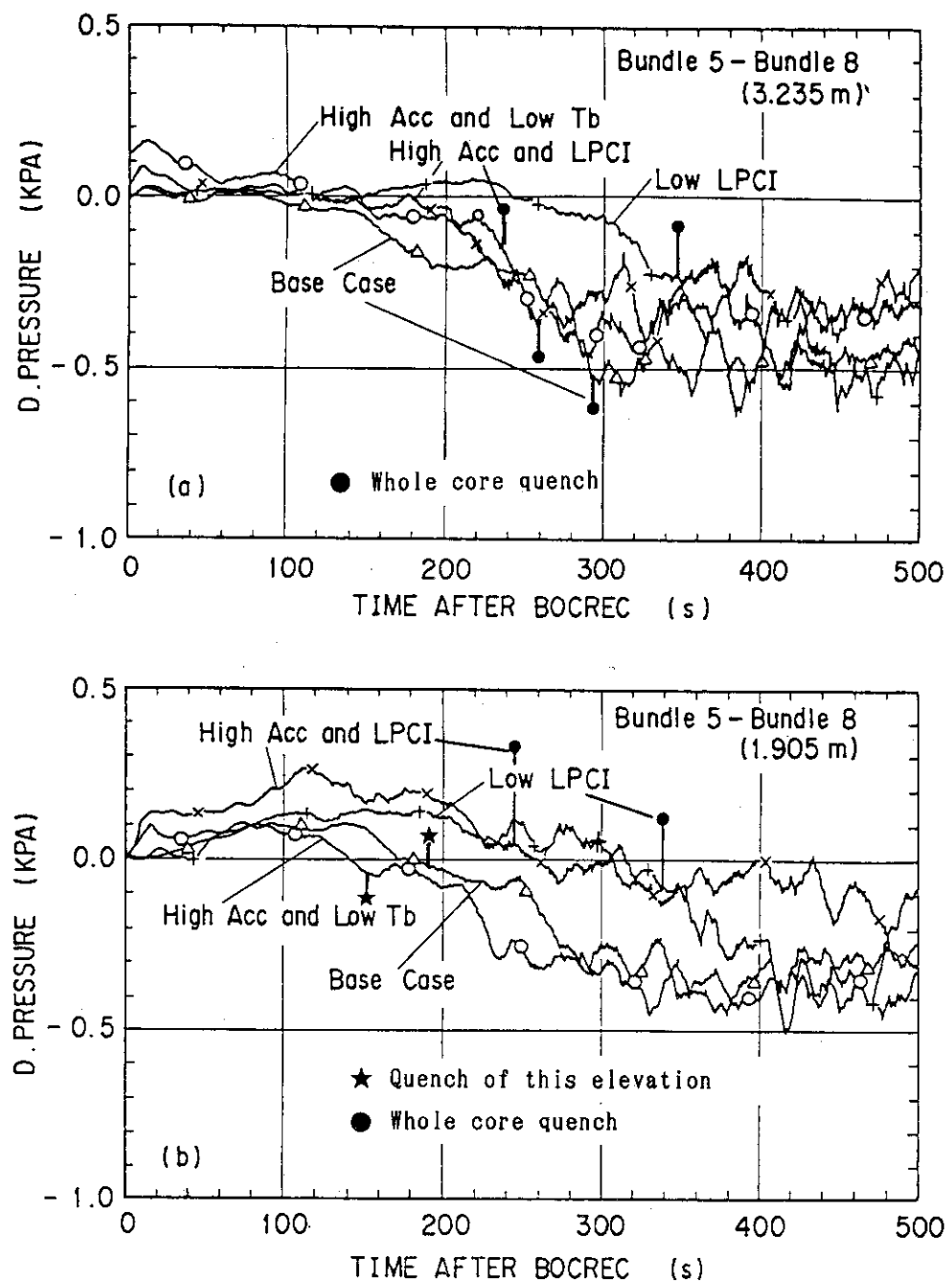


Fig. 3-13 Comparison of Horizontal Differential Pressure between Bundles 5 and 8 at 1.905m and 3.235m elevations

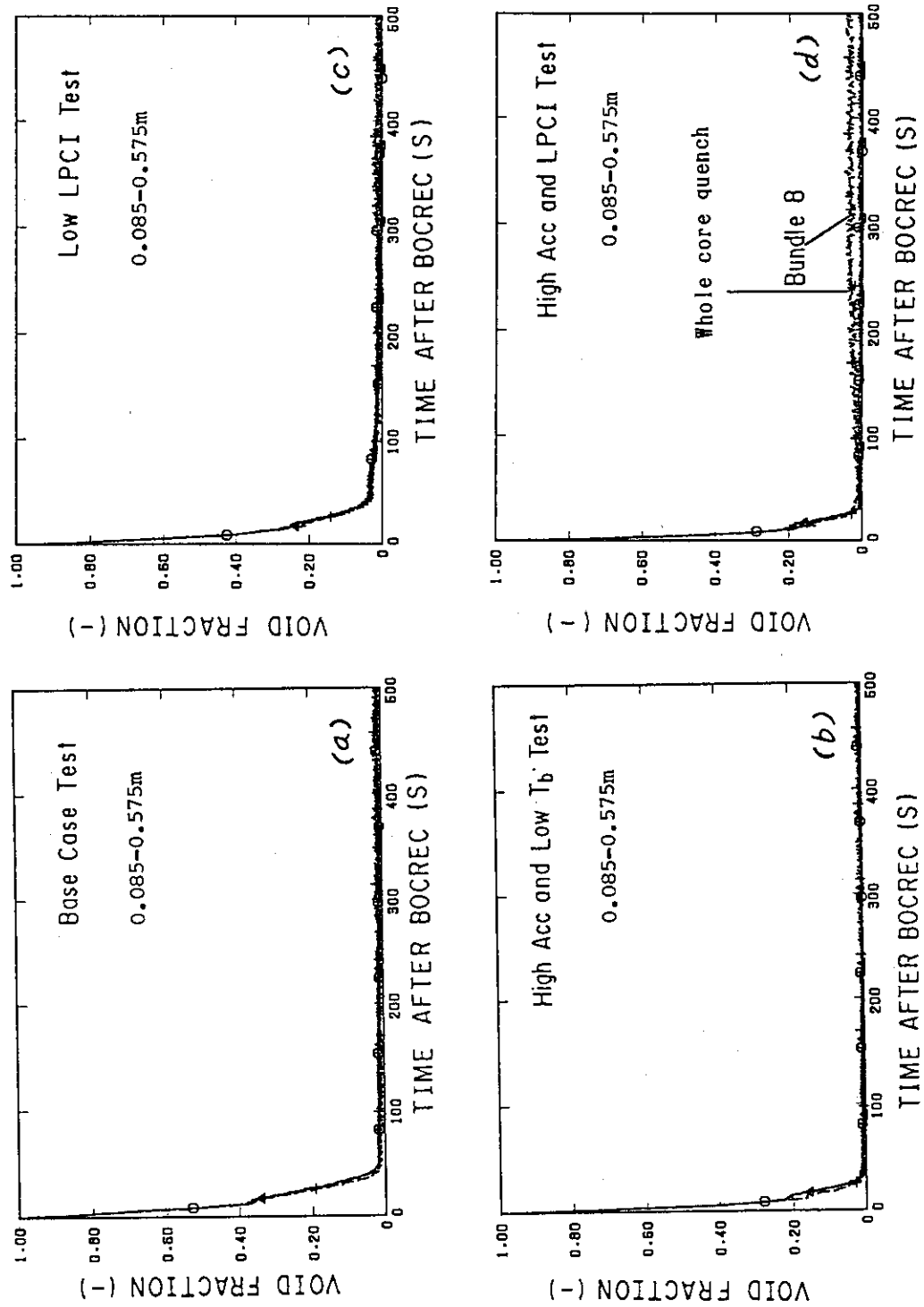


Fig. 3-14(1) Comparison of Sectional Void Fraction between 0.085m and 0.575m elevations in Bundles 2, 4 and 8

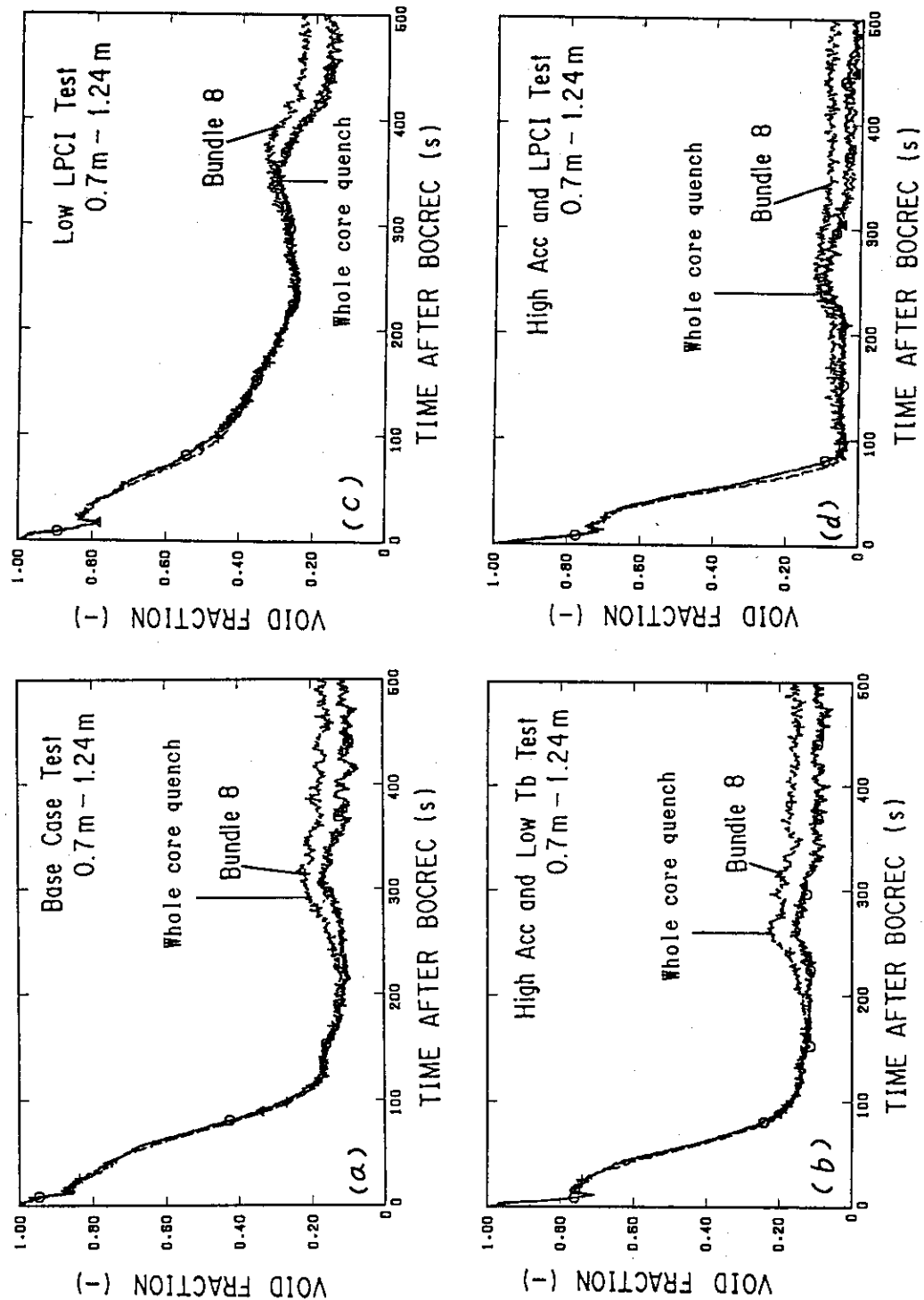


Fig. 3-14(2) Comparison of Sectional Void Fraction between 0.7m and 1.24m elevations in Bundles 2, 4 and 8

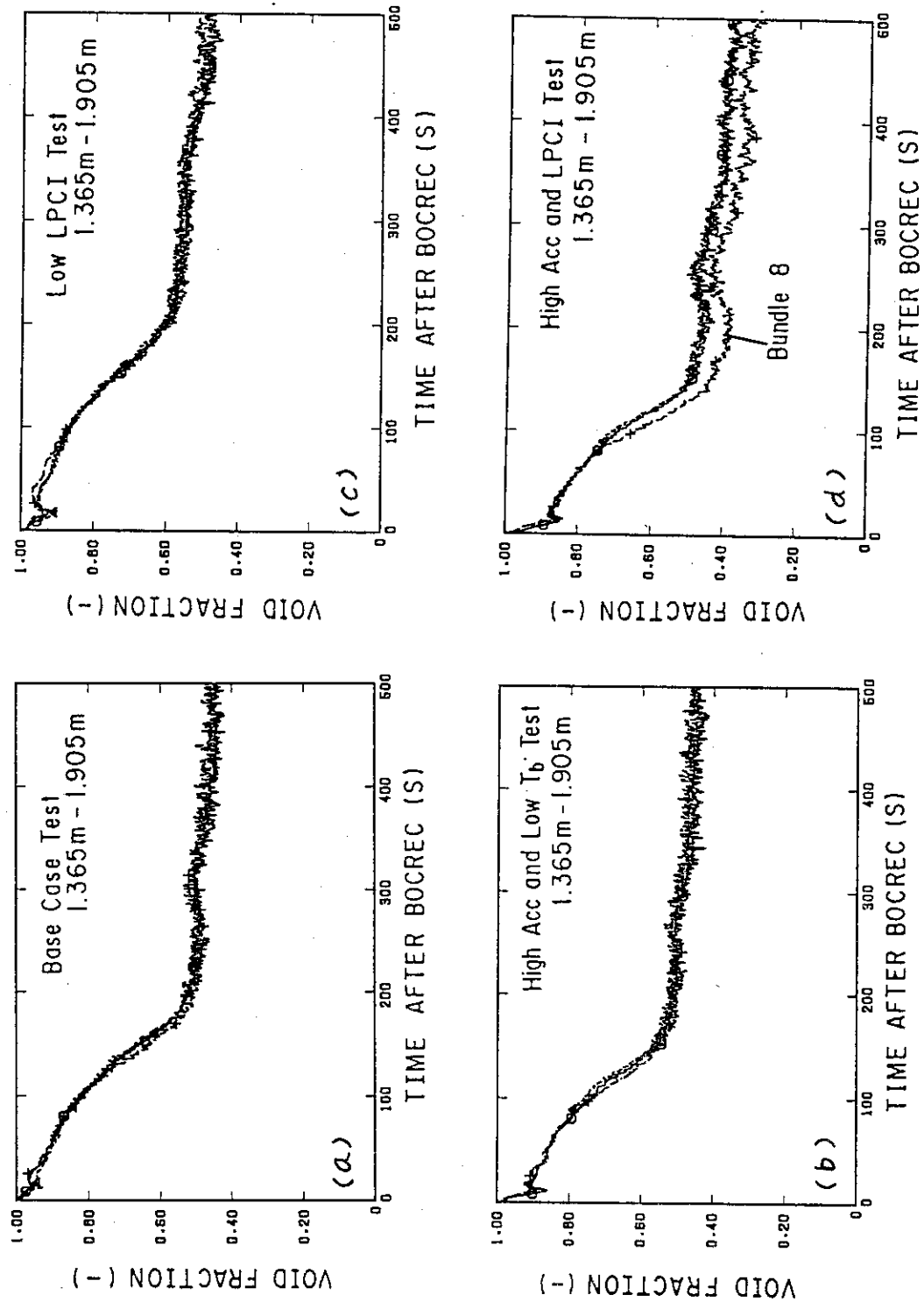


Fig. 3-14(3) Comparison of Sectional Void Fraction between 1.365m and 1.905m elevations in Bundles 2, 4 and 8

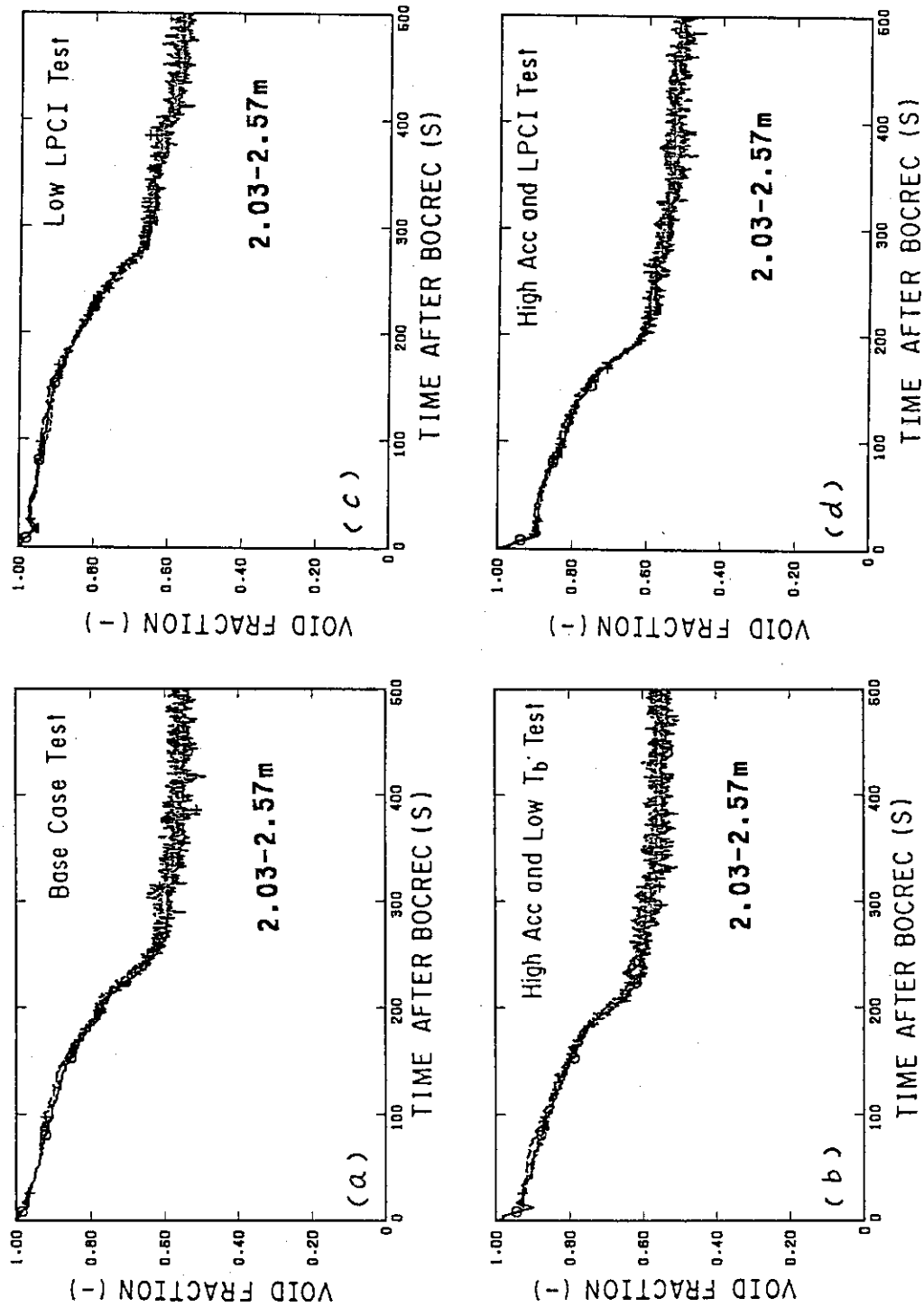


Fig. 3-14(4) Comparison of Sectional Void Fraction between 2.03m and 2.57m elevations in Bundles 2, 4 and 8

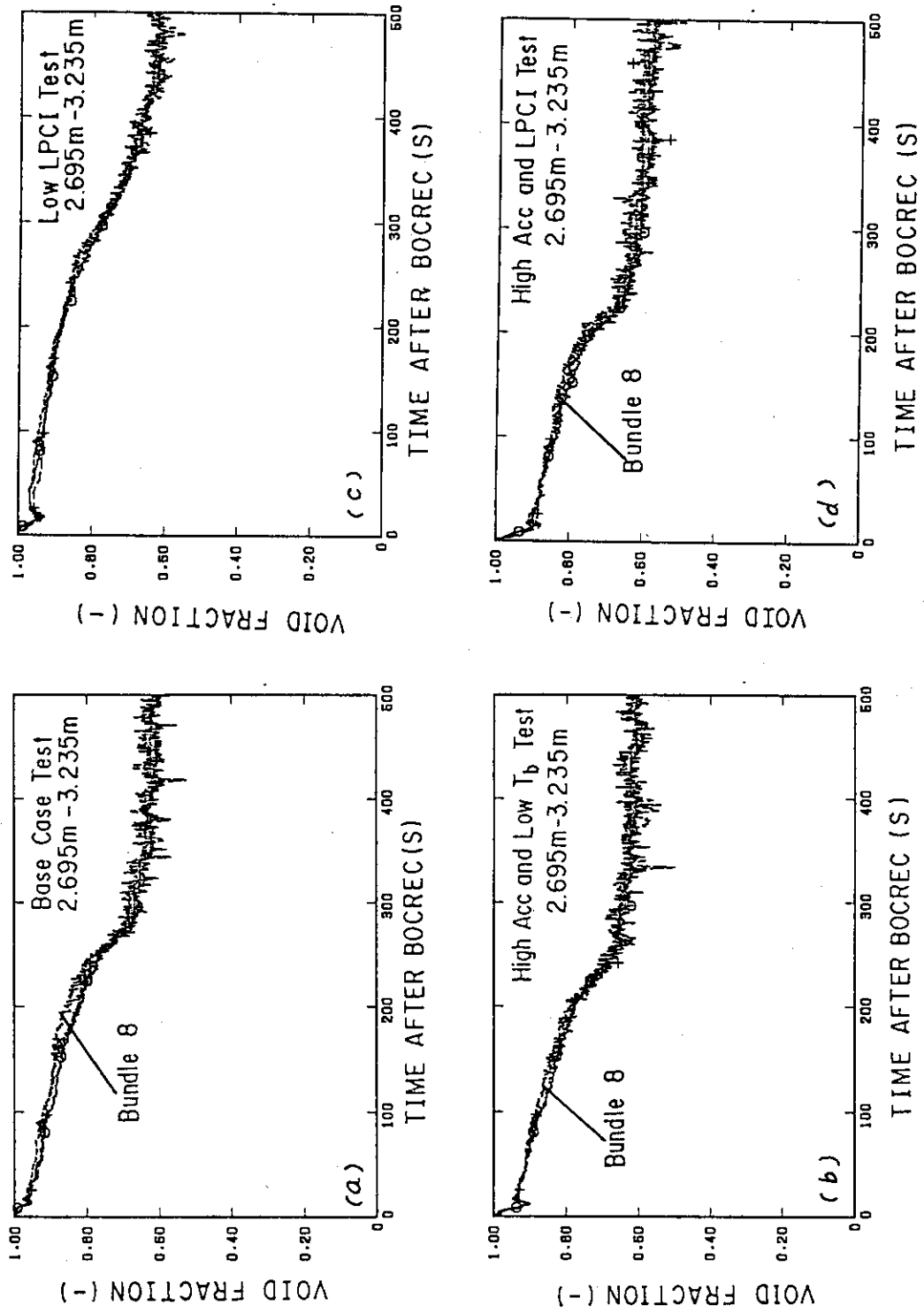


Fig. 3-14(5) Comparison of Sectional Void Fraction between 2.695m and 3.235m elevations in Bundles 2, 4 and 8

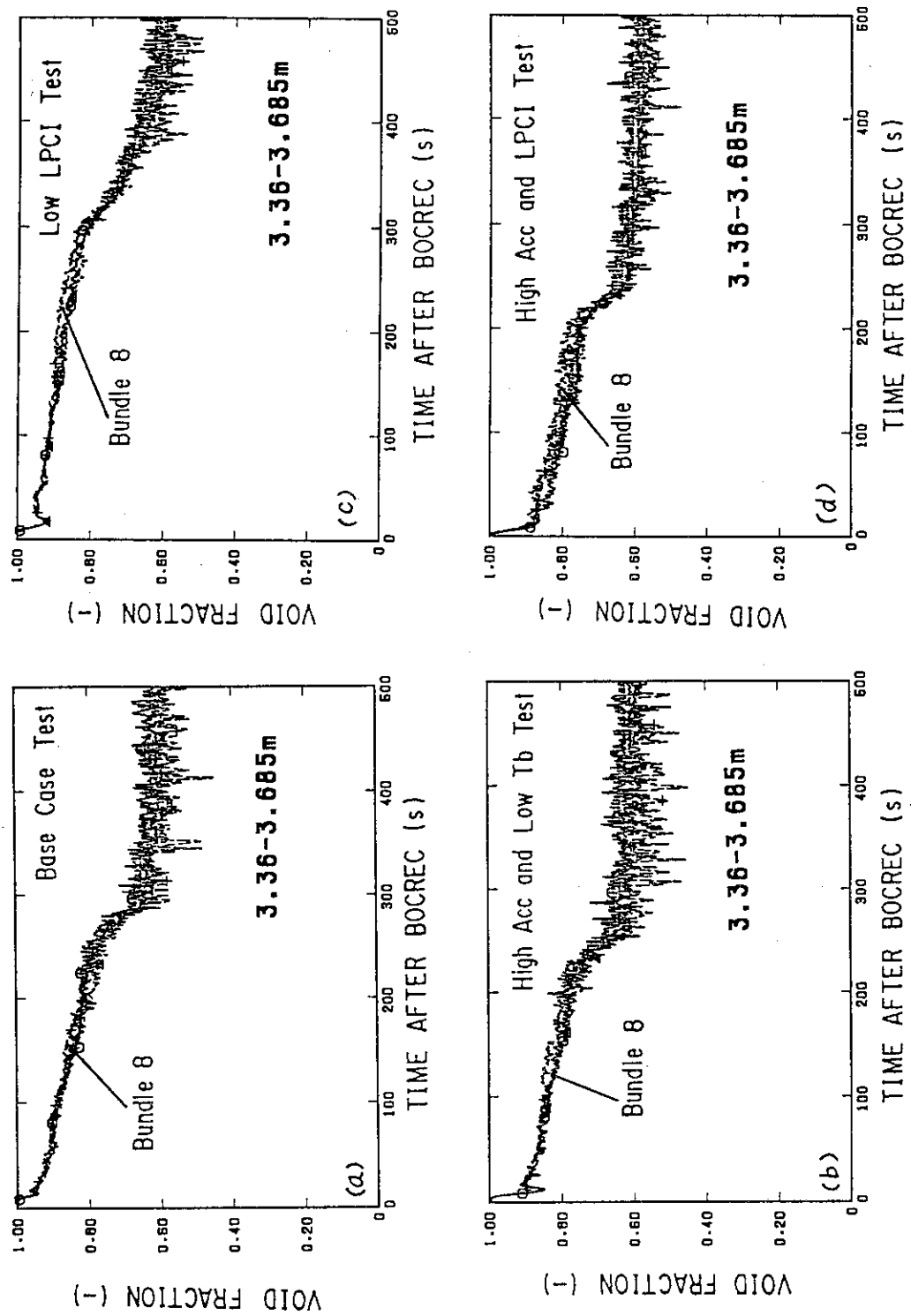


Fig. 3-14(6) Comparison of Sectional Void Fraction between 3.36m and 3.685m elevations in Bundles 2, 4 and 8

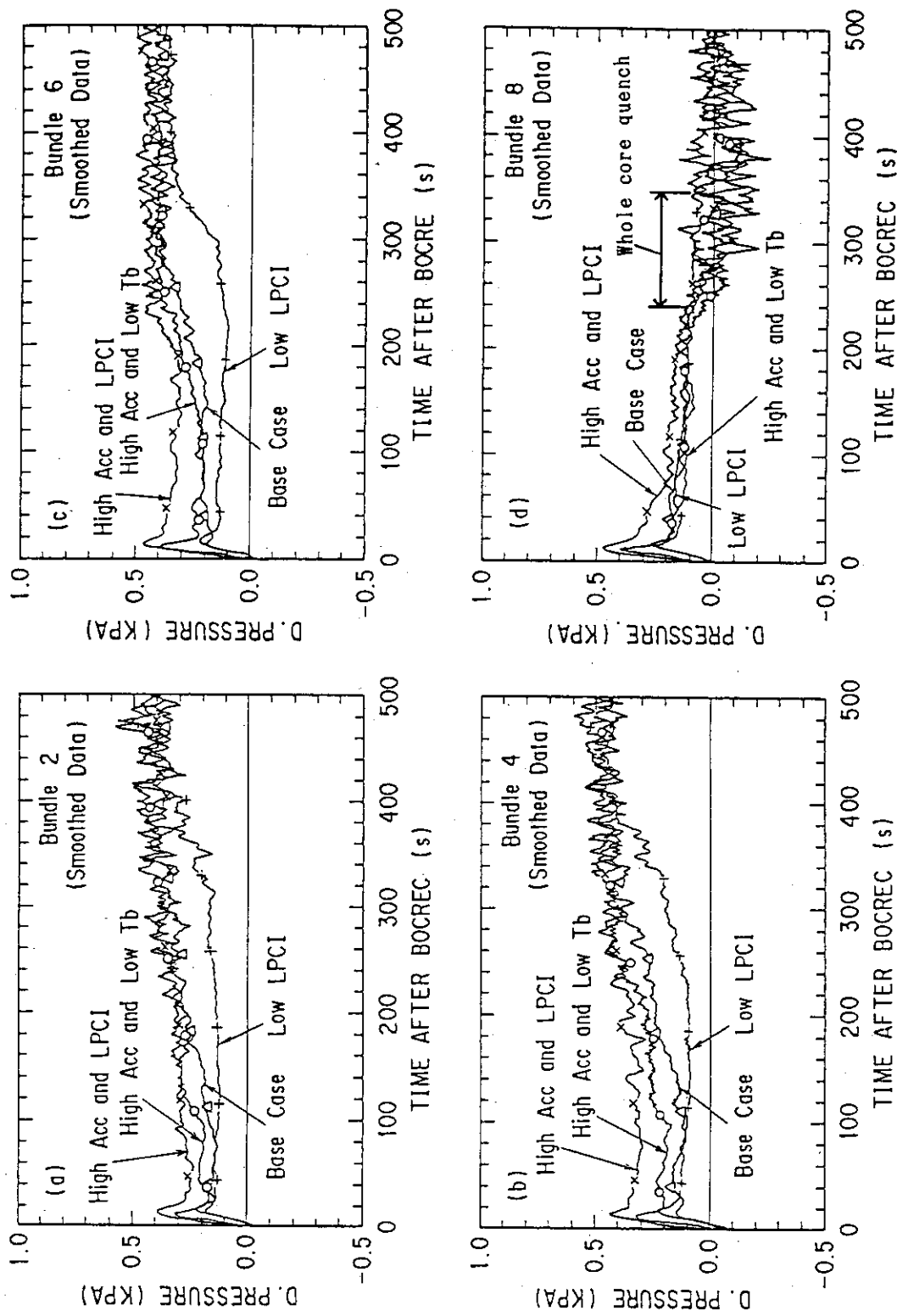


Fig. 3-15 Comparison of Differential Pressure across End Box Tie Plate  
above Bundles 2, 4, 6 and 8

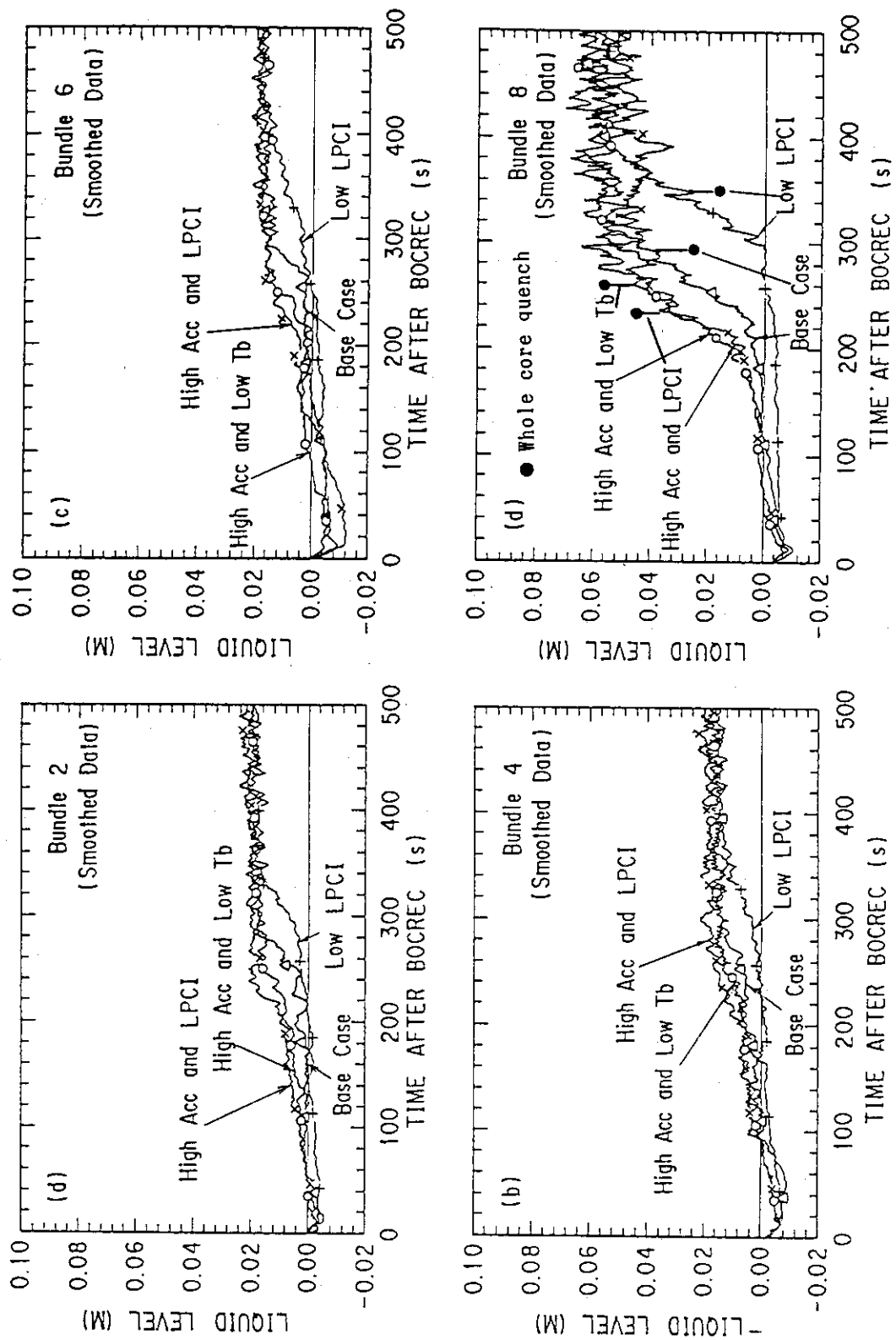


Fig. 3-16 Comparison of Liquid Level in End Box above Bundles 2, 4, 6  
and 8

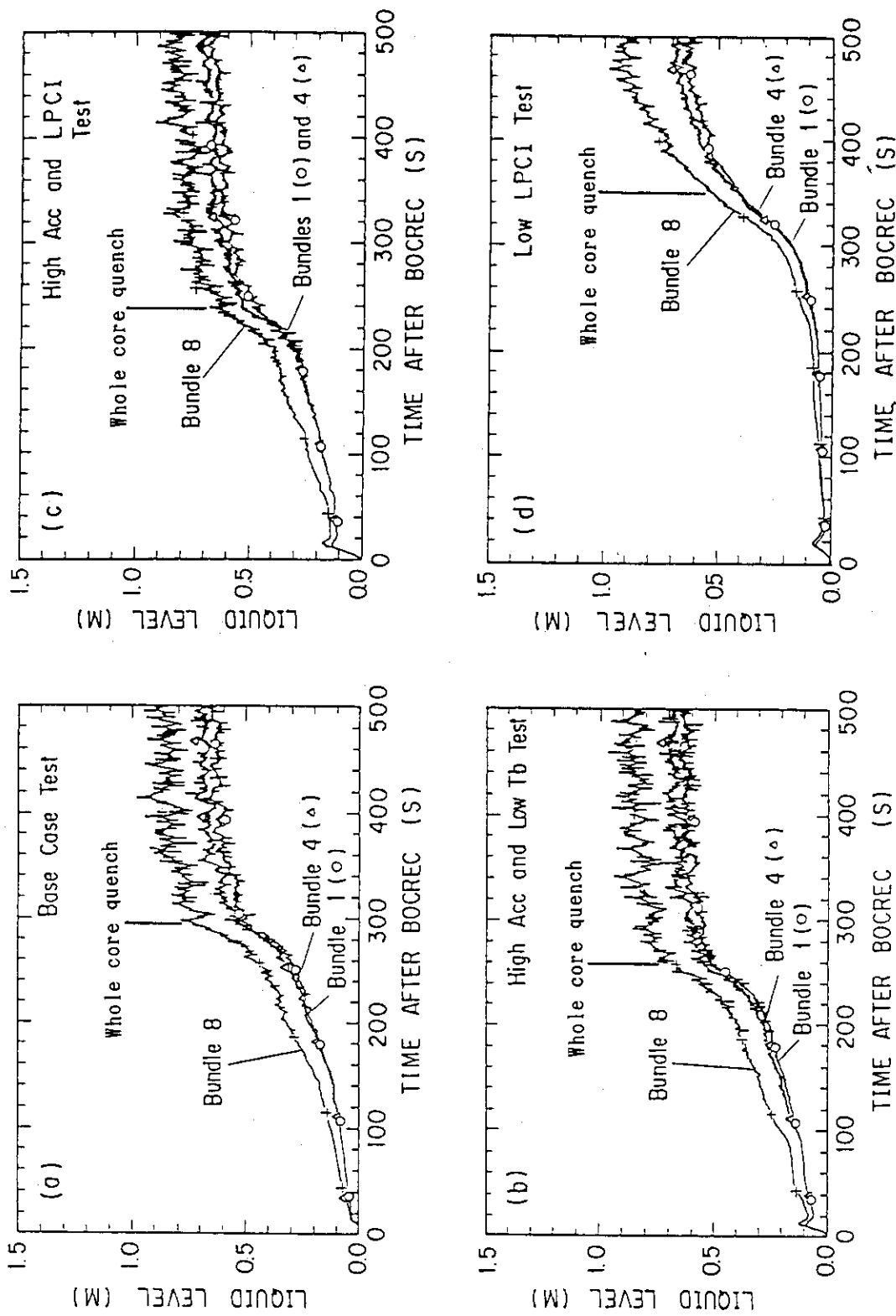


Fig. 3-17 Comparison of Liquid level in Upper Plenum above Bundles 1, 4 and 8

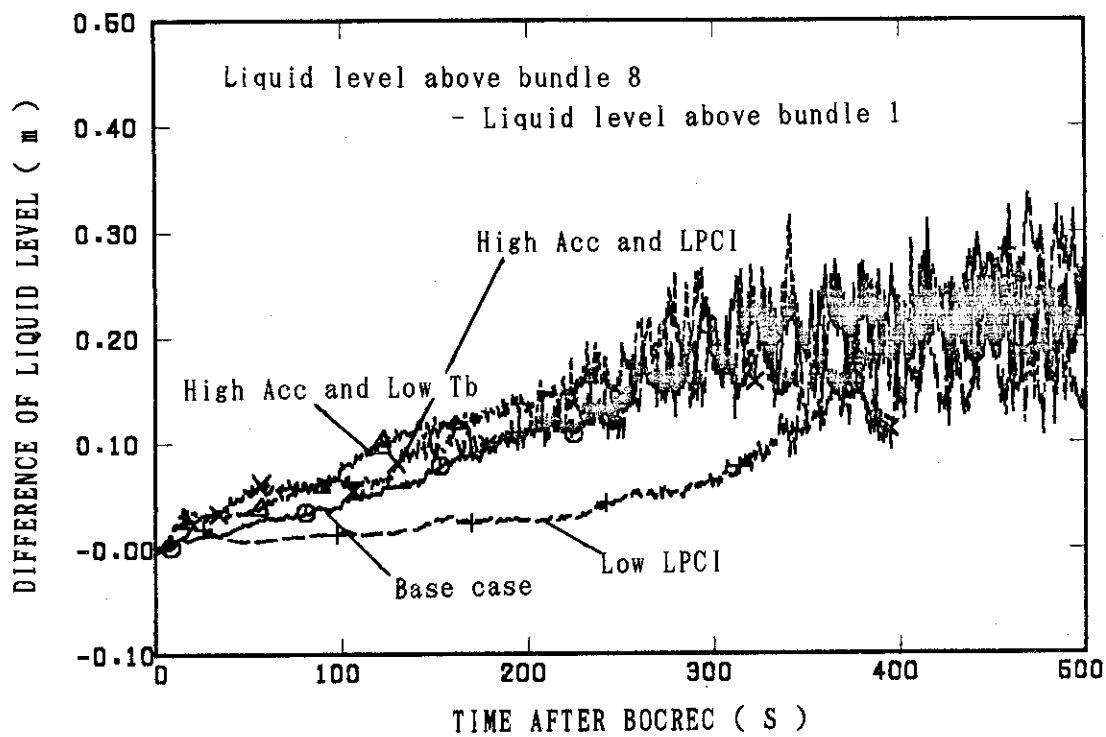


Fig. 3-18 Comparison of Difference of Liquid Level between above Bundles 1 and 8

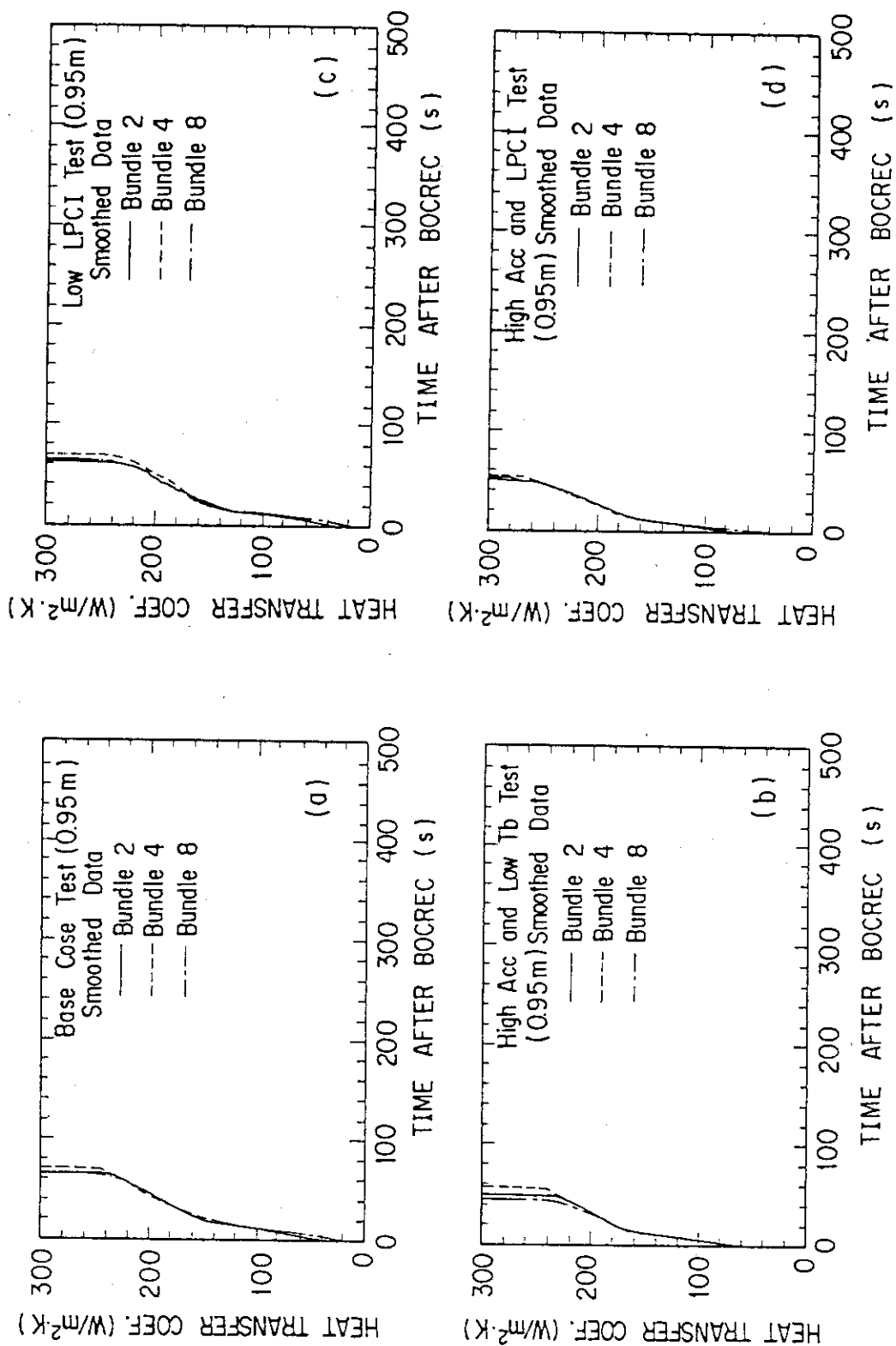


Fig. 3-19(1) Comparison of HTC at 0.95m elevation in Bundles 2, 4 and 8

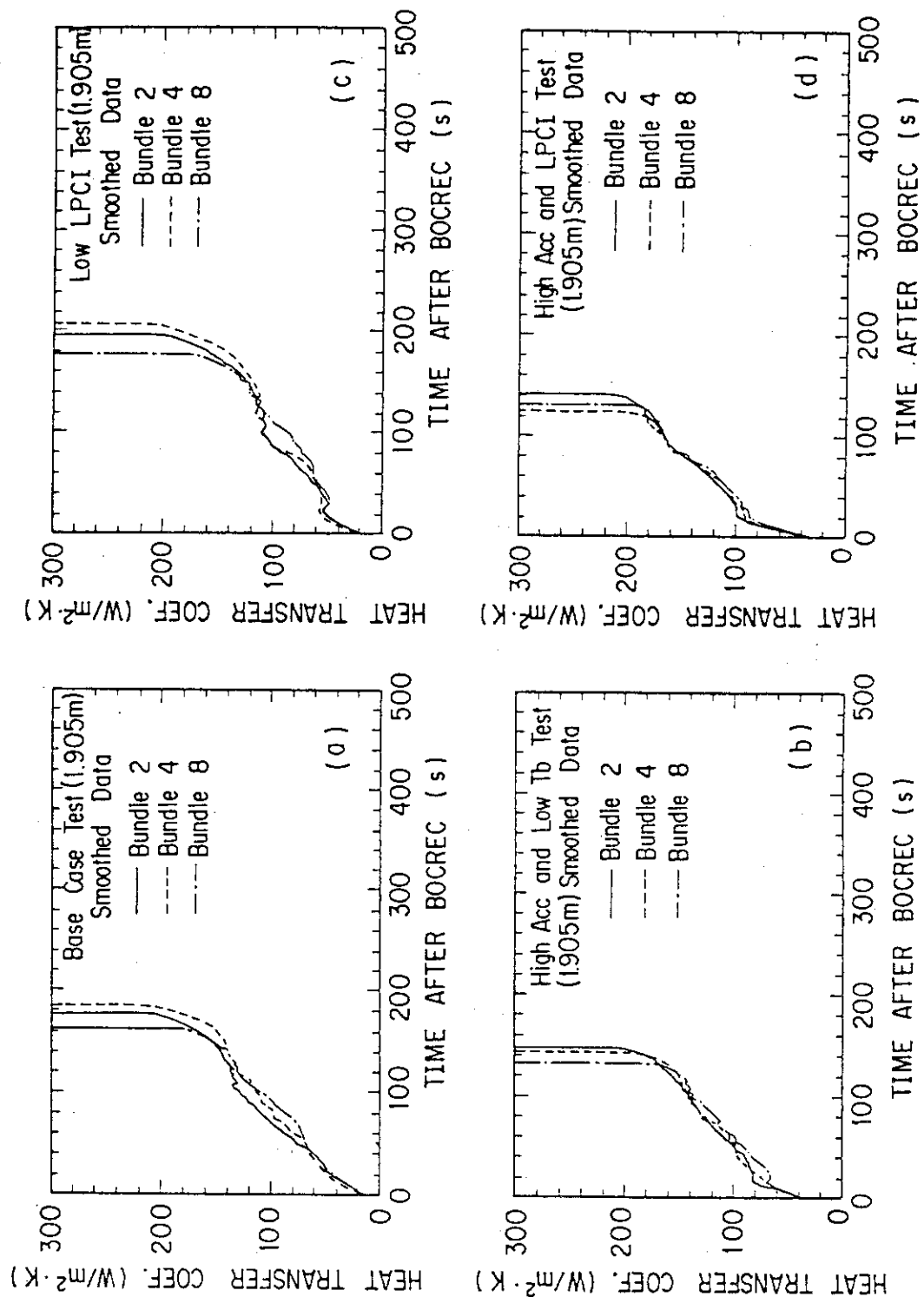


Fig. 3-19(2) Comparison of HTC at 1.905m elevation in Bundles 2, 4 and 8

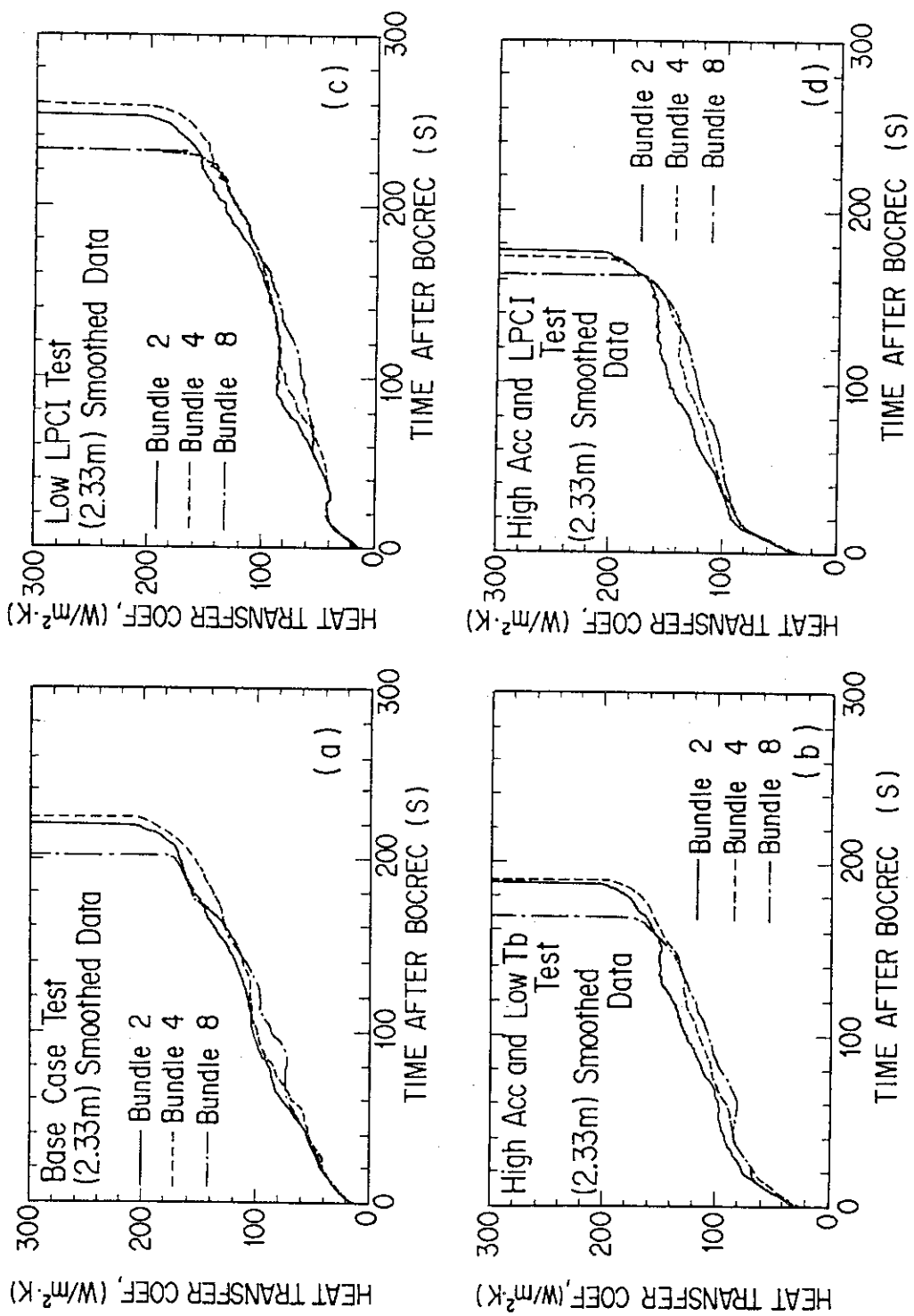


Fig. 3-19(3) Comparison of HTC at 2.33m elevation in Bundles 2, 4 and 8

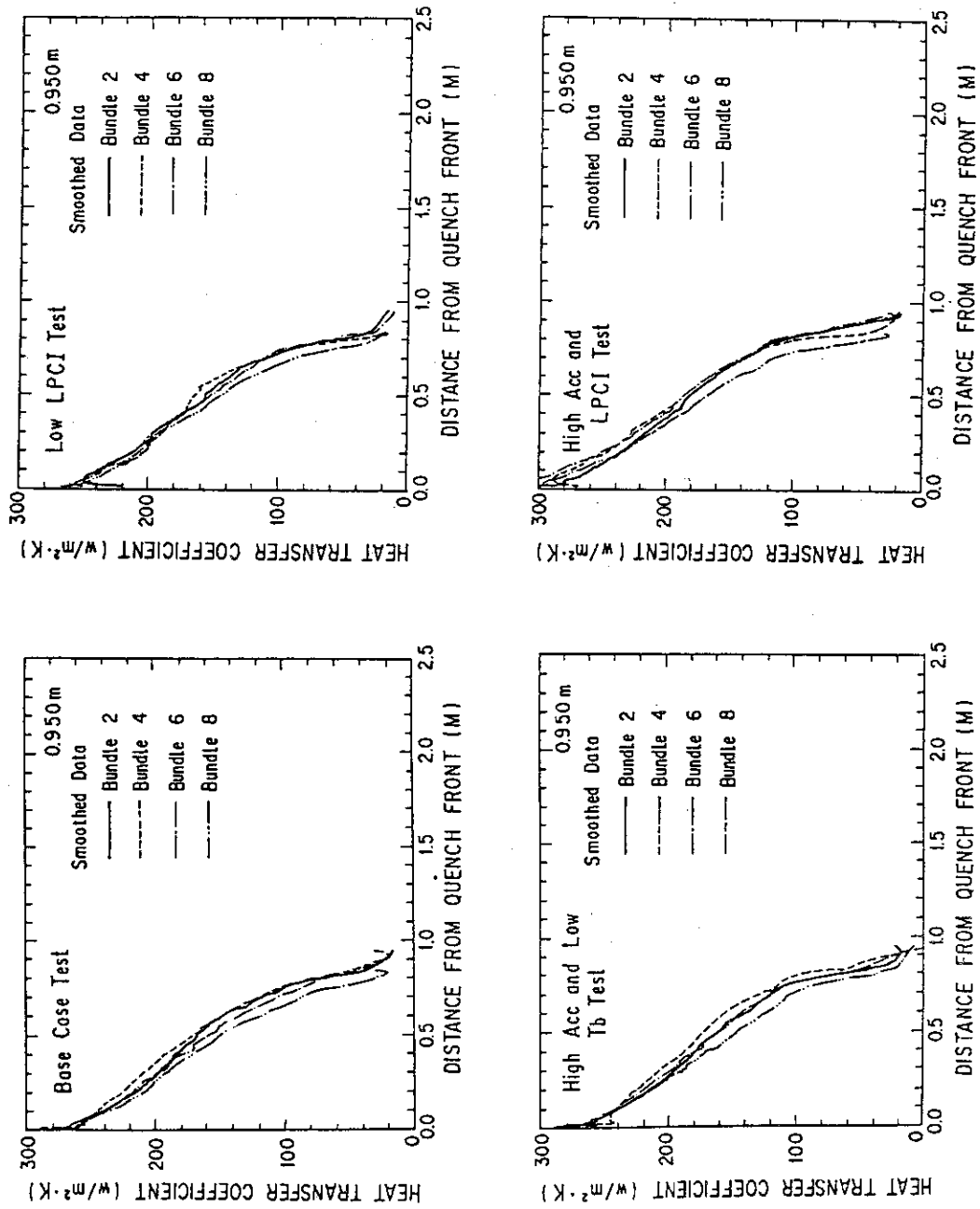


Fig. 3-20(1) Relationship between HTC and Distance from Quench Front at 0.95m elevation in Bundles 2, 4, 6 and 8

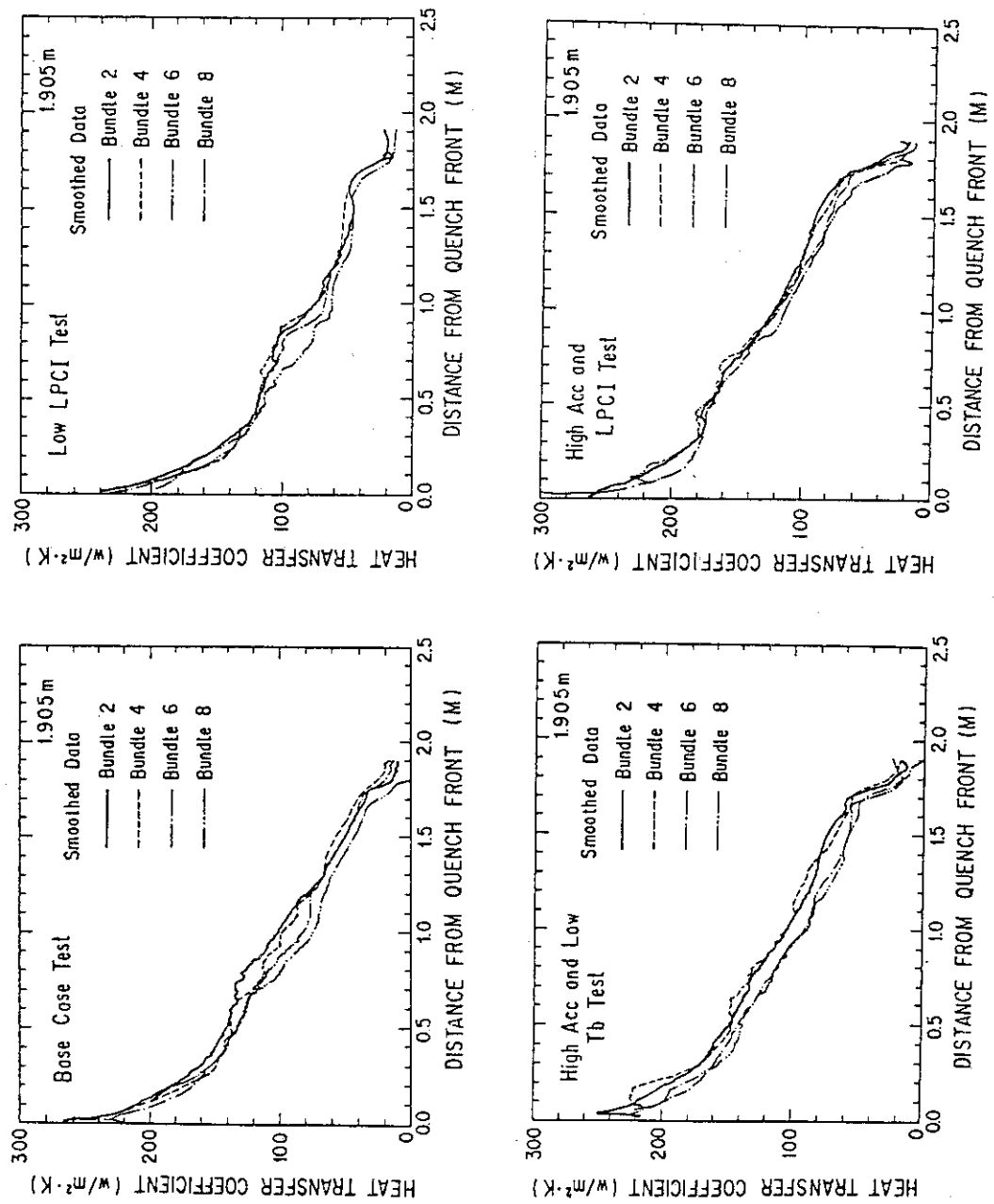


Fig. 3-20(2) Relationship between HTC and Distance from Quench Front at 1.905m elevation in Bundles 2, 4, 6 and 8

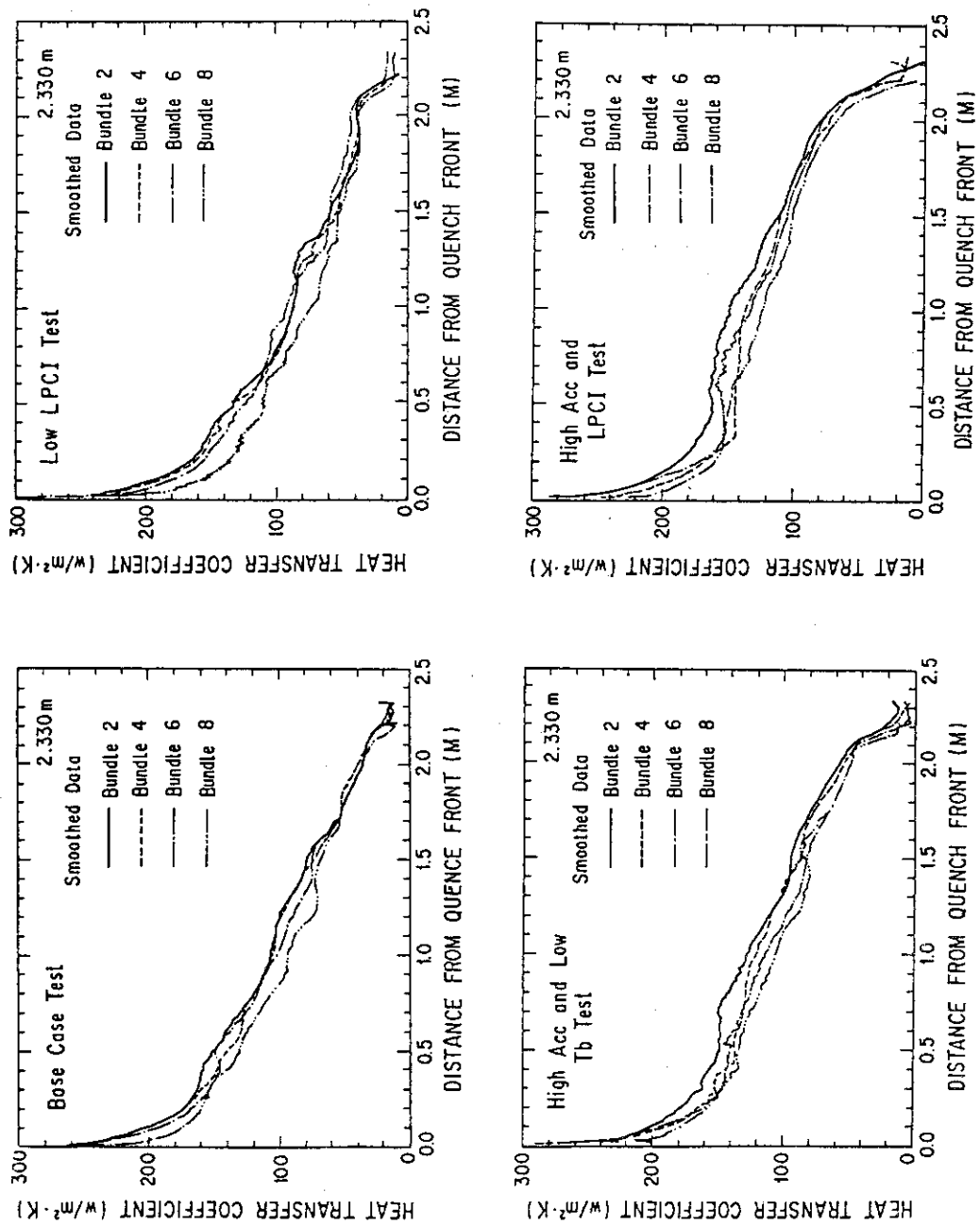


Fig. 3-20(3) Relationship between HTC and Distance from Quench Front at 2.33m elevation in Bundles 2, 4, 6 and 8

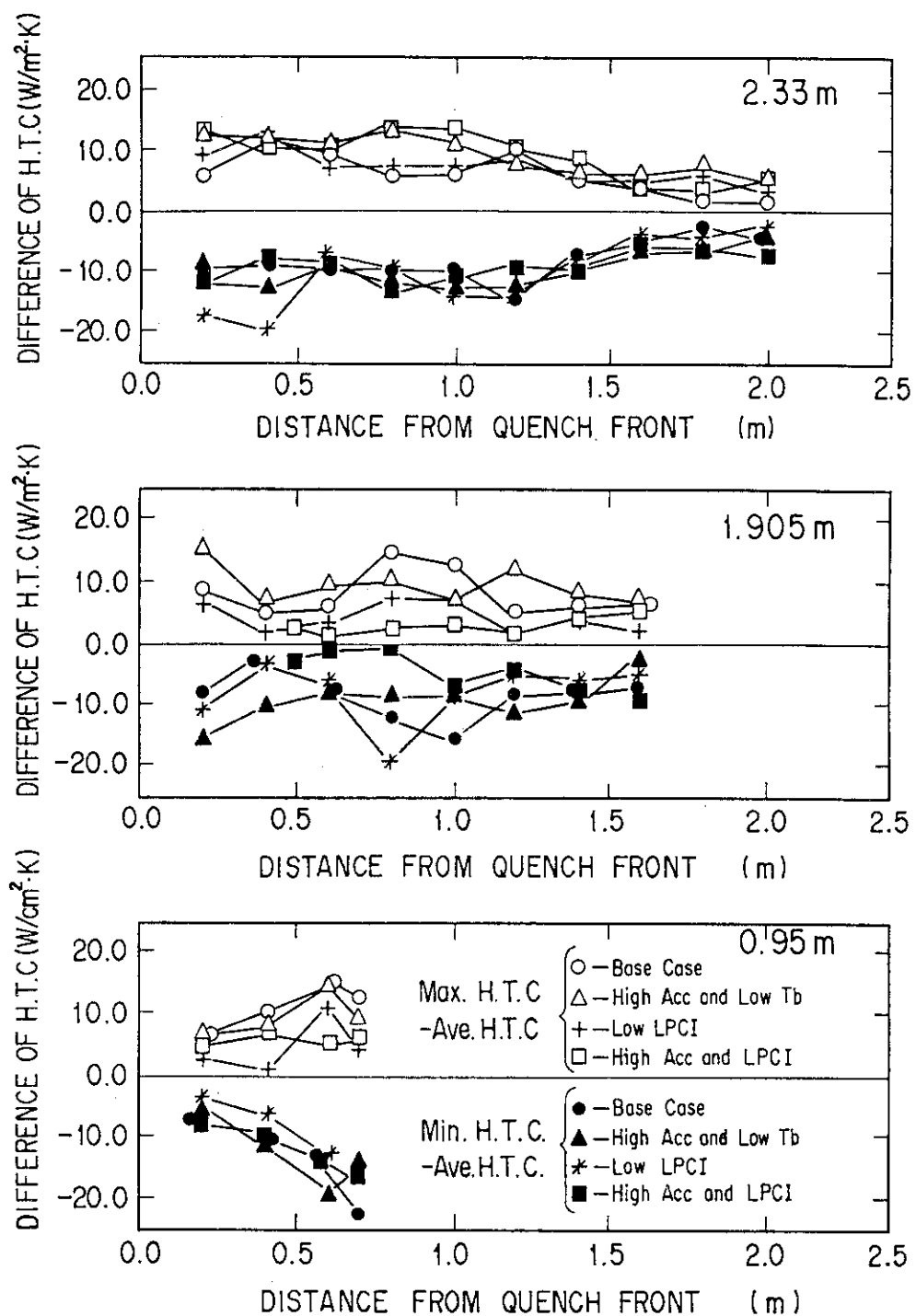


Fig. 3-21 Difference of HTC between Maximum or Minimum HTC and Average HTC at Three Axial Elevations

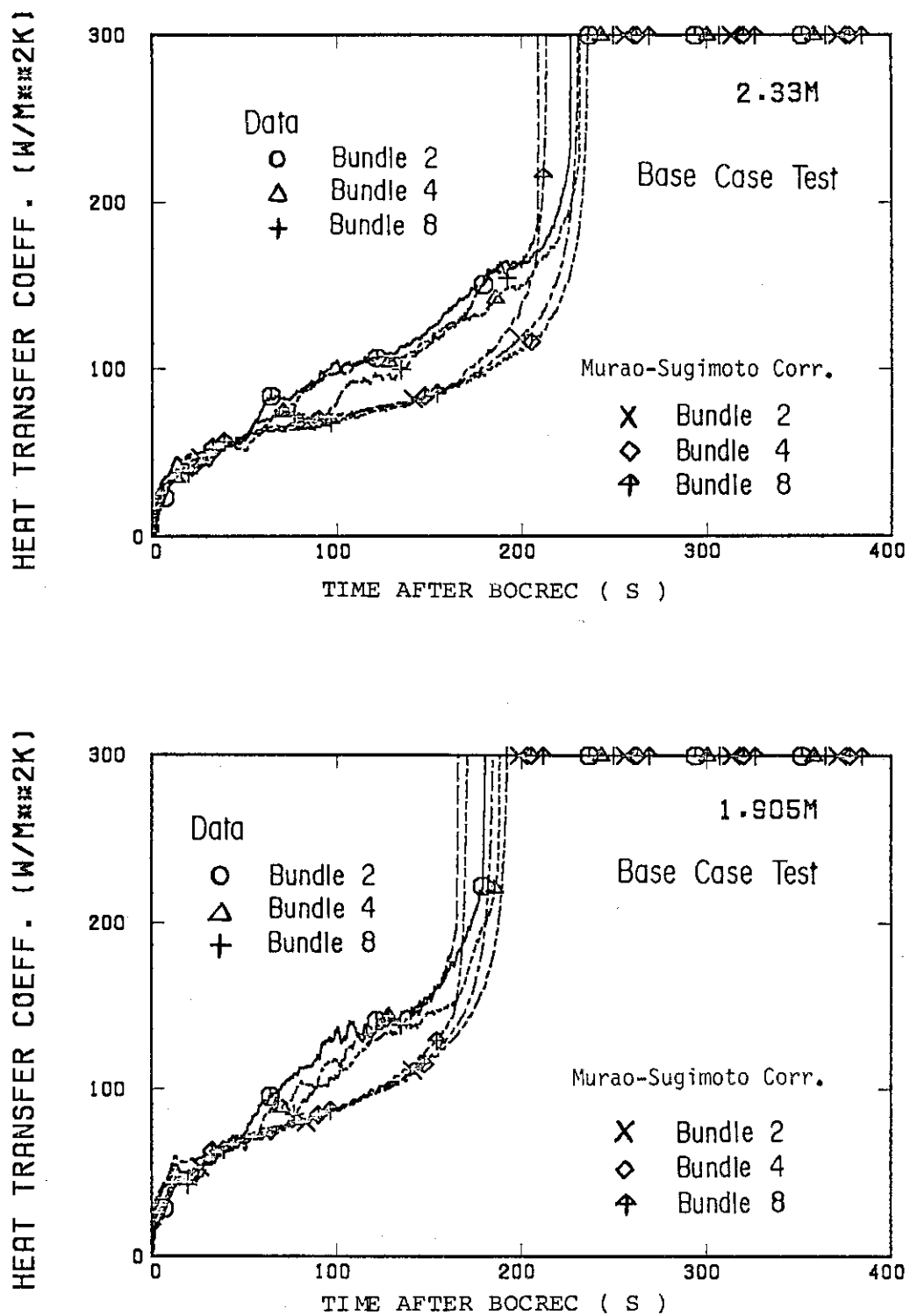


Fig. 3-22(1) Comparison of HTC at 1.905m and 2.33m elevations in Bundles 2,4 and 8 with Murao-Sugimoto Correlation in Base Case Test

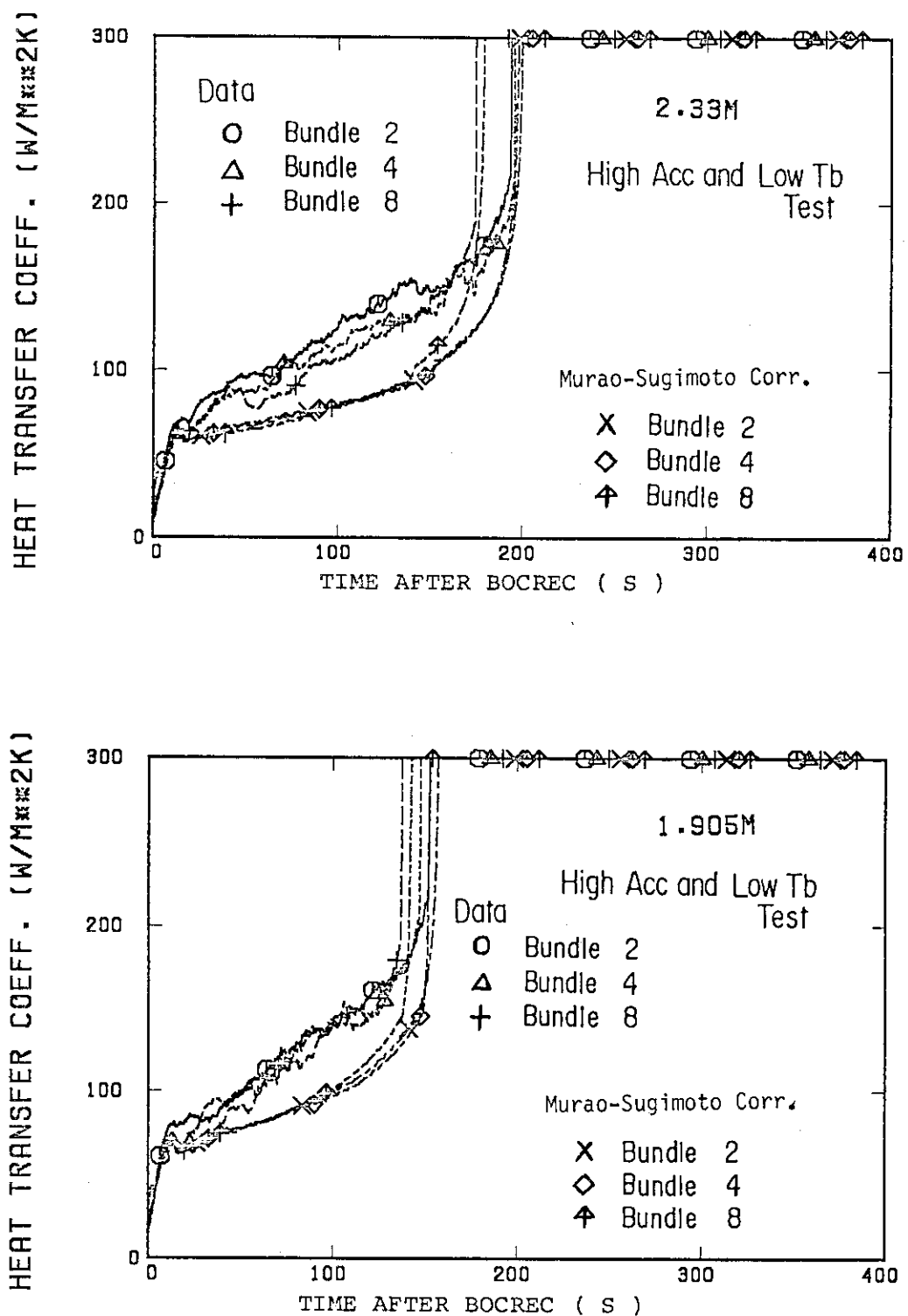


Fig. 3-22(2) Comparison of HTC at 1.905m and 2.33m elevations in Bundles 2,4 and 8 with Murao-Sugimoto Correlation in High Acc and Low Tb Test

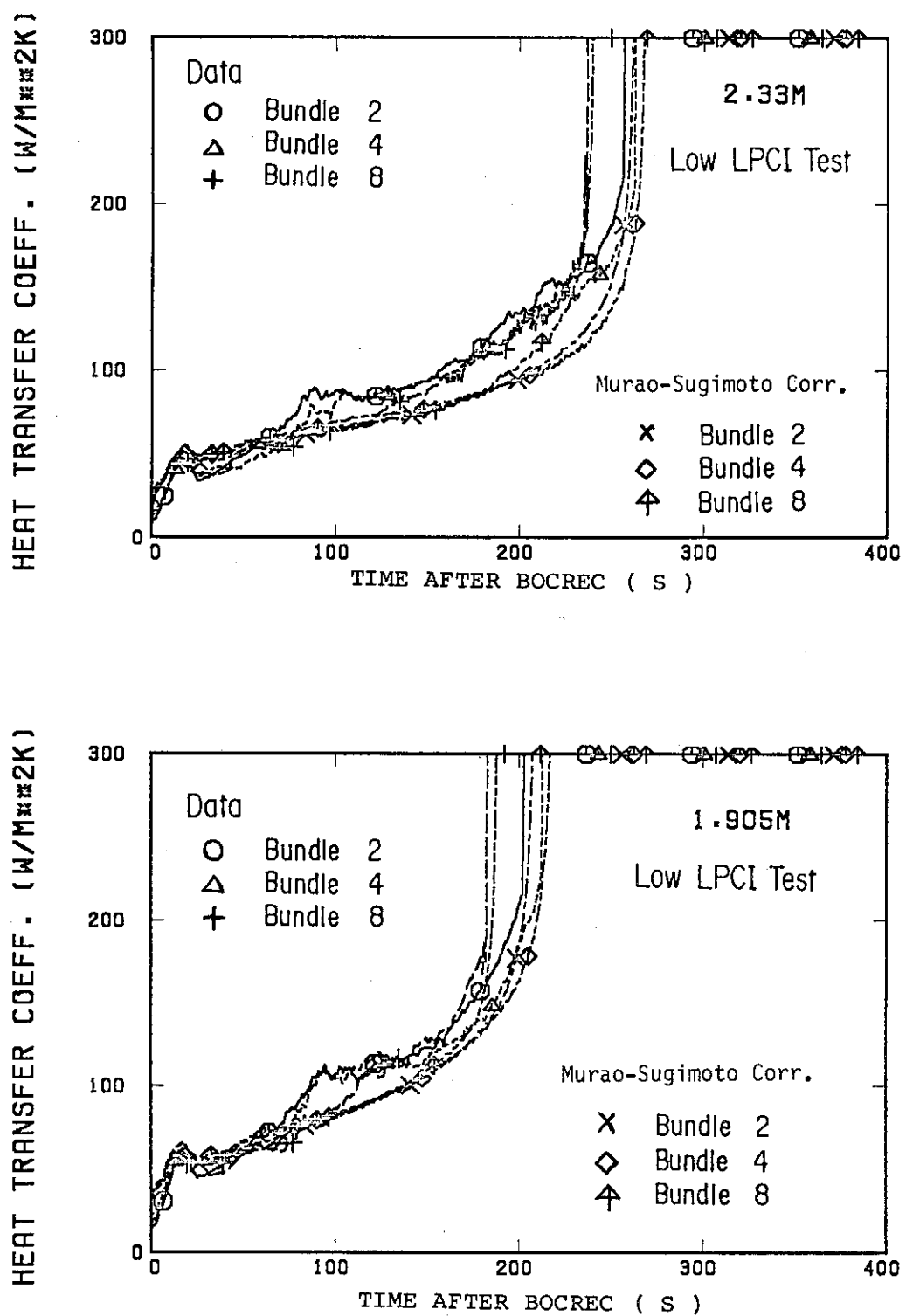


Fig. 3-22(3) Comparison of HTC at 1.905m and 2.33m elevations in Bundles 2,4 and 8 with Murao-Sugimoto Correlation in Low LPCI Test

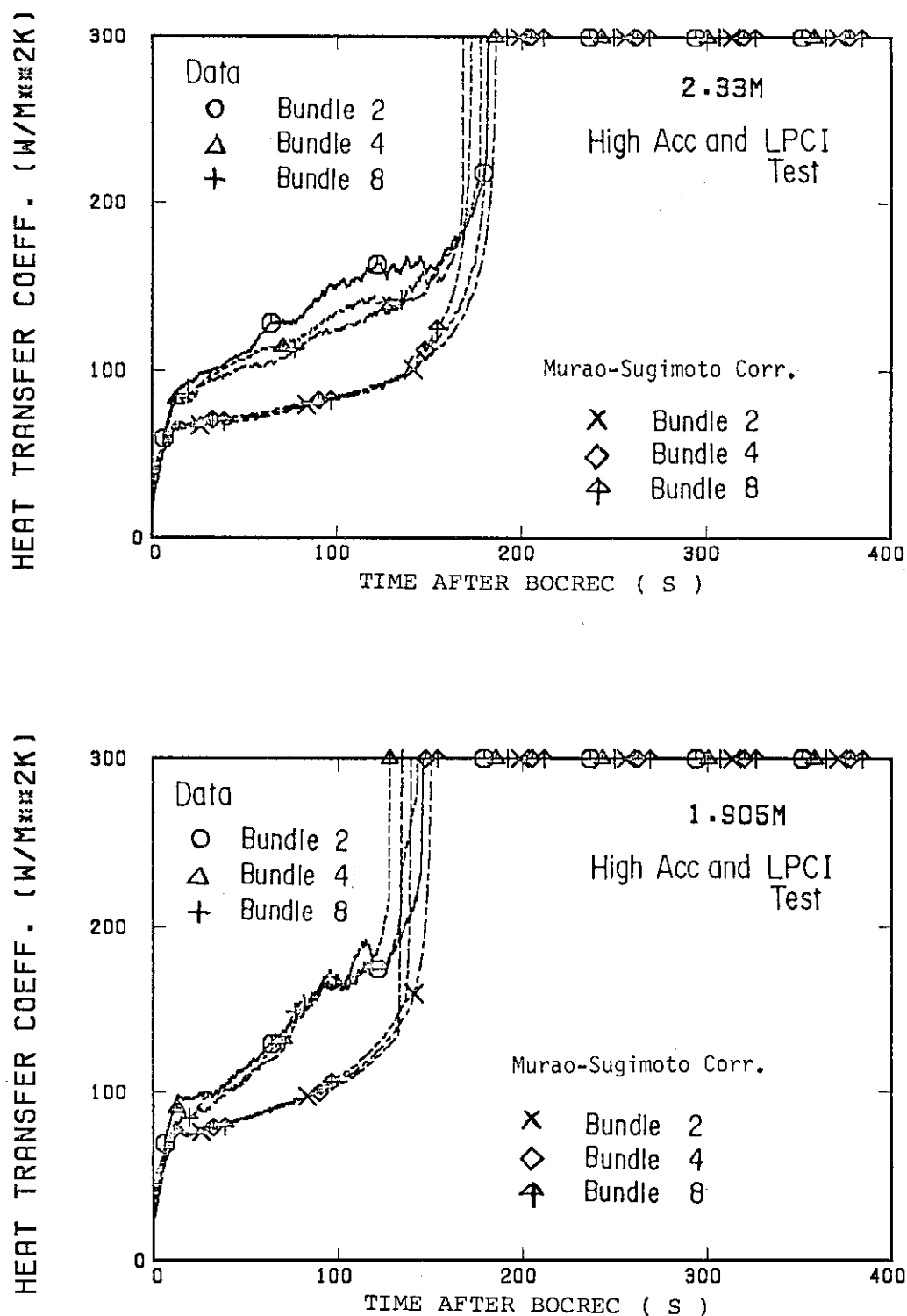


Fig. 3-22(4) Comparison of HTC at 1.905m and 2.33m elevations in Bundles 2,4 and 8 with Murao-Sugimoto Correlation in High Acc and LPCI Test

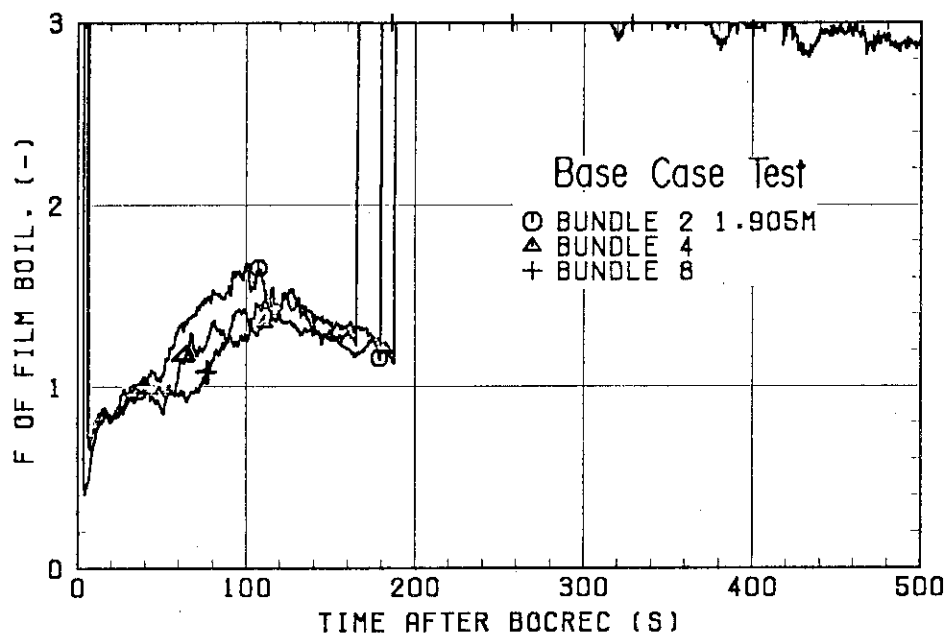
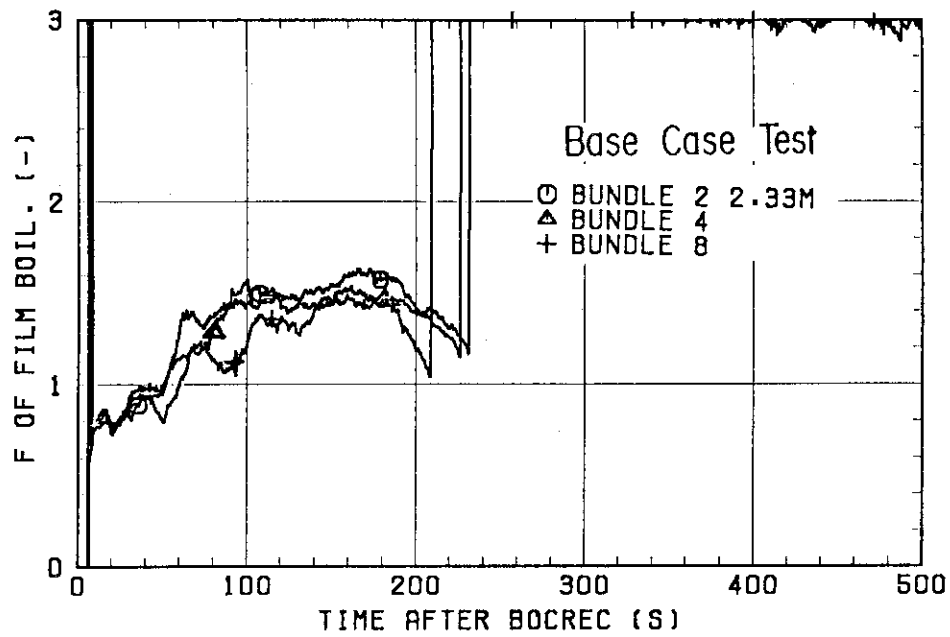


Fig. 3-23(1) Correction Factor for Film Boiling Term of Murao-Sugimoto Correlation in Base Case Test

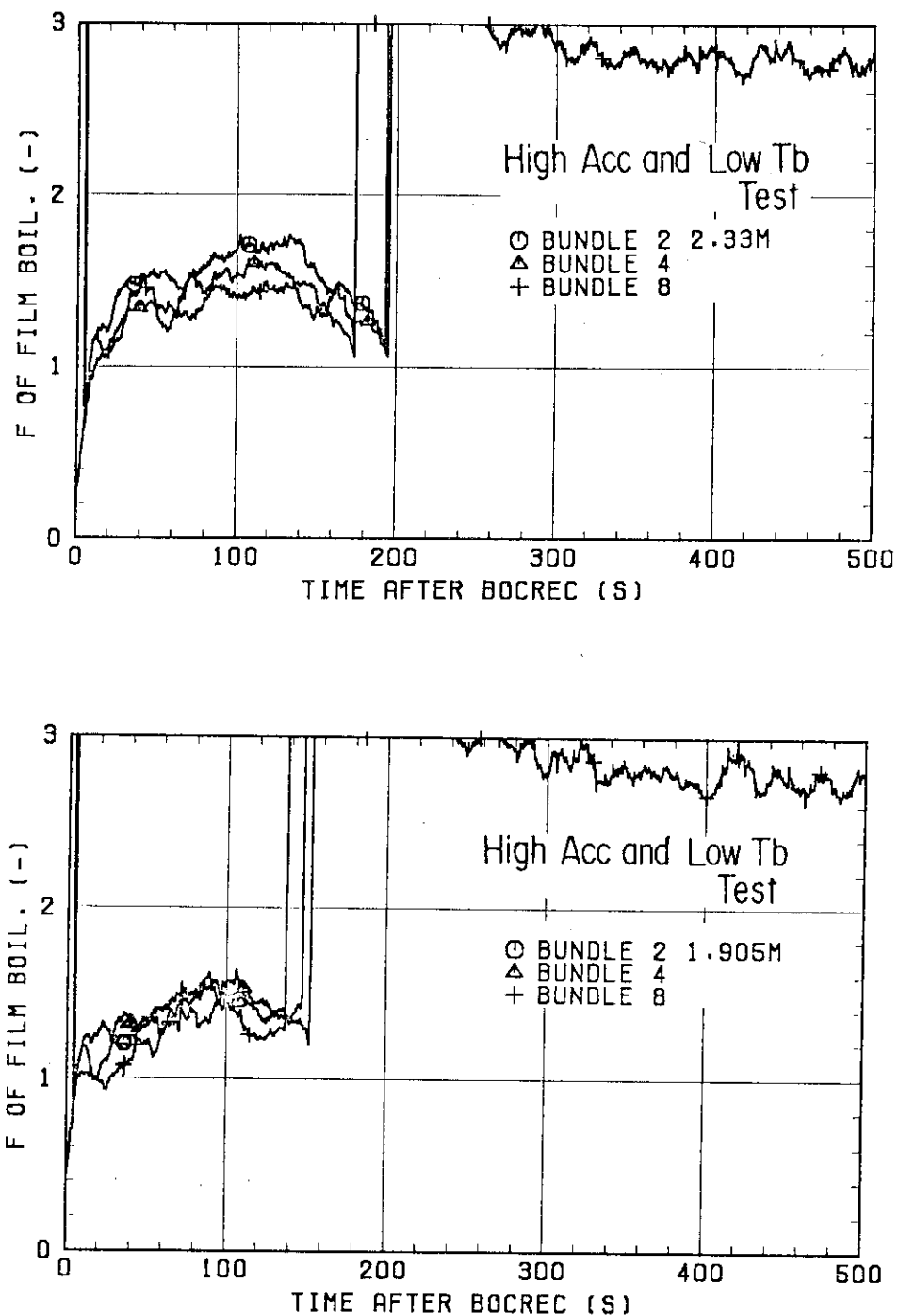


Fig. 3-23(2) Correction Factor for Film Boiling Term of Murao-Sugimoto Correlation in High Acc and Low Tb Test

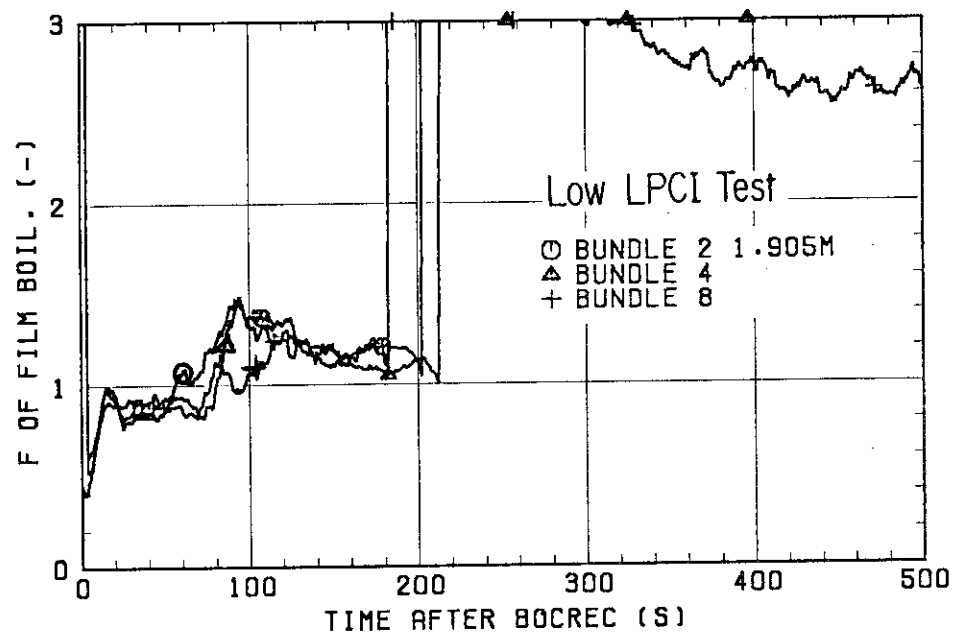
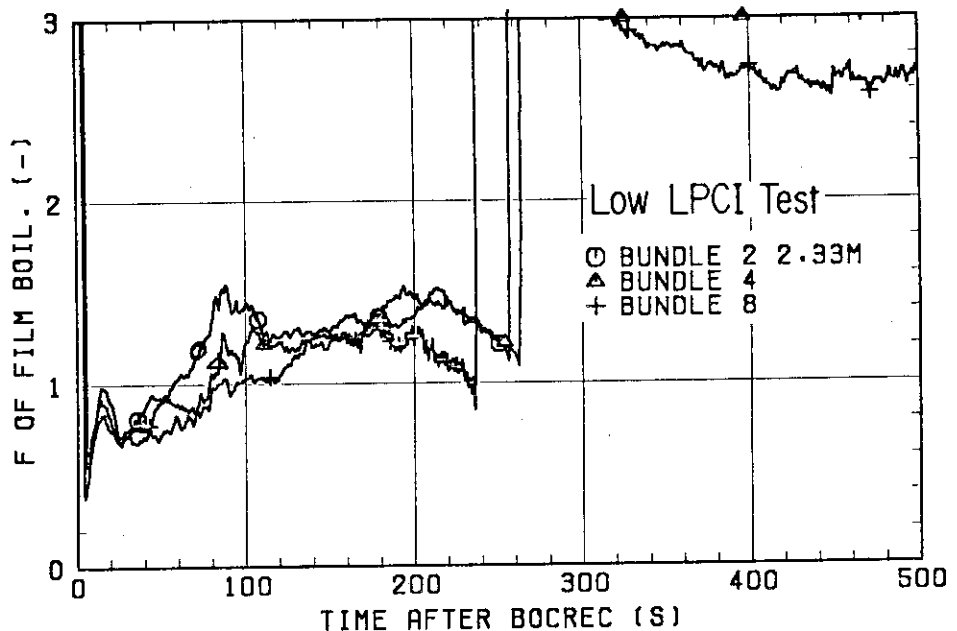


Fig. 3-23(3) Correction Factor for Film Boiling Term of Murao-Sugimoto Correlation in Low LPCI Test

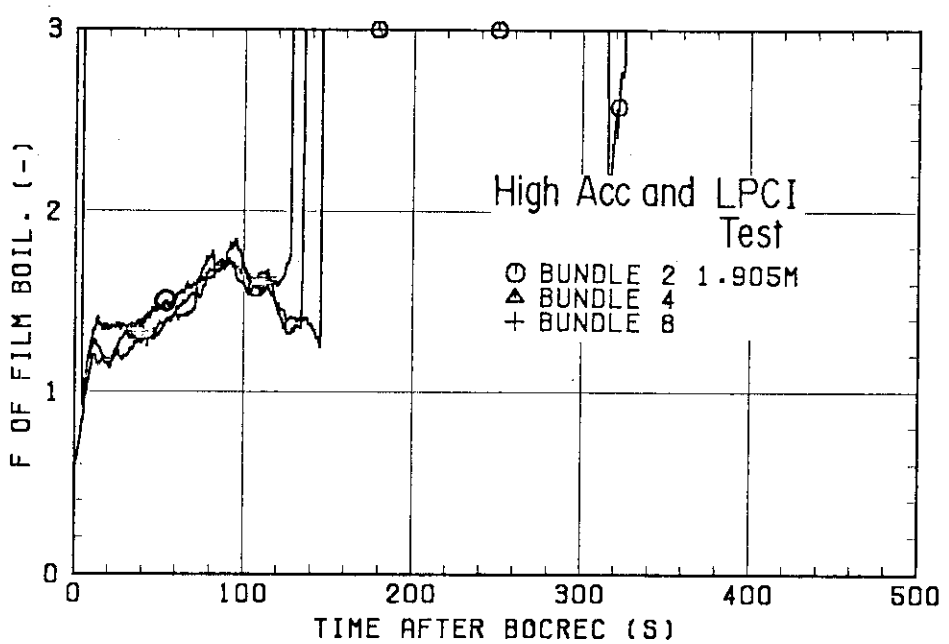
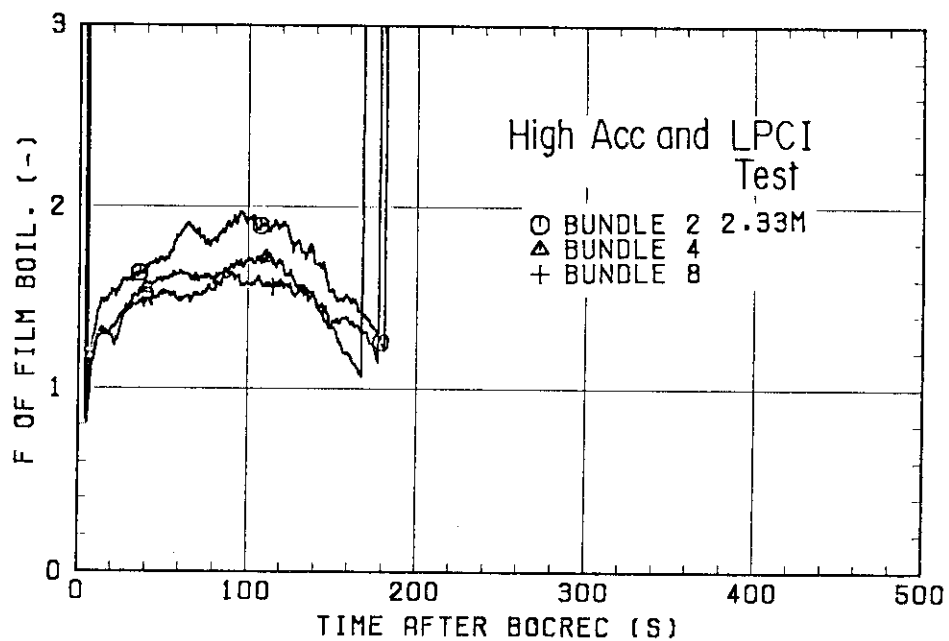


Fig. 3-23(4) Correction Factor for Film Boiling Term of Murao-Sugimoto Correlation in High Acc and LPCI Test

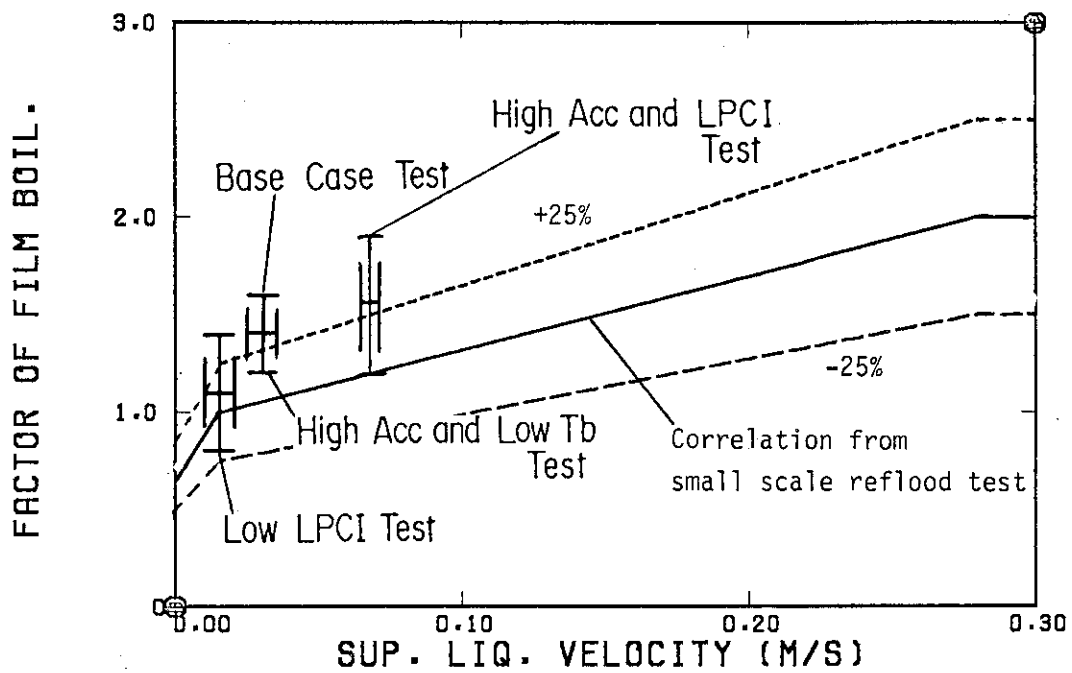


Fig. 3-24 Comparison of Correction Factor in SCTF Tests with Correlation from Small Scale Reflood Test

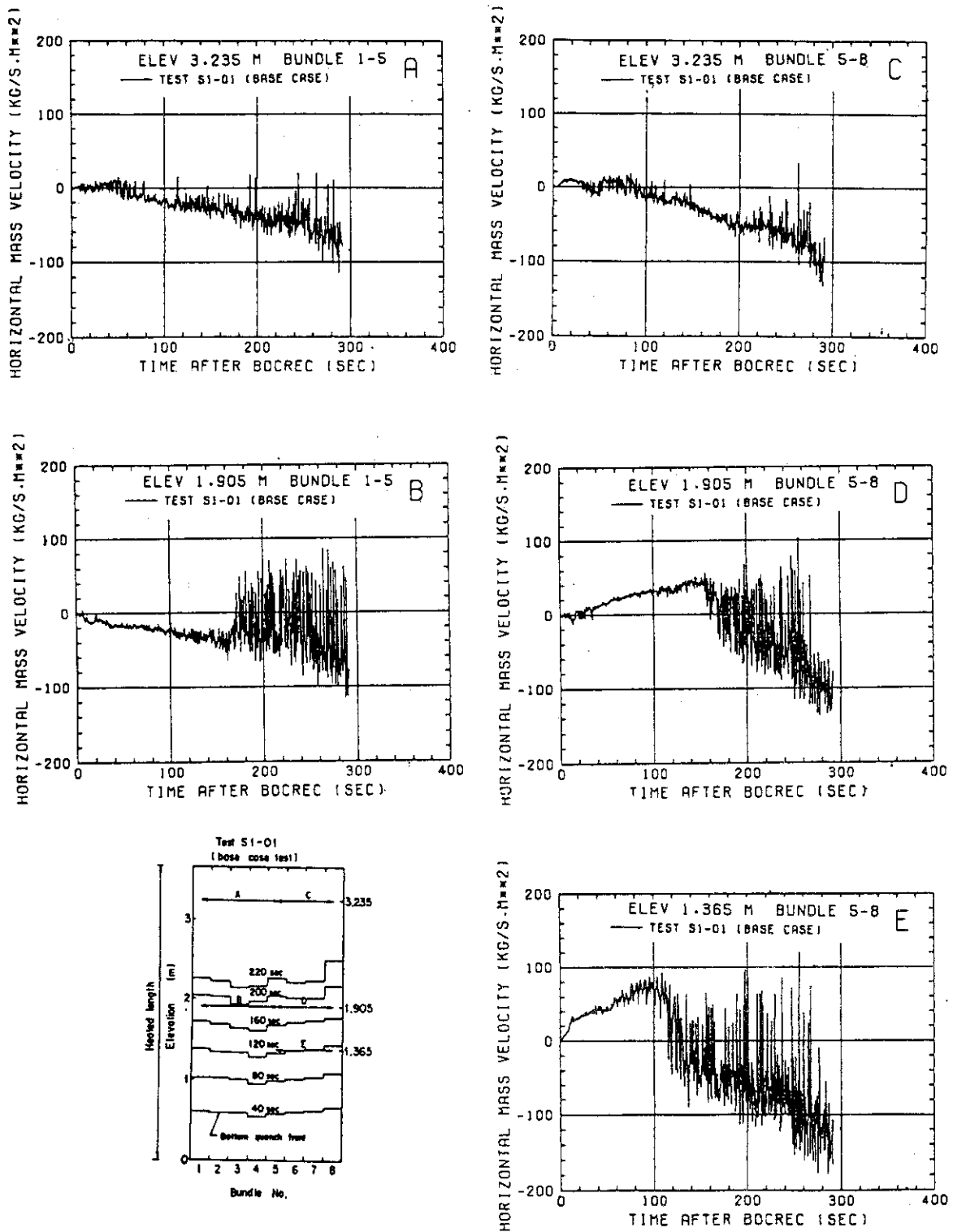


Fig. 3-25(1) Horizontal Mass Velocities in Base Case Test

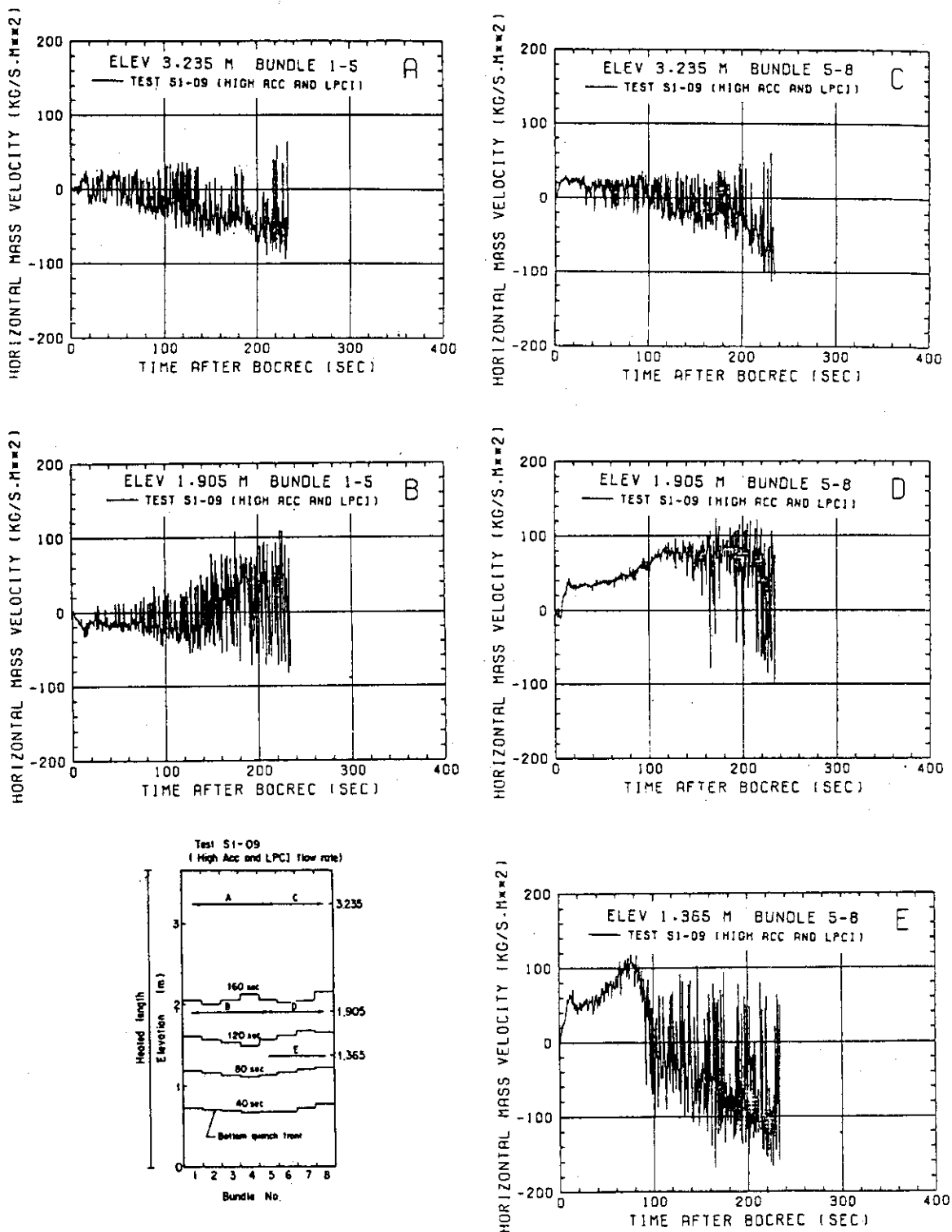


Fig. 3-25(2) Horizontal Mass Velocities in High Acc and LPCI Test

## Appendix A Schematic of Slab Core Test Facility (SCTF) Core-I

The Slab Core Test Facility was designed under the following design philosophy and design criteria:

### A.1.1 Design Philosophy

To properly simulate the two-dimensional core heat transfer and hydraulic behaviors, a special emphasis is put on the proper simulation of the components in the pressure vessel. Provided as the components in the pressure vessel are a simulated core, downcomer, core baffle region, lower plenum, upper plenum and upper head. On the other hand, simplified primary coolant loops are provided. Provided as the primary coolant loops are a hot leg, an intact cold leg, broken cold legs and a steam water separator. The objective of the steam/water separator is to measure the flow rate of carry-over water coming out of the upper plenum through the hot leg.

### A.1.2 Design Criteria

- (1) The reference reactor for simulation to the SCTF should be the Trojan reactor in the United States which is a four loop 3300 Mwt PWR. The Ooi reactor, etc. in Japan should be also referred to which are of similar types to the Trojan reactor.
- (2) A full scale radial and axial section of a pressurized water reactor should be provided as a simulated core of the SCTF with single bundle width.
- (3) The simulated core should consist of 8 bundles arranged in a row. Each bundle has electrically heated rods simulating fuel rods and non-heated rods with 16 x 16 array.
- (4) The flow area and fluid volume of components should be scaled in accordance with the core flow area scaling.
- (5) To properly simulate the flow behavior of carry-over water and entrainment, the elevations of hot leg and cold legs should be designed so as to be the same as the PWRs as much as possible.
- (6) To investigate the effect of flow resistance in the primary loops should be provided the orifices of which dimension is changeable.
- (7) The maximum allowable temperature of the simulated fuel rods should be 900 °C and the maximum allowable pressure of the facility should be 6

kg/cm<sup>2</sup> absolute.

- (8) The facility should be provided with a hot leg equivalent to four actual hot legs on the flow area scaling, an intact cold leg equivalent to three actual intact cold legs on the flow area scaling and two broken cold legs, one is for the steam water separator side and the other for the pressure vessel side.
- (9) The ECCS should consist of an Acc and a LPCI.
- (10) ECC water injection ports should be the cold leg, upper plenum, downcomer and lower plenum. These portions should be chosen according to the objective of the test.
- (11) For better simulation of lower plenum flow resistance, simulated fuel rods should not penetrate through the bottom plate of the lower plenum but terminate below the bottom of the core.
- (12) For measurements in the pressure vessel including core measurements, the feature of the slab geometry of the pressure vessel should be utilized as much as possible. Design and arrangement of the instruments should be done so as to be able to carry out installation calibration and removal of the instruments.
- (13) View windows should be provided where flow pattern recognition is important. The locations are, the interface between the core and the upper plenum, hot leg, pressure vessel side broken cold leg and the downcomer.
- (14) The blocked bundle test should be carried out in Core-I in order to investigate the effect of the ballooned fuel rods.
- (15) Simulated types of break should be cold leg break and hot leg break.
- (16) The components and systems such as the containment tanks and ECC water supply system in the cylindrical core test facility (CCTF) should be shared with the SCTF to the maximum extent.

The overall schematic diagram of the SCTF is shown in Fig. A-1. The principal dimensions of the facility is shown in Table A-1, and the comparison of dimensions between the SCTF and the referred PWR is shown in Fig. A-2.

#### A.2 Pressure Vessel and Internals

The pressure vessel is of slab geometry as shown in Fig. A-3. The height of the components in the pressure vessel is almost the same as the

reference reactor's, and the flow area and the fluid volume of each component are scaled down based on the nominal core flow area scaling.

The core consists of 8 bundles in a row and each bundles include simulated fuel rods and non-heated rods with 16 x 16 array. The core arrangement for the SCTF Core-I is shown in Fig. A-4, which includes 6 normal bundles and 2 blocked bundles. The core is enveloped by the honeycomb thermal insulator which is attached on the barrel.

The downcomer is located at one end of the pressure vessel which corresponds to the periphery of the actual PWR. The core baffle region is, on the other hand, located between the core and the downcomer.

The design of upper plenum internals is based on that of the new Westinghouse 17 x 17 array fuel assemblies. The internals consist of control rod guide tubes, support columns, orifice plates and open holes and the arrangement is shown in Fig. A-5. The radius of each internal is scaled down by factor 8/15 from that of an actual reactor. Flow resistance baffles are inserted into the guide tubes. The elevation and the configuration of baffle plates are shown in Figs. A-6 and A-7.

The height of the hot leg and cold legs are designed as close to the actual PWR as possible. However, in order to avoid the interference of the nozzles in the downcomer, the height of nozzles for broken cold leg and the intact cold leg are shifted down compared to that of the hot leg as shown in Fig. A-3.

### A.3 Heater Rod Assembly

The heater rod assembly for the SCTF Core-I consists of 8 bundles arranged in a row. These bundles are composed of 6 normal unblocked bundles which are located at the 1st, 2nd and 5th to 8th bundles and 2 blocked bundles which are 3rd and 4th bundles as shown in Fig. A-4. Each bundle has 234 electrically heated rods and 22 non-heated rods. The dimensions of the heater rods are based on a 15 x 15 fuel rod bundle and the heated length and the outer diameter of each heater rod are 3.66 m and 10.7 mm, respectively. A heater rod consists of a nichrome heater element, magnesium oxide (MgO) and Nichrofer-7216 sheath (equivalent to Inconel 600). The sheath wall thickness is about 1.0 mm and is thicker than the actual fuel cladding because of the requirements for thermocouple installation. The heating element is a helical coil and has a 17 step chopped cosine axial power profile as shown in Fig. A-8. The peaking factor is 1.4.

Non-heated rods are either stainless steel pipes or solid rods of 13.8 mm O.D. The heater rods and non-heated rods are fixed at the top of the core allowing the rods to move downward when the thermal expansion occurs. In Fig. A-9 the axial position where blockage sleeves for simulating the ballooned fuel rod are equipped is shown.

For better simulation for flow resistance in the lower plenum the simulated rods do not penetrate through the bottom plate of the lower plenum as shown in Fig. A-9.

The thermocouple locations on the heater rods and the tag identification numbers are shown in Fig. A-10.

#### A.4 Primary Loops and ECCS

Primary loops consist of a hot leg equivalent to the four actual hot legs on the flow area scaling, a steam/water separator for measuring the flow rate of carry-over water, an intact cold leg equivalent to the three actual intact loops on the flow area scaling, a broken cold leg at the pressure vessel side and a broken cold leg at the steam water separator side. These two broken cold legs are connected with two containment tanks through break valves, respectively. The arrangement of the primary loops is shown in Fig. A-11. The flow area of each loop is scaled down based on the core flow area scaling. It should be emphasized that the cross section of the hot leg is an elongated circle to realize the proper flow pattern in the hot leg. The steam/water separator has a steam generator inlet plenum simulator to realize the flow characteristics of carry-over water.

A pump simulator and a loop seal part are provided for the intact cold leg. The loop resistance is adjusted with the orifice plate.

In principle, ECCS consists of an accumulator and a low pressure coolant injection system. The injection port is located as already described in the design criteria.

#### A.5 Containment Tanks and Auxiliary System

Two containment tanks are provided to the SCTF. The containment tank-I is connected with the downcomer through the pressure vessel side broken cold leg and the containment tank-II is connected with the steam/water separator through the steam/water separator side broken cold leg. Especially in the containment tank-I, carry-over from the downcomer is measured by phase

separation. These containment tanks and auxiliary system such as a presurizer for injecting water from the Acc tank, etc. are shared with the CCTF.

List of Table and Figures

Table A-1 Principal Dimensions of Test Facility

Fig. A-1 Schematic Diagram of Slab Core Test Facility

Fig. A-2 Comparison of Dimensions between SCTF and a Reference PWR

Fig. A-3 Vertical Cross Section of the Pressure Vessel

Fig. A-4 Arrangement of Heater Bundles

Fig. A-5 Horizontal Cross Section of the Upper Plenum

Fig. A-6 Dimension of Guide Tube (1)

Fig. A-7 Dimension of Guide Tube (2)

Fig. A-8 Axial Power Distribution of Heater Rod

Fig. A-9 Relative Elevation and Dimension of the Core in SCTF

Fig. A-10 Locations and Tag Identification of Thermocouples on the  
Heater Rods

Fig. A-11 Overview of SCTF Arrangements

Table A-1 Principal Dimensions of Test Facility

## 1. Core Dimension

(1) Quantity of Bundle	8 Bundles
(2) Bundle Array	1 × 8
(3) bundle Pitch	230 mm
(4) Rod Array in a Bundle	16 × 16
(5) Rod Pitch in a Bundle	14.3 mm
(6) Quantity of Heater Rod in a Bundle	234 rods
(7) quantity of Non-Heated Rod in a Bundle	22 rods
(8) Total Quantity of Heater Rods	234 × 8 = 1872 rods
(9) Total Quantity of Non-Heated Rods	22 × 8 = 176 rods
(10) Effective Heated Length of Heater Rod	3360 mm
(11) Diameter of Heater Rod	10.7 mm
(12) Diameter of Non-Heated Rod	13.8 mm

## 2. Flow Area &amp; Fluid Volume

(1) Core Flow Area	0.259 m <sup>2</sup>
(2) Core Fluid Volume	0.92 m <sup>3</sup>
(3) Baffle Ragion Flow Area	0.10 m <sup>2</sup>
(4) Baffle Region Fluid Volume (nominal)	0.36 m <sup>3</sup>
(5) Effective Core Flow Area Based on the Measured Level-Volume Relationship Including Gap between Core Barrel and Pressure Vessel Wall and Various Penetration Holes	0.35 m <sup>2</sup>
(6) Downcomer Flow Area	0.121 m <sup>2</sup>
(7) Upper Annulus Flow Area	0.158 m <sup>2</sup>
(8) Upper Plenum Horizontal Flow Area	0.525 m <sup>2</sup>
(9) Upper Plenum Fluid Volume	1.16 m <sup>3</sup>
(10) Upper Head Fluid Volume	0.86 m <sup>3</sup>
(11) Lower Plenum Fluid Volume	1.305 m <sup>3</sup>
(12) Steam Generator Inlet Plenum Simulator Flow Area	0.626 m <sup>2</sup>
(13) Steam Generator Inlet Plenum Simulator Fluid Volume	0.931 m <sup>3</sup>
(14) Steam Water Separator Fluid Volume	5.3 m <sup>3</sup>
(15) Flow Area at the Top Plate of Steam Generator Inlet Plenum Simulator	0.195 m <sup>2</sup>
(16) Hot Leg Flow Area	0.0826 m <sup>2</sup>

Table A-1 (Continued)

(17) Intact Cold Leg Flow Area (Diameter = 297.9 mm)	0.0697	$\text{m}^2$
(18) Broken Cold Leg Flow Area (Diameter = 151.0 mm)	0.0179	$\text{m}^2$
(19) Containment Tank-I Fluid Volume	30	$\text{m}^3$
(20) Containment Tank-II Fluid Volume	50	$\text{m}^3$

## 3. Elevation &amp; Height

(1) Top Surface of Upper Core Support Plate (UCSP)	0	mm
(2) Bottom Surface of UCSP	- 76	mm
(3) Top of the Effective Heated Length of Heater Rod	- 393	mm
(4) Bottom of the Skirt in the Lower Plenum	-5270	mm
(5) Bottom of Intact Cold Leg	+ 724	mm
(6) Bottom of Hot Leg	+1050	mm
(7) Top of Upper Plenum	+2200	mm
(8) Bottom of Steam Generator Inlet Plenum Simulator	+1933	mm
(9) Centerline of Loop Seal Bottom	-2281	mm
(10) Bottom Surface of End Box	- 185.1	mm
(11) Top of Upper Annulus of Downcomer	+2234	mm
(12) Height of Steam Generator Inlet Plenum Simulator	1595	mm
(13) Height of Loop Seal	3140	mm
(14) Inner Height of Hot Leg Pipe	737	mm
(15) Bottom of Lower Plenum	-5770	mm
(16) Top of Upper Head	+2887	mm

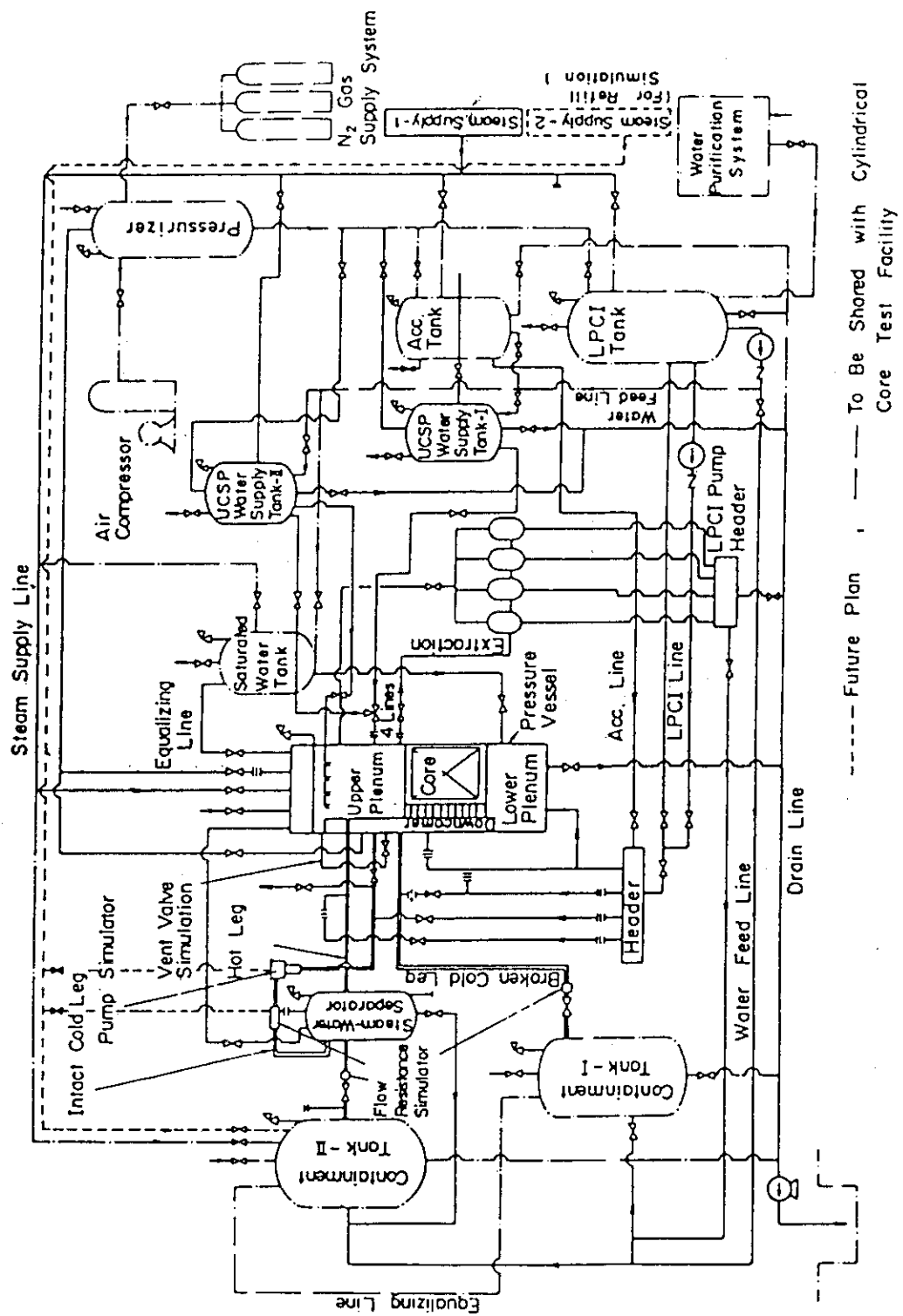


Fig. A-1 Schematic Diagram of Slab Core Test Facility

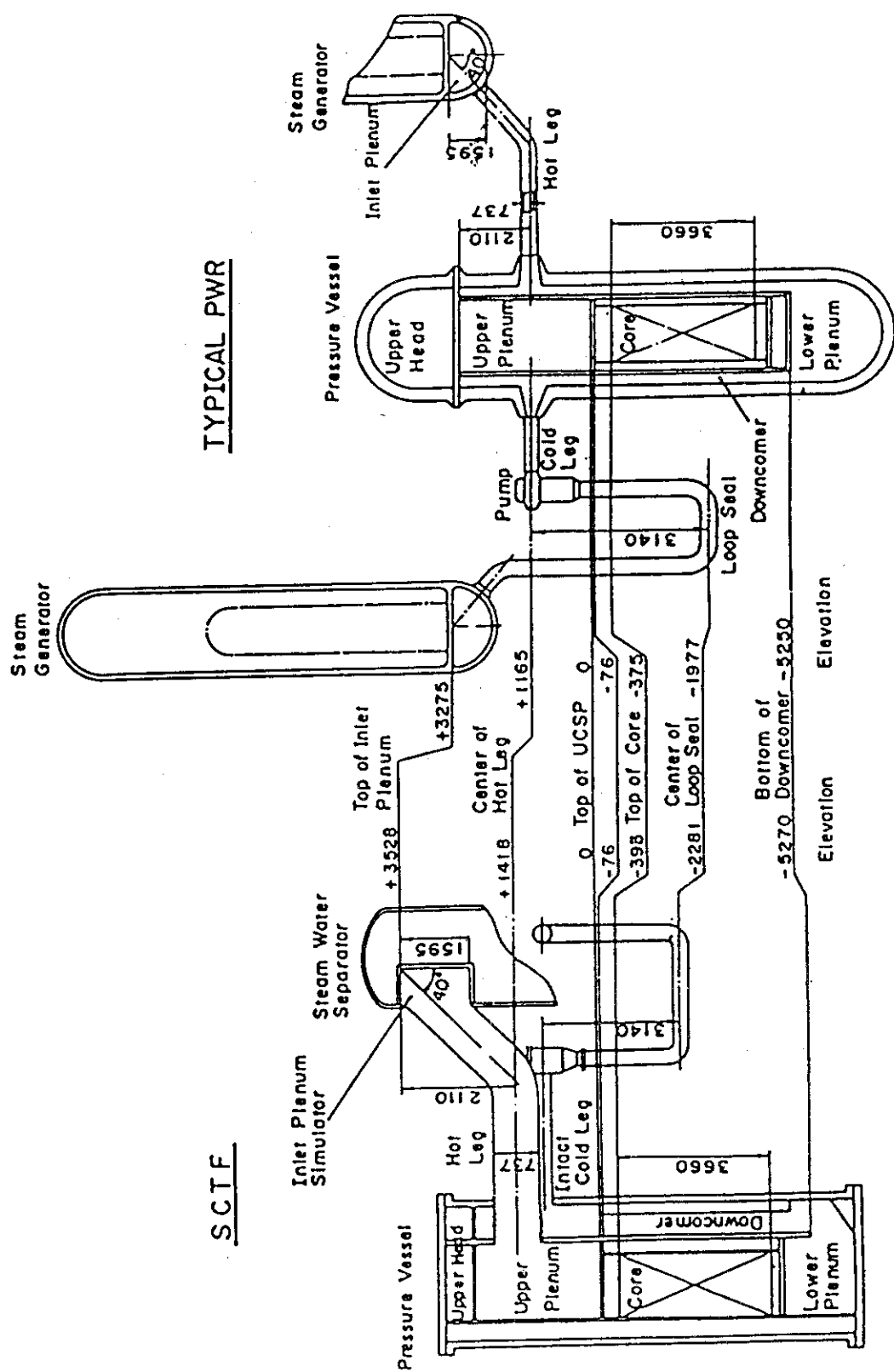


Fig. A-2 Comparison of Dimensions between SCTF and a Reference PWR

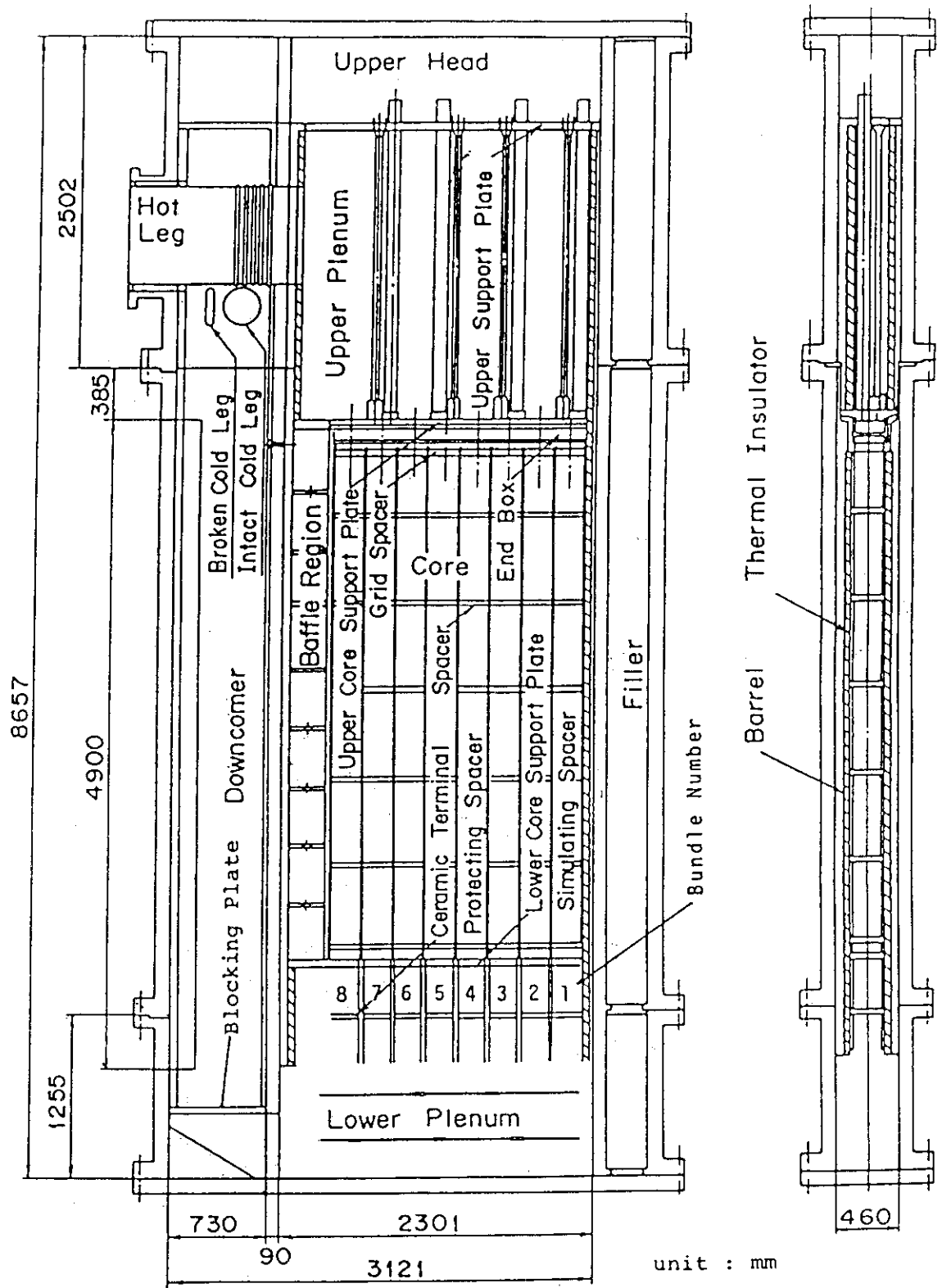


Fig. A-3 Vertical Cross Section of the Pressure Vessel

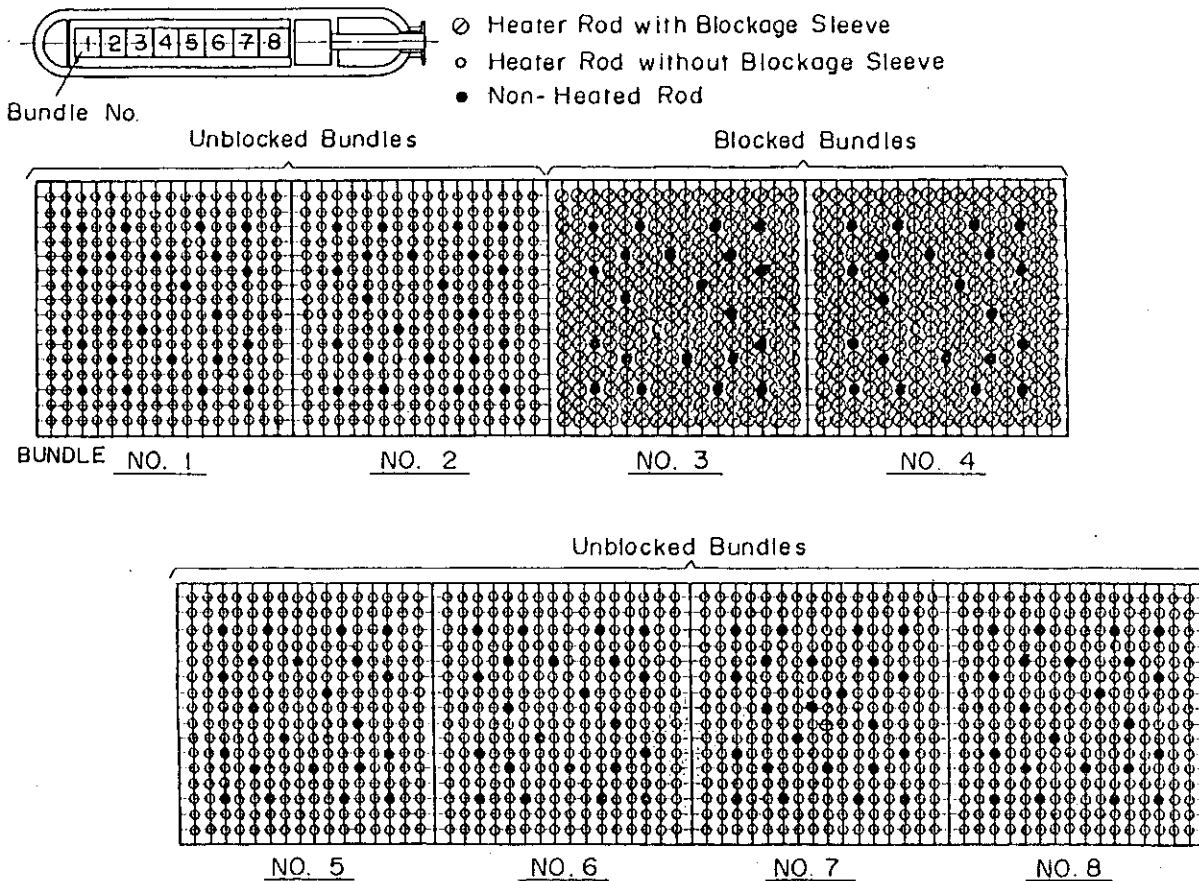


Fig. A-4 Arrangement of Heater Bundles

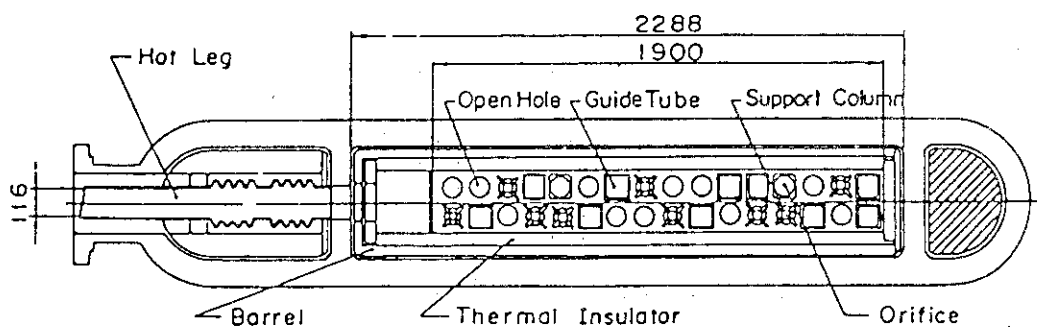


Fig. A-5 Horizontal Cross Section of the Upper Plenum

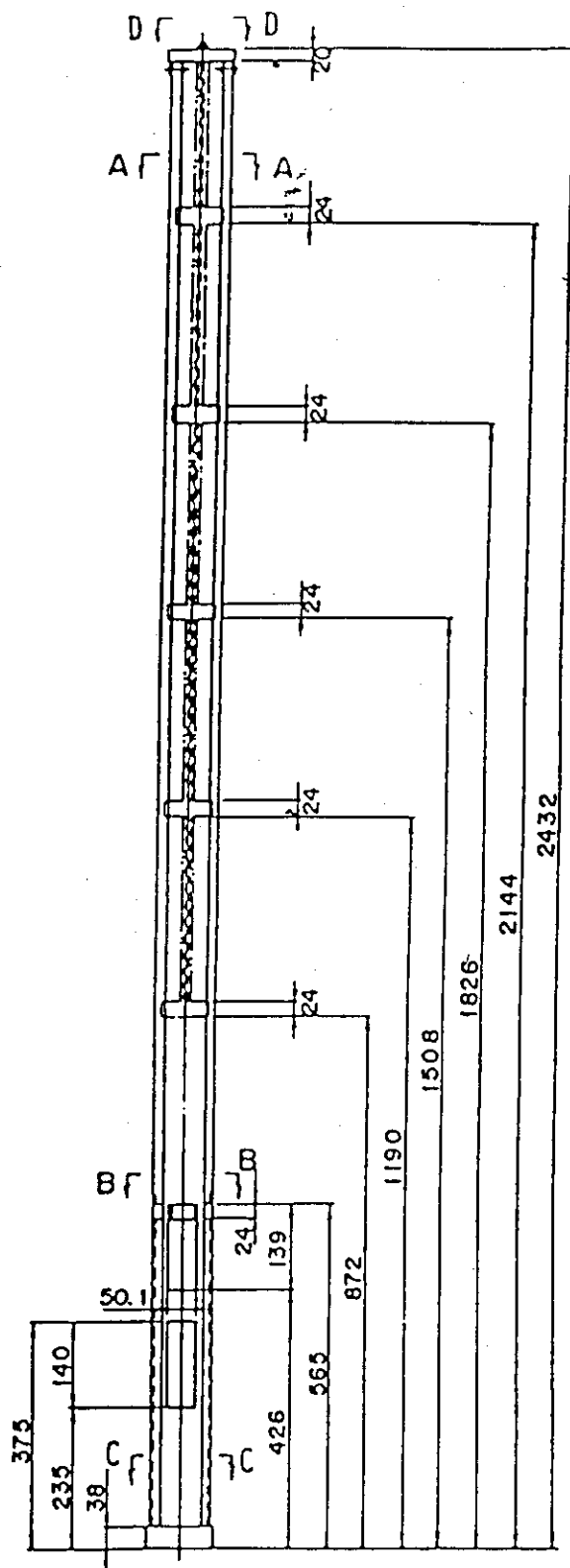
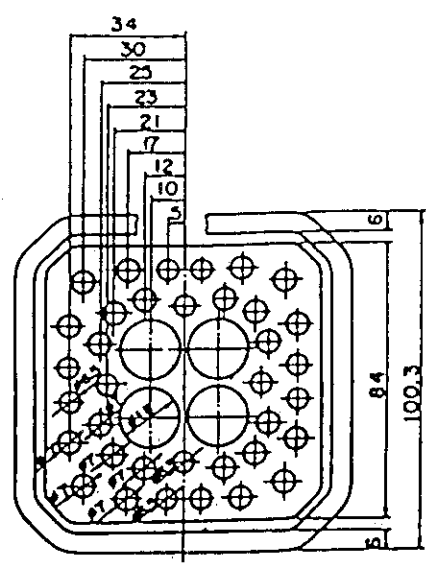
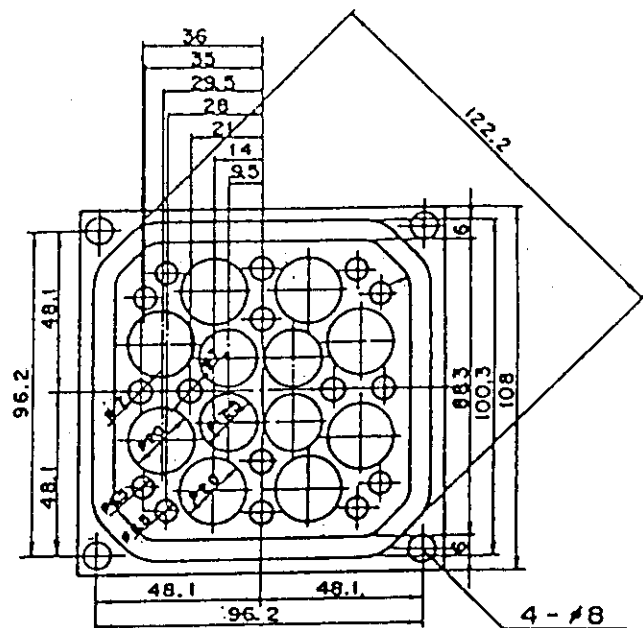


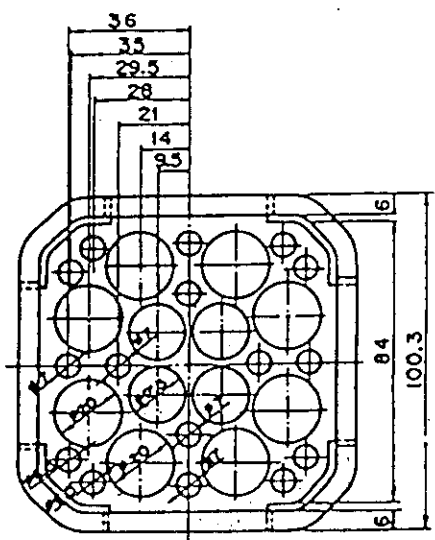
Fig. A-6 Dimension of Guide Tube (1)



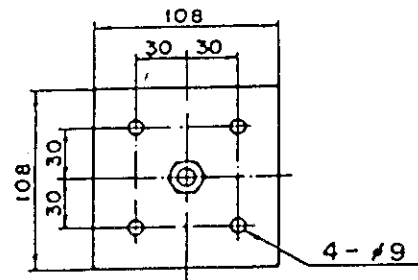
SECTION A-A



SECTION C-C



SECTION B-B



SECTION D-D

Fig. A-7 Dimension of Guide Tube (2)

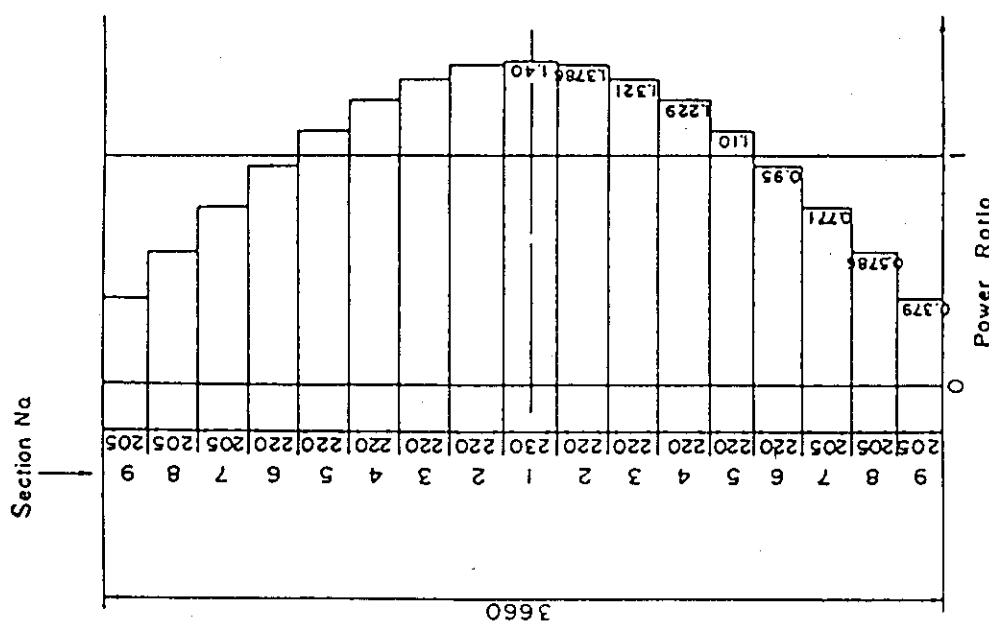


Fig. A-8 Axial Power Distribution of Heater Rod

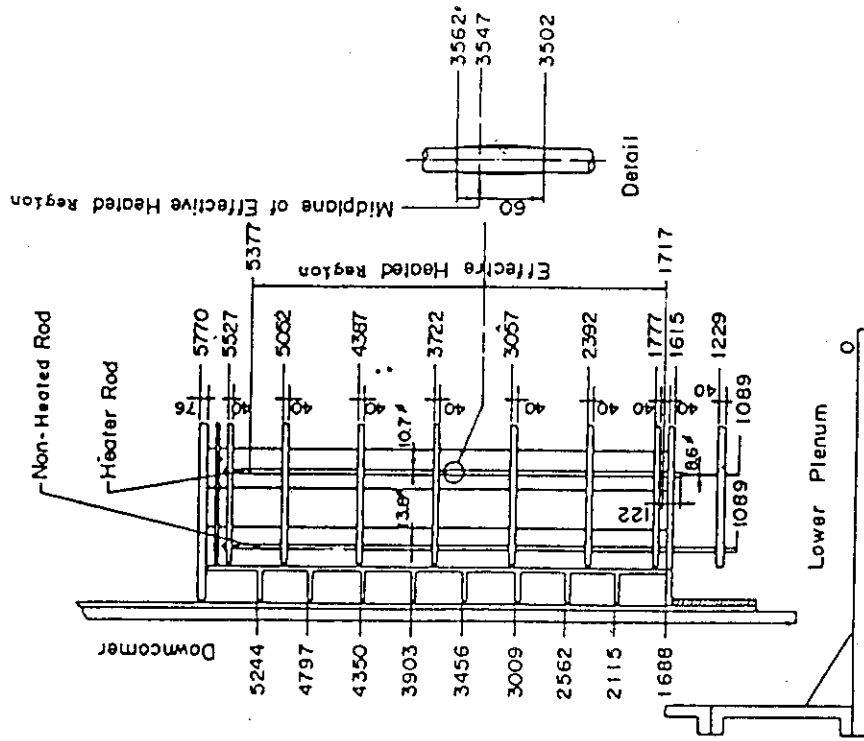


Fig. A-9 Relative Elevation and Dimension of the Core in SCTF

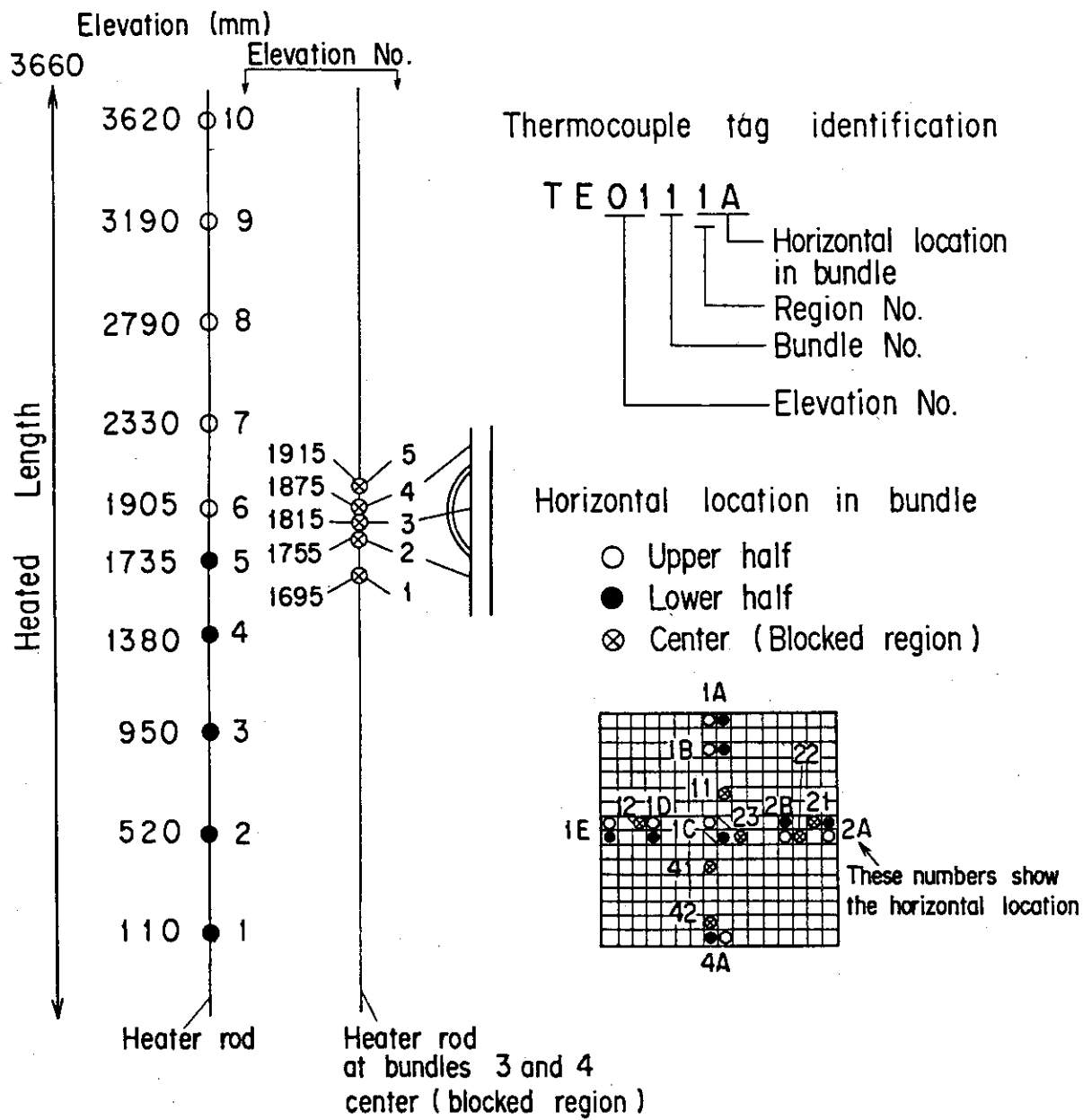


Fig. A-10 Locations and Tag Identification of Thermocouples on the Heater Rods

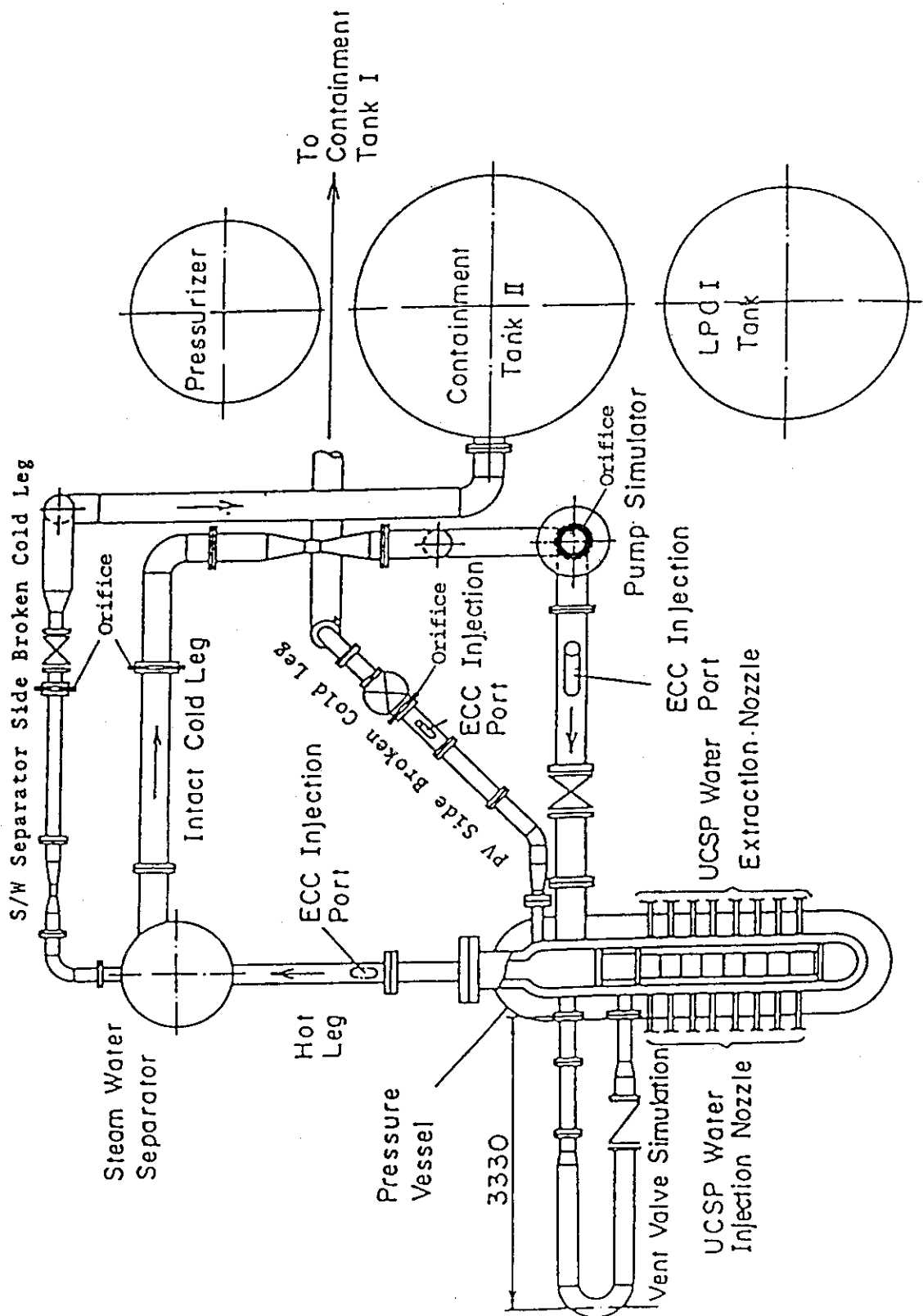


Fig. A-11 Overview of SCTF Arrangements

Appendix B Selected Heater Rod Cladding Temperatures of SCTF Test S1-SH1

Note:

\* Figs. B-1 through B-8: Heater rod cladding temperatures at the center of bundles 2, 4, 6 and 8 are shown in these figures. Identification mark and measuring elevation from the bottom of heated length for each curve are as follows:

○	110 mm	Lower half
△	520 mm	
+	950 mm	
×	1380 mm	
◊	1735 mm	Upper half
○	1905 mm	
△	2330 mm	
+	2760 mm	
×	3190 mm	
◊	3620 mm	

List of Figures

- Fig. B-1 Heater Rod Temperature (Bundle 2-1C, Lower Half)
- Fig. B-2 Heater Rod Temperature (Bundle 2-1C, Upper Half)
- Fig. B-3 Heater Rod Temperature (Bundle 4-1C, Lower Half)
- Fig. B-4 Heater Rod Temperature (Bundle 4-1C, Upper Half)
- Fig. B-5 Heater Rod Temperature (Bundle 6-1C, Lower Half)
- Fig. B-6 Heater Rod Temperature (Bundle 6-1C, Upper Half)
- Fig. B-7 Heater Rod Temperature (Bundle 8-1C, Lower Half)
- Fig. B-8 Heater Rod Temperature (Bundle 8-1C, Upper Half)

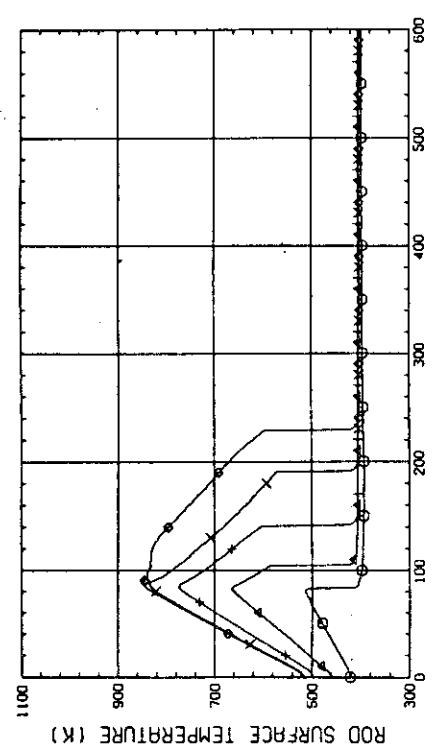


Fig. B-1 Heater Rod Temperature  
(Bundle 2-1C, Lower Half)

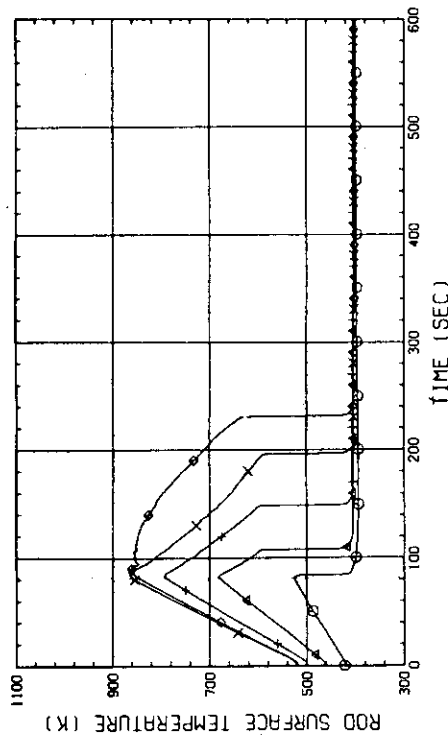


Fig. B-3 Heater Rod Temperature  
(Bundle 4-1C, Lower Half)

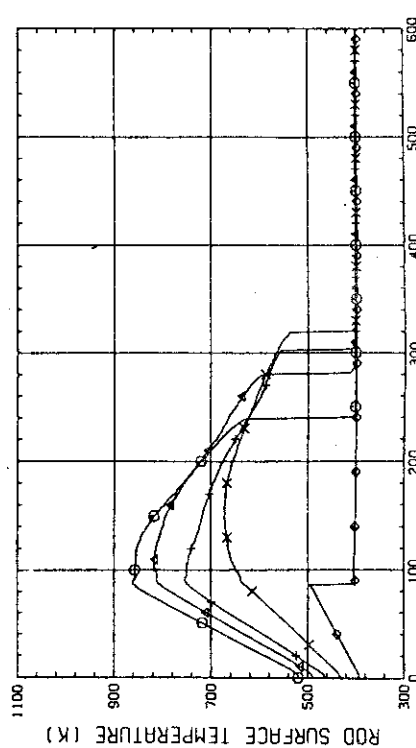


Fig. B-2 Heater Rod Temperature  
(Bundle 2-1C, Upper Half)

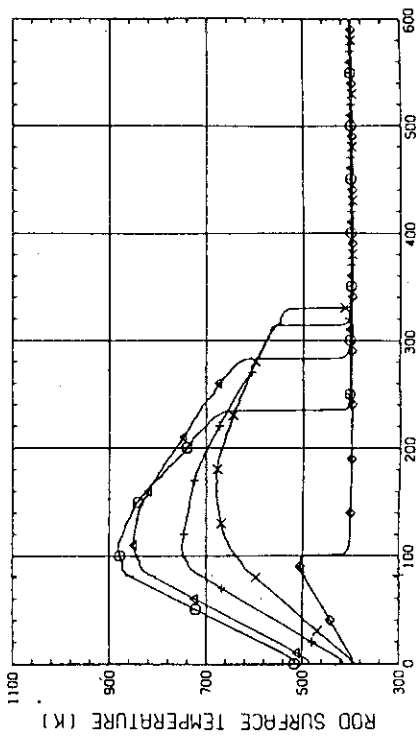


Fig. B-4 Heater Rod Temperature  
(Bundle 4-1C, Upper Half)

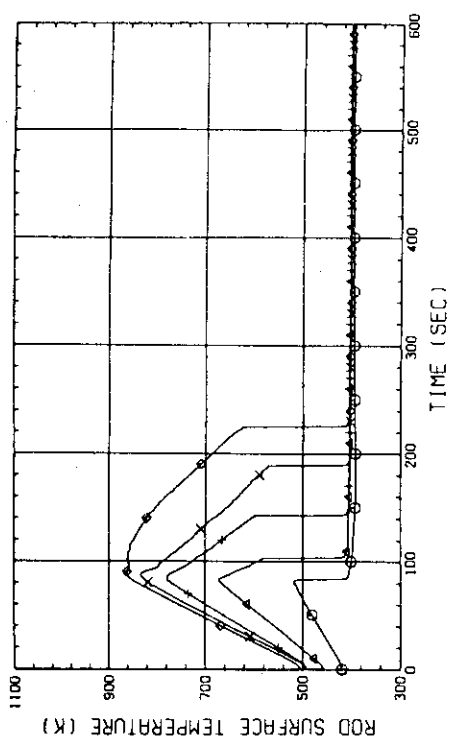


Fig. B-5 Heater Rod Temperature  
(Bundle 6-1C, Lower Half)

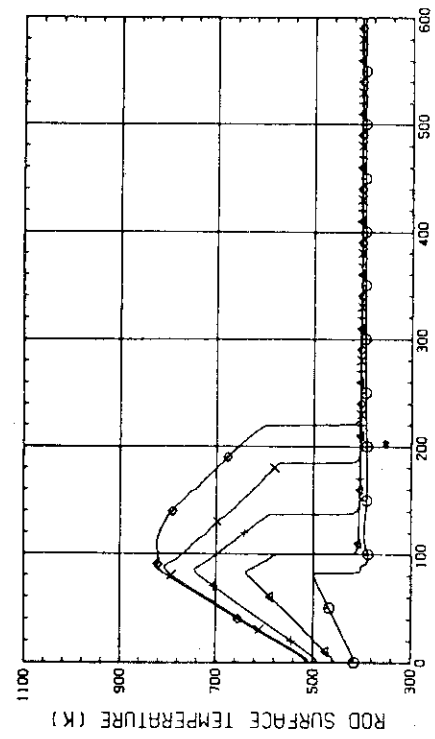


Fig. B-7 Heater Rod Temperature  
(Bundle 8-1C, Lower Half)

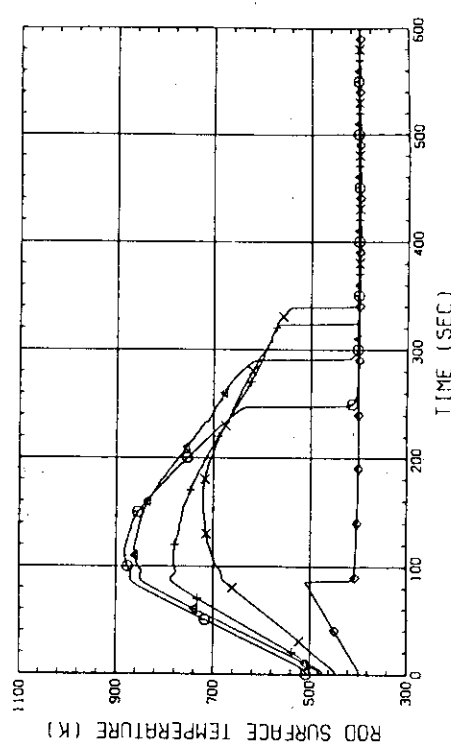


Fig. B-6 Heater Rod Temperature  
(Bundle 6-1C, Upper Half)

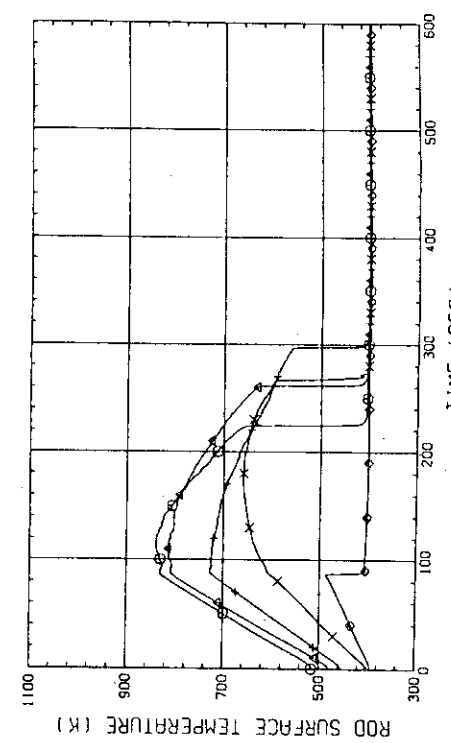


Fig. B-8 Heater Rod Temperature  
(Bundle 8-1C, Upper Half)

Appendix C Selected Heater Rod Cladding Temperature of SCTF Test S1-05

Note:

In Appendix C, selected data from Test S1-05 are introduced.  
Definitions of identification marks for each figure are the same  
as those described in Appendix B.

List of Figures

- Fig. C-1 Heater Rod Temperature (Bundle 2-1C, Lower Half)
- Fig. C-2 Heater Rod Temperature (Bundle 2-1C, Upper Half)
- Fig. C-3 Heater Rod Temperature (Bundle 4-1C, Lower Half)
- Fig. C-4 Heater Rod Temperature (Bundle 4-1C, Upper Half)
- Fig. C-5 Heater Rod Temperature (Bundle 6-1C, Lower Half)
- Fig. C-6 Heater Rod Temperature (Bundle 6-1C, Upper Half)
- Fig. C-7 Heater Rod Temperature (Bundle 8-1C, Lower Half)
- Fig. C-8 Heater Rod Temperature (Bundle 8-1C, Upper Half)

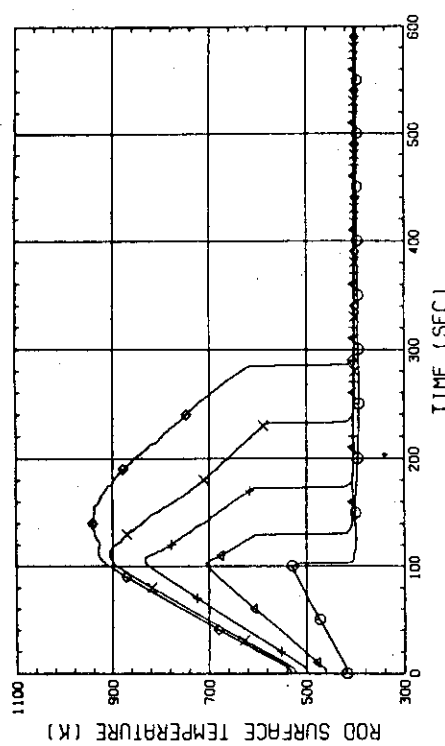


Fig. C-1 Heater Rod Temperature  
(Bundle 2-1C, Lower Half)

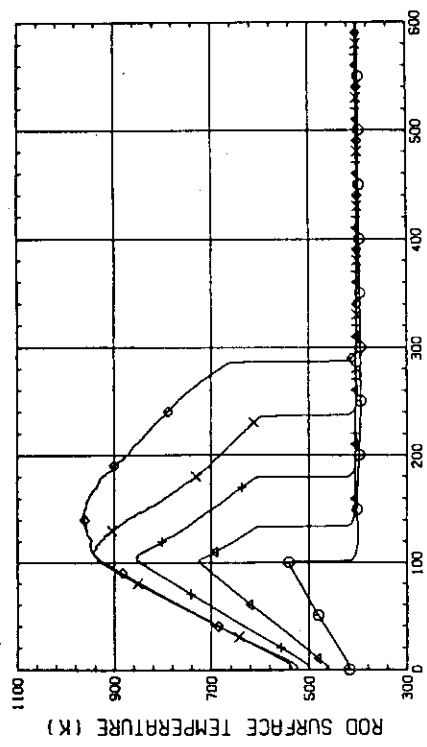


Fig. C-3 Heater Rod Temperature  
(Bundle 4-1C, Lower Half)

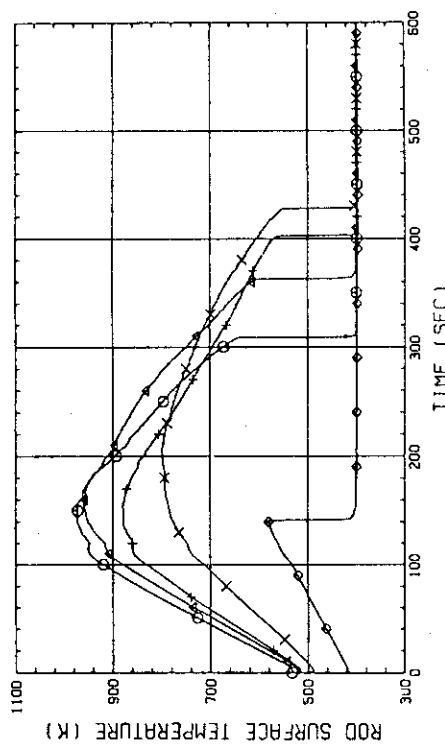


Fig. C-2 Heater Rod Temperature  
(Bundle 2-1C, Upper Half)

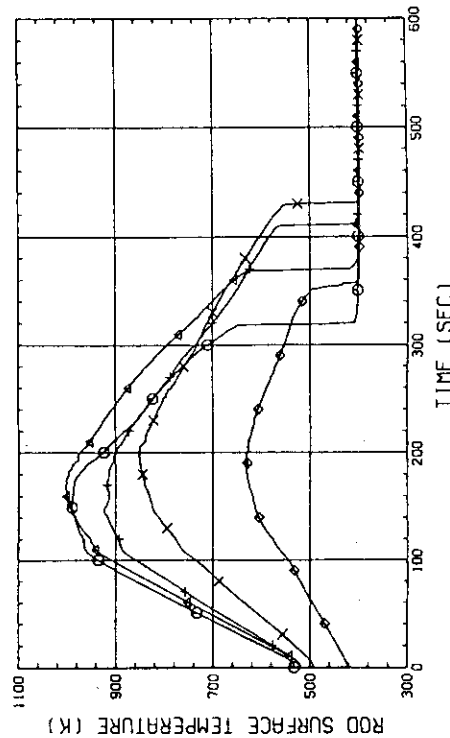


Fig. C-4 Heater Rod Temperature  
(Bundle 4-1C, Upper Half)

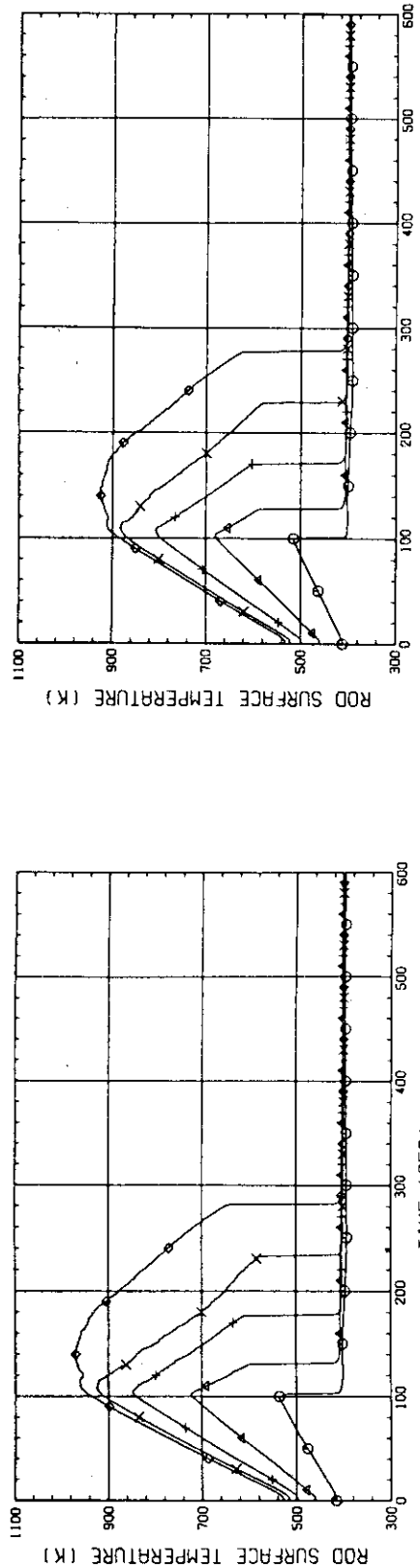


Fig. C-5 Heater Rod Temperature  
(Bundle 6-1C, Lower Half)

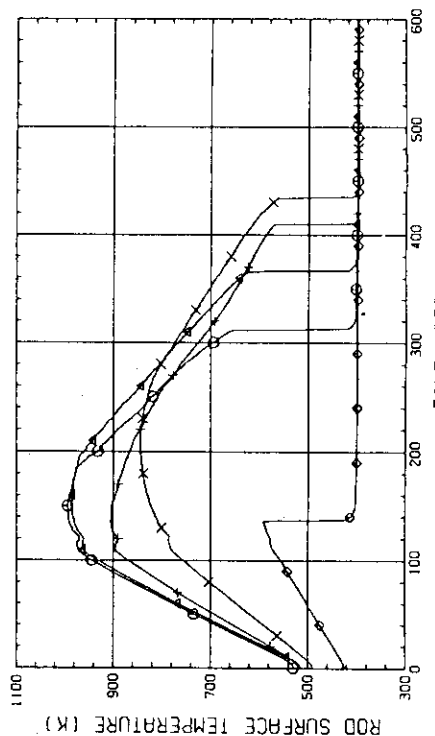


Fig. C-6 Heater Rod Temperature  
(Bundle 6-1C, Upper Half)

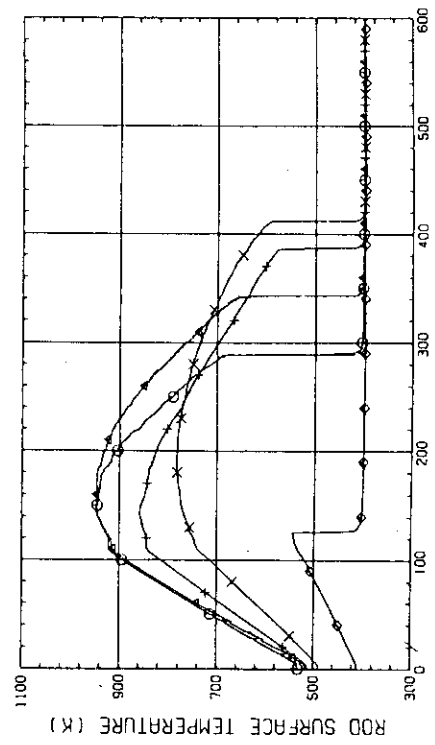


Fig. C-7 Heater Rod Temperature  
(Bundle 8-1C, Lower Half)

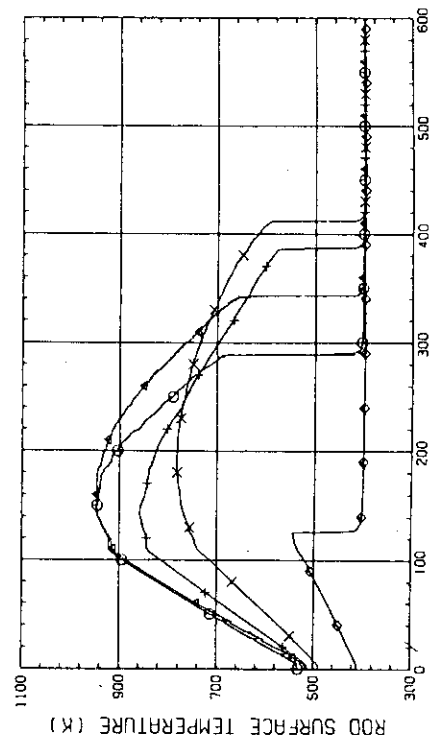


Fig. C-8 Heater Rod Temperature  
(Bundle 8-1C, Upper Half)

Appendix D Selected Heater Rod Cladding Temperatures of SCTF Test S1-09

Note:

In Appendix D, selected data from Test S1-09 are introduced.  
Definitions of identification marks for each figure are the same  
as those described in Appendix B.

List of Figures

- Fig. D-1 Heater Rod Temperature (Bundle 2-1C, Lower Half)
- Fig. D-2 Heater Rod Temperature (Bundle 2-1C, Upper Half)
- Fig. D-3 Heater Rod Temperature (Bundle 4-1C, Lower Half)
- Fig. D-4 Heater Rod Temperature (Bundle 4-1C, Upper Half)
- Fig. D-5 Heater Rod Temperature (Bundle 6-1C, Lower Half)
- Fig. D-6 Heater Rod Temperature (Bundle 6-1C, Upper Half)
- Fig. D-7 Heater Rod Temperature (Bundle 8-1C, Lower Half)
- Fig. D-8 Heater Rod Temperature (Bundle 8-1C, Upper Half)

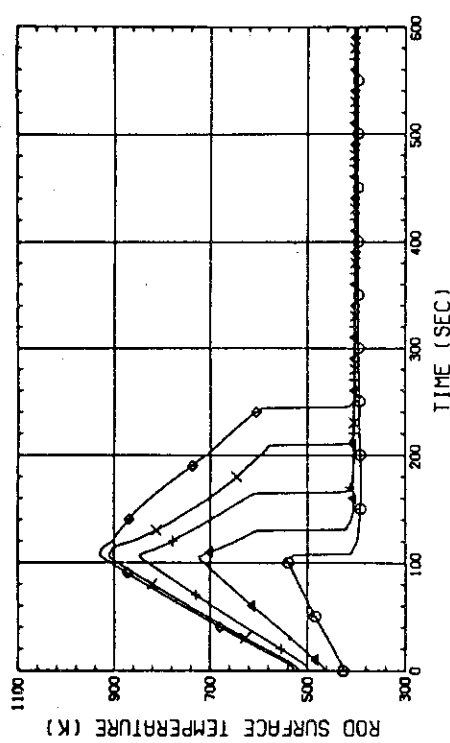


Fig. D-1 Heater Rod Temperature  
(Bundle 2-1C, Lower Half)

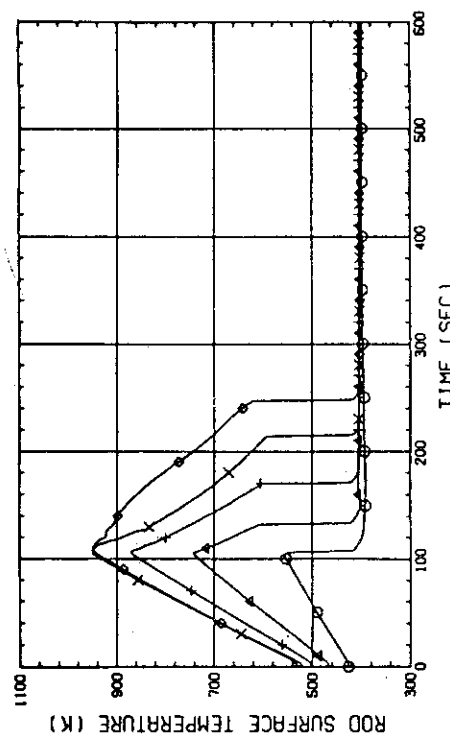


Fig. D-3 Heater Rod Temperature  
(Bundle 4-1C, Lower Half)

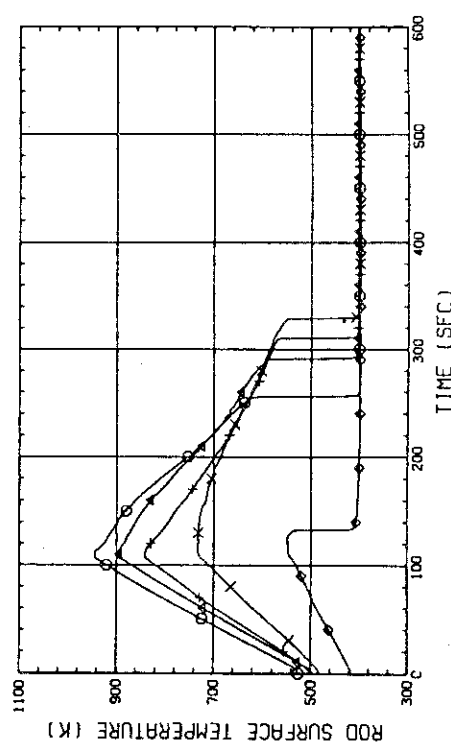


Fig. D-2 Heater Rod Temperature  
(Bundle 2-1C, Upper Half)

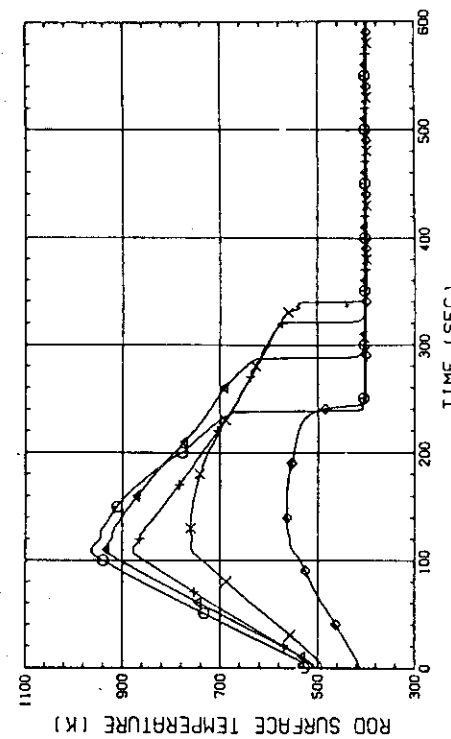


Fig. D-4 Heater Rod Temperature  
(Bundle 4-1C, Upper Half)

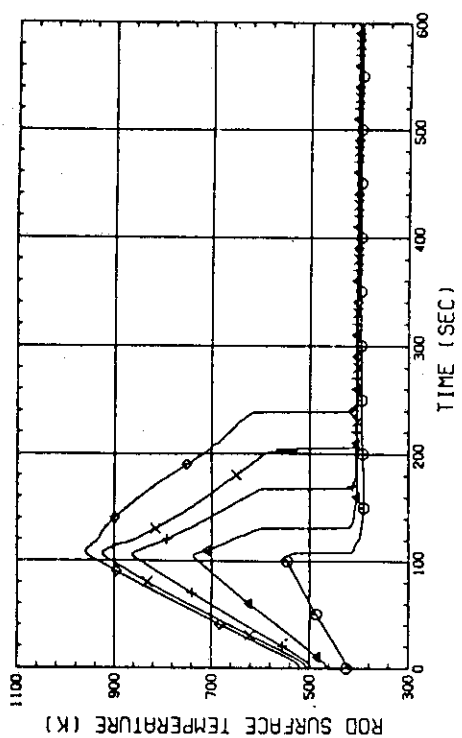


Fig. D-5 Heater Rod Temperature  
(Bundle 6-1C, Lower Half)

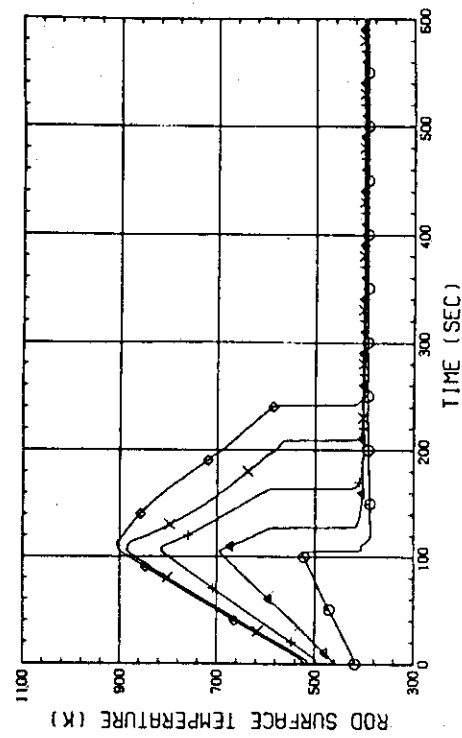


Fig. D-7 Heater Rod Temperature  
(Bundle 8-1C, Lower Half)

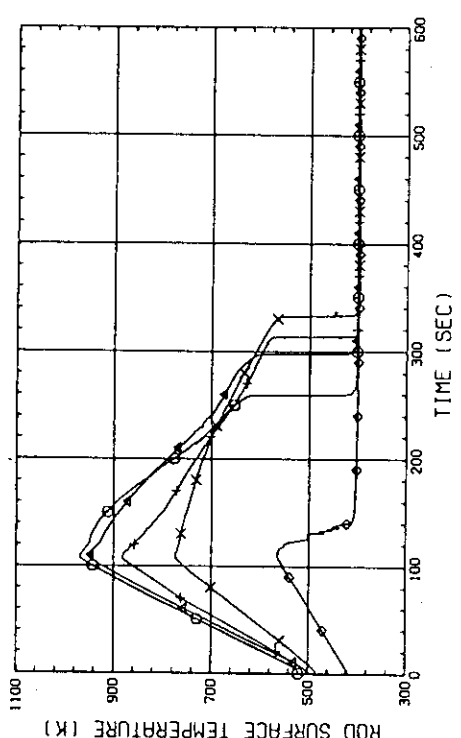


Fig. D-6 Heater Rod Temperature  
(Bundle 6-1C, Upper Half)

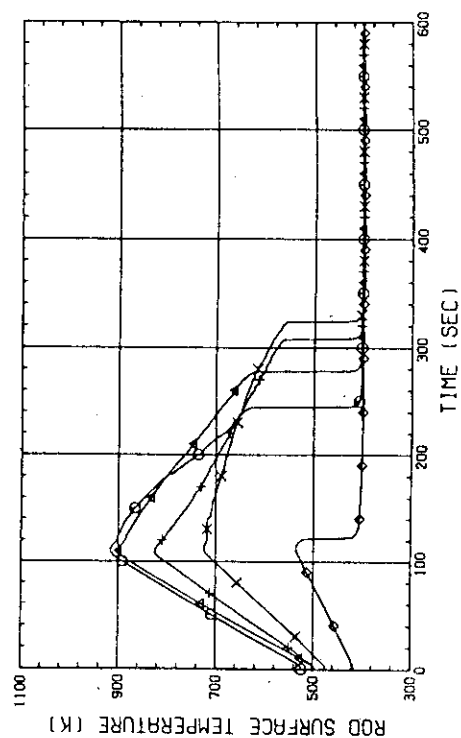


Fig. D-8 Heater Rod Temperature  
(Bundle 8-1C, Upper Half)